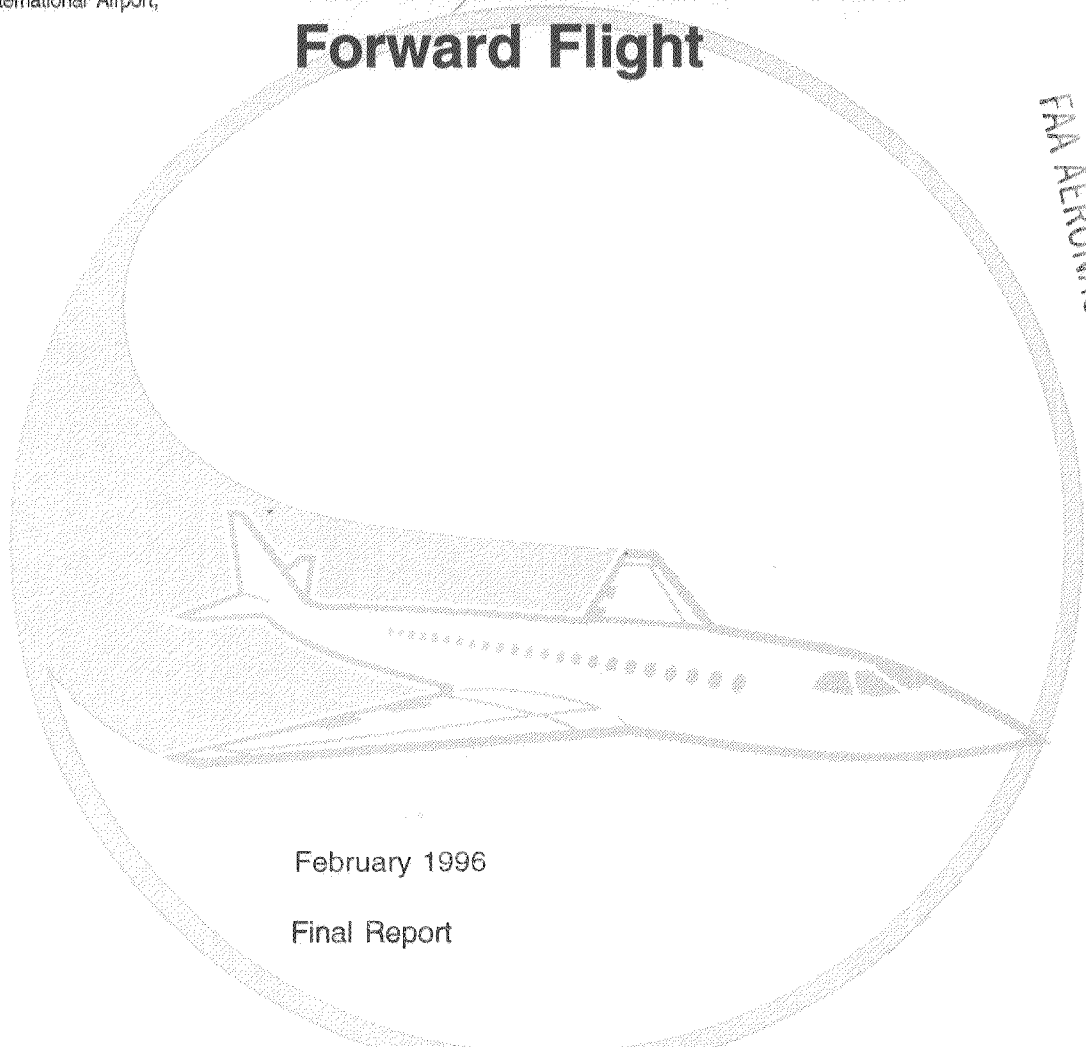


0002312

DOT/FAA/CT-94/117

FAA Technical Center  
Atlantic City International Airport,  
N.J. 08405

# Flight Test Investigation of Rotorcraft Wake Vortices in Forward Flight



FAA AERONAUTICAL CENTER LIBRARY

February 1996

Final Report

This document is available to the public  
through the National Technical Information  
Service Springfield, Virginia 22161



U.S. Department of Transportation  
Federal Aviation Administration

## NOTICE

This document is disseminated under the sponsorship of the U.S. Department of Transportation in the interest of information exchange. The United States Government assumes no liability for the contents or use thereof. The United States Government does not endorse products or manufacturers. Trade or manufacturer's names appear herein solely because they are considered essential to the objective of this report.

1. Report No. <p>DOT/FAA/CT-94/117</p>	2. Government Accession No.	3. Recipient's Catalog No.	
4. Title and Subtitle <p>FLIGHT TEST INVESTIGATION OF ROTORCRAFT WAKE VORTICES IN FORWARD FLIGHT</p>		5. Report Date <p>February 1996</p>	
		6. Performing Organization Code <p>ACT-370</p>	
7. Author(s) <p>Stephen A. Teager, Keith J. Biehl (FAA Technical Center) Leo J. Garodz, Joseph J. Tymczyszyn (FAA retired) David C. Burnham (Scientific &amp; Engineering Solutions, Inc.)</p>		8. Performing Organization Report No. <p>DOT/FAA/CT-94/117</p>	
9. Performing Organization Name and Address <p>Federal Aviation Administration Technical Center Atlantic City International Airport, NJ 08405</p>		10. Work Unit No. (TRAIS)	
		11. Contract or Grant No.	
12. Sponsoring Agency Name and Address <p>U.S. Department of Transportation Federal Aviation Administration Technical Center Atlantic City International Airport, NJ 08405</p>		13. Type of Report and Period Covered <p>Final Report</p>	
		14. Sponsoring Agency Code	
15. Supplementary Notes <p>This report resulted from a collaborative effort by ACT-370, AAR-420, AND-630, and the Volpe National Transportation Systems Center.</p>			
16. Abstract <p>This report presents the results of helicopter flight tests and wake vortex measurements which were designed to provide data necessary for the assessment of hazards to following aircraft. The tests described in this report were conducted using small probe airplanes and a Laser Doppler Velocimeter for wake vortex measurements during forward-flight helicopter operations. Four helicopters, having weights ranging from 7,600 to 70,000 pounds, were used in the tests as the wake vortex generating aircraft. Wake vortex strength and decay characteristics as determined from the flight test results are discussed. In the absence of encounter measurements for the case of hover flight, it is recommended that small airplanes, at the same altitude and downwind of a hovering helicopter, maintain at least 500 feet of separation.</p>			
17. Key Words <p>Wake vortex, Rotorcraft, Flight test, Separation standards, Hazard</p>		18. Distribution Statement <p>This document is available to the public through the National Technical Information Service, Springfield, Virginia 22161.</p>	
19. Security Classif. (of this report) <p>Unclassified</p>	20. Security Classif. (of this page) <p>Unclassified</p>	21. No. of Pages <p>94</p>	22. Price



## PREFACE

This report was part of an effort by the Federal Aviation Administration (FAA) to assess the need for rotorcraft separation standards based on wake vortex hazards. The data in this report, on the strength and duration of the wake vortices generated by helicopters, is needed to assess the vortex hazard to following aircraft. Preliminary tests were conducted in October 1984 to validate experimental techniques for measuring helicopter wake vortices out-of-ground effect using a laser doppler velocimeter (LDV). In the fall of 1985, flight tests were conducted using three small aircraft to probe helicopter wake vortices. The tests described in this report, and conducted from late 1985 through 1987, were designed to include complete characterization of helicopter wake vortex parameters and meteorological conditions during forward flight operations. This test program was originally conducted under the direction of the Wake Vortex Program Manager, John O'Neill, formerly of the FAA Technical Center and now retired. This report, which describes the results of the test program, was developed under the direction of the current Wake Vortex Program Manager, George C. Hay and the Wake Vortex Program Deputy Manager, Robert Passman.

The tests were conducted jointly by the Federal Aviation Administration (FAA) Technical Center, Atlantic City International Airport, New Jersey, which was responsible for the full-scale flight test and the Transportation Systems Center, Cambridge, Mass., which was responsible for the LDV data. Special acknowledgement is given to David C. Burnham, formerly of the Volpe National Transportation Center and to Thomas D. Talbot of the Unisys Corporation for their contributions in the collection and analysis of the LDV data. The documentation of the results of the LDV data analysis presented in chapters 3 and 4 was contributed by Mr. Burnham. The authors wish to express their sincere appreciation and gratitude to the personnel of Lockheed, Huntsville, Alabama, and NOAA, Idaho Falls, Idaho, for their support during the program. Special appreciation is noted for the following military organizations and their personnel for their assistance and cooperation during the tests: the Pennsylvania National Guard, for use of the UH-1H rotorcraft; the U.S. Marine Corps, HMX-1, Quantico, VA, for use of the CH-53E; the U.S. Army, Fort Eustis, VA, for use of the CH-47D; the U.S. Army, Fort Dix, NJ, for use of the UH-60A; and the U.S. Navy, Pensacola, FL, for the use of the T-34C aircraft.

The authors also wish to acknowledge the exceptional efforts and dedication of their many coworkers, both at the FAA Technical Center and the John Volpe National Transportation Systems Center, in completing this program.



## TABLE OF CONTENTS

	Page
EXECUTIVE SUMMARY	xi
1. INTRODUCTION	1-1
1.1 Objective	1-1
1.2 Prior Tests	1-1
1.3 Summary of Huntsville Tests	1-4
1.4 Description of Present Study	1-6
1.5 Analytical Background	1-9
1.6 Hazard Model	1-11
2. TEST DESCRIPTION	2-1
2.1 Aircraft Types	2-1
2.2 Flow Visualization	2-1
2.2.1 CH-53E	2-3
2.2.2 CH-47D	2-4
2.2.3 UH-60A	2-4
2.2.4 S-76A	2-4
2.3 Test Schedule	2-8
2.4 Test Procedures	2-8
3. LDV MEASUREMENTS	3-1
3.1 Meteorological Measurements	3-1
3.2 Aircraft Tracking	3-4
3.3 Photography	3-4
3.4 Airspeed/Ground Speed	3-4
3.5 LDV System	3-5
3.6 Data Collection	3-6
3.7 Data Reduction	3-8
3.8 Data Analysis	3-9
4. LDV RESULTS	4-1
4.1 Initial Vortex Strength	4-1
4.2 Initial Vortex Separation	4-7
4.3 Vortex Decay	4-10
4.3.1 Predicted Hazard Duration	4-11
4.3.2 Predicted Hazard Distance	4-15

5.	PROBE TESTING	5-1
5.1	Probe Airplanes	5-1
5.2	Probe Test Pilot's Hazard Criteria	5-1
5.3	Test Procedures	5-2
	5.3.1 Vortex Probing Techniques	5-2
	5.3.2 Aircraft Separation	5-5
	5.3.3 Data Recording and Photo-Video Coverage	5-5
5.4	Test Results	5-7
	5.4.1 Vortex Upsets	5-7
	5.4.2 Roll Control Power	5-7
	5.4.3 Vortex Upset Hazard	5-12
5.5	Structural Damage Considerations	5-13
5.6	Qualitative Observations	5-13
	5.6.1 Visual Characteristics	5-14
	5.6.2 Wake Vortex Trajectories	5-14
	5.6.3 Wake Vortex Hazard Volume	5-14
5.7	Probe Test Comments	5-15
6.	DISCUSSION	6-1
6.1	Comparison of LDV and Probe Results	6-1
	6.1.1 Hazard Definition	6-1
	6.1.2 Hazard Distance	6-1
	6.1.3 Hazard Duration	6-3
	6.1.4 Vortex Core Spacing	6-5
6.2	Comparison with Calculations	6-5
6.3	Operational Considerations	6-7
	6.3.1 Current Separation Standards	6-8
	6.3.2 Decelerating Approach	6-9
	6.3.3 Comparison with Fixed-Wing Vortices	6-10
	6.3.4 Uncontrolled Airports	6-11
7.	CONCLUSIONS	7-1
8.	RECOMMENDATIONS	8-1
9.	REFERENCES	9-1

APPENDIX A - Probe Aircraft

## LIST OF FIGURES

		Page
1-1	S-58 Helicopter Wake Flight Test Site (Tower Flyby Technique)	1-2
1-2	S-58 Helicopter Wake Vortex Time History, Crosswind Run Number Four	1-3
1-3	HO4S-3 Helicopter Used for Wake Vortex Tests	1-4
1-4	Bell UH-1H Helicopter Schematic	1-5
1-5	Sikorsky CH-54 Helicopter	1-6
1-6	Sikorsky S-76A Helicopter Schematic	1-7
1-7	Sikorsky CH-53E Helicopter Schematic	1-8
1-8	Boeing Vertol CH-47D Helicopter Schematic	1-8
1-9	Sikorsky UH-60A Helicopter Schematic	1-9
2-1	Bell UH-1H Smoke Generator	2-2
2-2	Bell UH-1H Smoke Trail	2-2
2-3	CH-53E Wake Vortex Flow Visualization System	2-3
2-4	CH-47D Wake Vortex Flow Visualization System	2-5
2-5	CH-47D Smoke Trail	2-5
2-6	UH-60A Wake Vortex Flow Visualization System	2-6
2-7	UH-60A Smoke Trail	2-6
2-8	S-76A Wake Vortex Flow Visualization System	2-7
2-9	S-76A Wake Vortex Flow	2-7
3-1	CH-53E Data Flight Over LDV Housing	3-1
3-2	LDV Installation at FAA Technical Center	3-2
3-3	S-76A Data Flight Over Equipment Van	3-2
3-4	Meteorological Measurement System at Test Site	3-3
3-5	LDV Scan Methodology	3-6
3-6	CH-53E Data Flight Over LDV Van	3-7
3-7	Range and Elevation Angle vs. Time	3-9
3-8	S-76A Vortex Velocity Profile Time History	3-10
3-9	Full-Size S-76A Wake Velocity Profile	3-11
3-10	CH-53E Circulation Profiles	3-11
3-11	S-76A Average Circulation vs. Time	3-12
4-1	S-76A 5-M Initial Average Circulation vs. Airspeed (Knots)	4-2
4-2	UH-60A 5-M Initial Average Circulation vs. Airspeed (Knots)	4-2
4-3	CH-47D 5-M Initial Average Circulation vs. Airspeed (Knots)	4-3
4-4	CH-53E 5-M Initial Average Circulation vs. Airspeed (Knots)	4-3
4-5	S-76A 5-M Initial Average Circulation X (V/100) vs. Airspeed (Knots)	4-4
4-6	UH-60A 5-M Initial Average Circulation X (V/100) vs. Airspeed (Knots)	4-5
4-7	CH-47A 5-M Initial Average Circulation X (V/100) vs. Airspeed (Knots)	4-5
4-8	CH-53E 5-M Initial Average Circulation X (V/100) vs. Airspeed (Knots)	4-6
4-9	S-76A Vortex Separation (Rotor Diameters) vs. Airspeed (Knots)	4-8

4-10	UH-60A Vortex Separation (Rotor Diameters) vs. Airspeed (Knots)	4-9
4-11	CH-47D Vortex Separation (Rotor Diameters) vs. Airspeed (Knots)	4-9
4-12	CH-53E Vortex Separation (Rotor Diameters) vs. Airspeed (Knots)	4-10
4-13	S-76A Modeled Vortex Hazard Duration vs. Airspeed (Knots)	4-12
4-14	UH-60A Modeled Vortex Hazard Duration vs. Airspeed (Knots)	4-12
4-15	CH-47D Modeled Vortex Hazard Duration vs. Airspeed (Knots)	4-13
4-16	CH-53E Modeled Vortex Hazard Duration vs. Airspeed (Knots)	4-13
4-17	S-76A Predicted Vortex Hazard Distance (nm) vs. Airspeed (Knots)	4-16
4-18	UH-60A Predicted Vortex Hazard Distance (nm) vs. Airspeed (Knots)	4-16
4-19	CH-47D Predicted Vortex Hazard Distance (nm) vs. Airspeed (Knots)	4-17
4-20	CH-53E Predicted Vortex Hazard Distance (nm) vs. Airspeed (Knots)	4-17
5-1	Vortex Probe Techniques: Parallel and Crosstrack Penetrations	5-3
5-2	Probe Test (Note Asymmetry of Wake Trail)	5-6
5-3	Probe Test (Note Probe Aircraft Excursion in the Vortex Core)	5-6
5-4	T-34C Upsets in the Wake of a UH-1H Helicopter	5-8
5-5	T-34C Upsets in the Wake of a UH-60A Helicopter	5-8
5-6	T-34C Upsets in the Wake of a CH-47D Helicopter	5-9
5-7	T-34C Upsets in the Wake of a CH-53E Helicopter	5-10
5-8	Bank Angle vs. Separation for CH-47D (45-75 Knots Airspeed)	5-11
5-9	Bank Angle vs. Separation for CH-47D (90-120 Knots Airspeed)	5-11
5-10	Bank Angle vs. Separation for CH-53E (80-120 Knots Airspeed)	5-12
6-1	Predicted Hazard Distance vs. Airspeed for S-76A (Tape 17)	6-2
6-2	Predicted Hazard Distance vs. Airspeed for CH-53E (Tape 12)	6-2
6-3	Probe Upset Bank Angle vs. Vortex Age for CH-47D	6-4
6-4	Probe Upset Bank Angle vs. Vortex Age for CH-53E	6-4
6-5	Recalculated Hazard Duration vs. Airspeed for S-76A	6-6
6-6	Recalculated Hazard Duration vs. Airspeed for CH-53E	6-6
6-7	S-76A Wake Visualization	6-8

## LIST OF TABLES

		Page
2-1	Characteristics of Wake Vortex Generating Helicopters	2-1
2-2	LDV Runs	2-8
4-1	Wake Vortex Circulation Analysis	4-7
4-2	Predicted Hazard Duration, T	4-14
4-3	Predicted Hazard Distance, D	4-18
5-1	Probe Test Separation Distances (nm)	5-13
6-1	Hazard Distance Comparison	6-3
6-2	Comparison of Observed and Calculated Roll Moments	6-7
6-3	Wake Vortex Class Weight Limits	6-8
6-4	IFR Wake Vortex Approach Separation Standards (Nautical Miles)	6-9

## LIST OF SYMBOLS, SUBSCRIPTS AND ABBREVIATIONS

### SYMBOLS

a	Deceleration ft/sec <sup>2</sup>
b	Aircraft Wingspan (ft)
b'	Spacing Between Vortices (ft, $b'=\pi/4b$ for Elliptical Wing Loading)
$C_L$	Airplane Lift Coefficient
D	Distance Behind Generating Helicopter (ft)
d	Rotor diameter (feet)
f	Ratio of Maximum Vortex-Induced Rolling Moment to Roll Control Capability of Encountering Airplane
$F_n$	Function
G	Helicopter Ground Speed (ft/sec or kts)
K	Span Load Factor — Depends on Shape of Lift Distribution
p	Roll Rate (degrees per second or radians per second)
$\hat{p}$	Maximum Nondimensional Roll Rate of Encountering Airplane
r	Vortex Radius (ft)
S	Longitudinal Separation Between Aircraft (ft)
T	Time
V	Aircraft True Airspeed (ft/sec or kts)
v	Vortex Tangential Velocity (ft/sec or kts)
W	Aircraft Weight (pounds)
$\Gamma$	Vortex Circulation (ft <sup>2</sup> /sec)
$\Gamma'(r)$	Vortex Average Circulation out to Radius r (ft <sup>2</sup> /sec)
$\Gamma_\infty$	Vortex Bound Circulation About Midpoint of Wing (ft <sup>2</sup> /sec)
$\rho$	Atmospheric Density (slugs/ft <sup>3</sup> )

### SUBSCRIPTS

c	Vortex Core
e	Encountering Aircraft
g	Generating Aircraft
r	Vortex Radial Distance
o	Initial
f	Final

### ABBREVIATIONS

LDV	Laser Doppler Velocimeter
ATC	Air Traffic Control
AGL	Above Ground Level
MSL	Mean Sea Level
IFR	Instrument Flight Rules
NM	Nautical Miles
PAPI	Precision Approach Path Indicator

## EXECUTIVE SUMMARY

This report is a part of an effort by the Federal Aviation Administration (FAA) to assess the need for rotorcraft separation standards based on wake vortex hazards to following aircraft. The specification of safe aircraft separation standards for operations behind rotorcraft requires an understanding of the strength, movement, and decay of rotorcraft wake vortices. This report presents the results of helicopter flight tests and wake vortex measurements which were designed to provide the data necessary for the assessment of hazards to following aircraft. The tests described in this report were conducted using four small probe airplanes and a laser doppler velocimeter (LDV) for wake vortex measurements during forward-flight helicopter operations. Four helicopters, having weights ranging from 7,600 to 70,000 pounds, were used in the tests as the wake vortex generating aircraft. Wake vortex strength, transport, and decay characteristics were determined for the test helicopters. Safe separation distances and wake vortex hazard durations were assessed for several helicopter speeds. The test results indicate that the classification for helicopters should be two weight classes with a break at 25,000 pounds. In the absence of encounter measurements for the case of hover flight, it is recommended that small airplanes, at the same altitude and downwind of a hovering helicopter, maintain at least 500 feet of separation.



## 1. INTRODUCTION.

Safe fixed wing aircraft operation behind rotorcraft depends upon an understanding of the strength, movement, and duration of rotorcraft wakes. The mechanisms involved in wake vortex generation and rollup are significantly different and much more complex for rotorcraft than for fixed-wing aircraft. Thus, the wake vortex behavior observed for fixed-wing aircraft is not necessarily the same as for rotorcraft.

Vortex strength for fixed- and rotary-wing aircraft is strongly dependent on airspeed. Prior studies have shown that vortex strength for fixed-wing aircraft varies inversely with airspeed. Rotorcraft can fly at extremely low airspeeds and can hover at an airspeed of zero. Therefore, if this inverse speed dependency is valid for rotorcraft, the strength of the wake vortex generated by a given rotorcraft can conceivably reach much higher values than that of a given fixed-wing aircraft of the same weight. Airspeed may therefore have a significant effect on separation criteria for rotorcraft.

Rotorcraft appear in a number of significantly different configurations, including single rotor, tandem rotor, tilt rotor, and the number of blades per rotor. The configuration of the rotorcraft may influence its wake vortex characteristics.

The flight test program described in this report attempted to provide an understanding of these issues and how they may apply to rotorcraft operations in terminal areas.

### 1.1 OBJECTIVE.

Currently there are no classification standards or separation standards pertaining specifically to rotorcraft on Instrument Flight Rule (IFR) approaches. Therefore, the objective of the test program reported here was to investigate the characteristics of strength, persistence, movement, and mode of decay of the wake vortices generated by rotorcraft. A second objective of the test program was to provide data to assess the need for Rotorcraft Classification Standards and Separation Standards.

This investigation was accomplished through use of laser doppler velocimeter (LDV) strength and persistence measurements of the rotorcraft generated wake vortex and the full-scale penetration of the wake vortex through the use of a probe aircraft to determine the actual hazard location.

### 1.2 PRIOR TESTS.

Before the Rotorcraft Wake/Downwash Program was initiated in 1984, three studies (references 1, 2, and 3) attempted to characterize the wake vortices generated by helicopters. The study of reference 1 used the tower flyby method to study the wake vortices generated by an S-58 helicopter (figure 1-1). The velocity measurements were rather crude (made with cup anemometers), but nevertheless, the measurements showed that the advancing blade generated

higher vortex tangential velocities than the retreating blade (figure 1-2). The study of reference 2 included some H-47 measurements made with the vortex sensing systems installed at the Toronto International Airport to study the wake vortices generated on departure. Reference 3 describes the results of H04S-3 helicopter (figure 1-3) wake vortex probing using a fixed-wing aircraft.

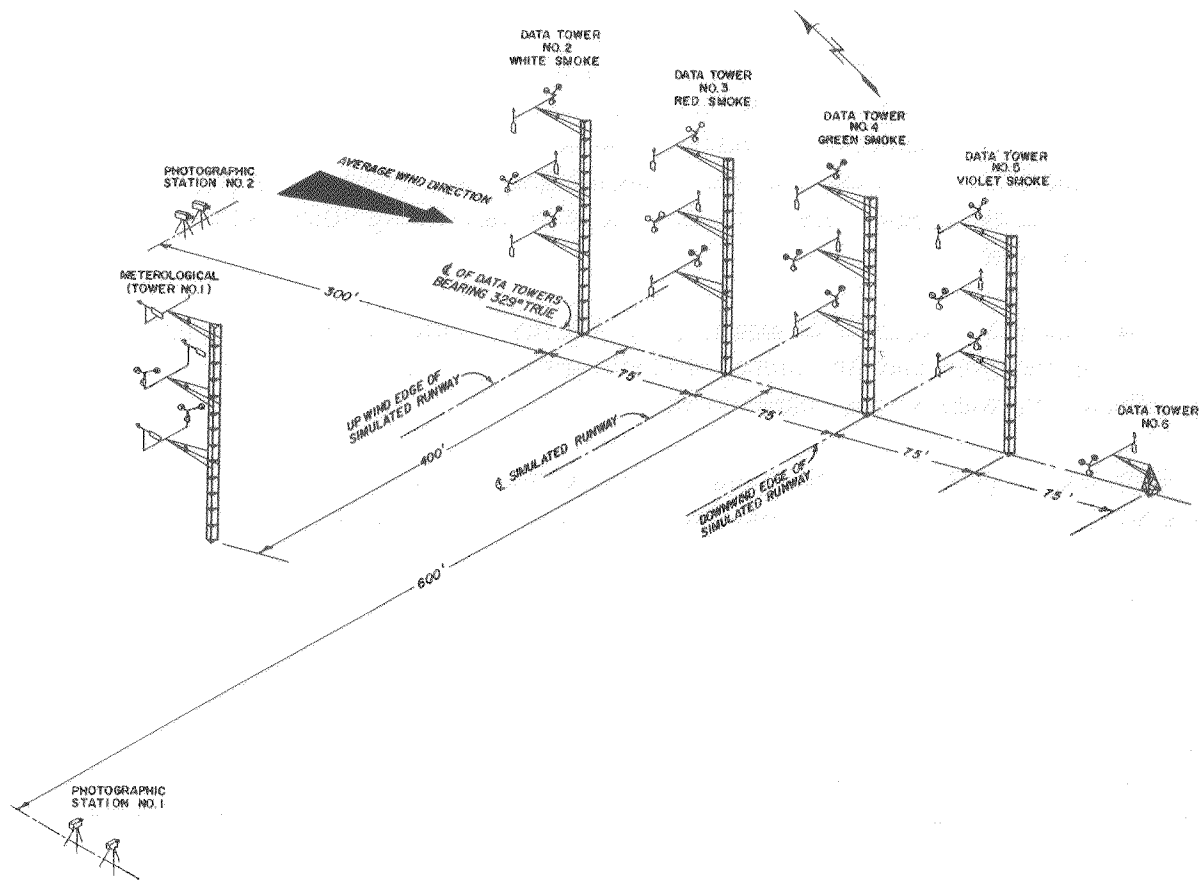
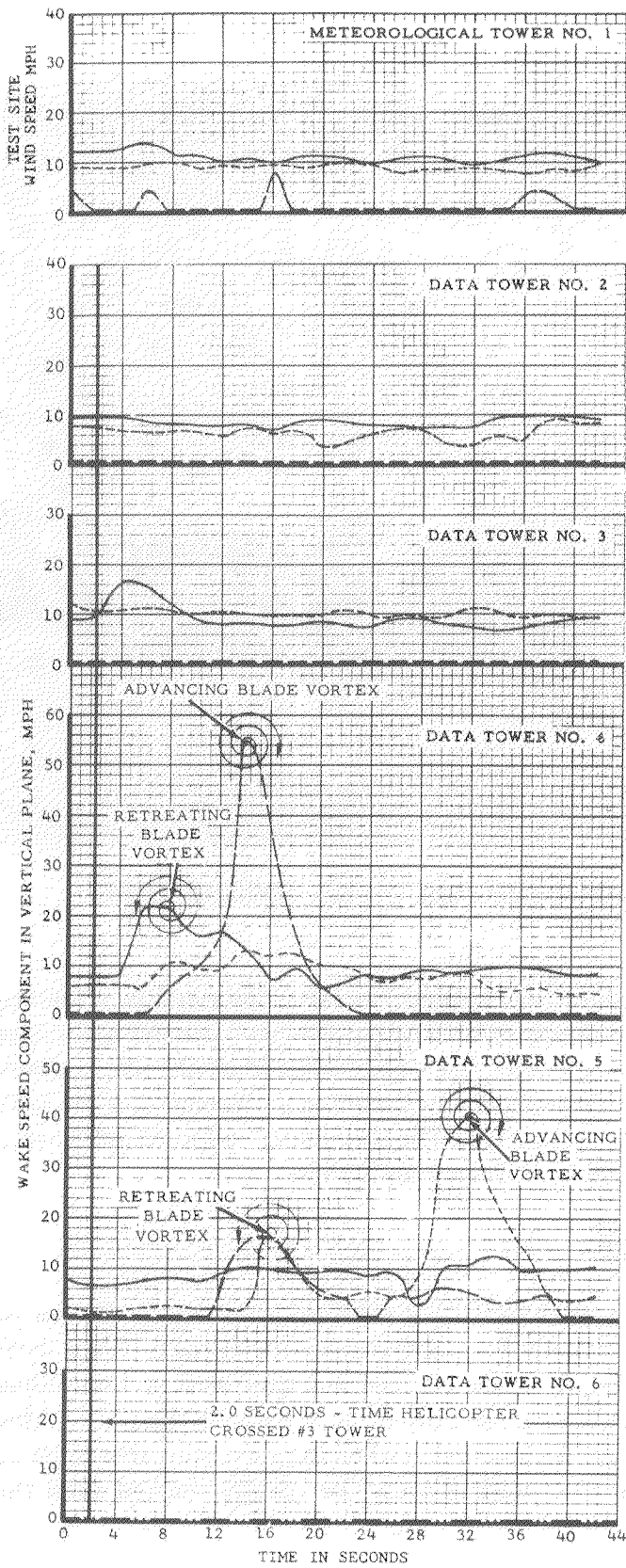


FIGURE 1-1. S-58 HELICOPTER WAKE FLIGHT TEST SITE (TOWER FLYBY TECHNIQUE)



RUN NUMBER 4

TYPE OF RUN CROSSWIND

DATE 1-3-63

TIME 1505

HELICOPTER SIKORSKY UH-34D

GROSS WEIGHT 12,125 LBS. APPROX.

ALTITUDE 80.3' TO ROTOR HUB

I.A.S. 45 KNOTS

GROUND SPEED 39.1 KNOTS

AVERAGE WIND SPEED  
AT 20' HEIGHT 9 M.P.H.

AVERAGE WIND  
DIRECTION 309° TRUE

LINE OF TOWERS 329° TRUE,  
TOWER SPACING 75'

LOCATION OF FLIGHT PATH  
75° TO THE LINE OF TOWERS,  
CROSSING TOWER #3

LEGEND

———— 50 FT. LEVEL

----- 35 FT. LEVEL

----- 20 FT. LEVEL

----- 6 FT. LEVEL

NOTE:

INSTRUMENTATION MEASURED THAT COMPONENT OF WAKE SPEED IN A VERTICAL PLANE ALIGNED PERPENDICULAR TO THE LINE OF TOWERS, PLUS THAT COMPONENT OF METEOROLOGICAL WIND IN THE SAME PLANE

FIGURE 1-2. S-58 HELICOPTER WAKE VORTEX TIME HISTORY, CROSSWIND RUN NUMBER FOUR



FIGURE 1-3. HO4S-3 HELICOPTER USED FOR WAKE VORTEX TESTS

The early work of the Rotorcraft Wake/Downwash Program has been described in an interim report (reference 4) which includes some additional analysis of the Toronto data and preliminary LDV measurements of rotorcraft wake vortex velocities that were studied in Huntsville, Alabama, in 1984. The main goal of the Huntsville testing was to check out the performance of the LDV, which was last used for measuring wake vortices in 1980. The data turned out to be quite useful, especially since no additional LDV data could be collected until 1986.

### 1.3 SUMMARY OF HUNTSVILLE TESTS.

The Huntsville tests showed that, in general, satisfactory LDV measurements require that aerosol particles be injected into the rotorcraft wake by some flow visualization mechanism. Some useful data can be obtained without flow visualization when vortices are generated at low altitude (around 300 feet), but these low altitude vortices can be difficult to track with the LDV. Much better data on vortex characteristics (i.e., decay) were obtained when the generating rotorcraft was at higher altitude (600 feet). In this case, the vortices could be readily tracked until they disintegrated.

The Huntsville tests included vortex velocity measurements of two types of helicopter, the 8,000 pound UH-1H (figure 1-4) and the 32,000 pound CH-54 (figure 1-5). At first, flow visualization for the UH-1H made use of canister smoke grenades taped to the ends of ten-foot hand-held steel

conduits. Later tests used a different UH-1H that was equipped with a battlefield smoke generator. Since the CH-54 had no flow visualization, an unsuccessful attempt was made to provide aerosols for the LDV by flying the CH-54 through the smokey wake of the UH-1H with the battlefield smoke generator. Data collected via this procedure was inconsistent in quality and was in general suspect since the residual wake of the UH-1H could have influenced the wake generated by the CH-54.

The Huntsville tests showed that UH-1H vortices remained hazardous (using the definition of a hazard cited later in this report) to small aircraft for up to 80 seconds and gave indications that the hazard from CH-54 vortices lasted longer than 100 seconds. The measured vortex strength (defined as the vortex circulation) was roughly comparable to that predicted by the classical circulation equation for fixed-wing aircraft, if one substitutes the rotorcraft rotor diameter for the aircraft wingspan. Although the classical equation gives a vortex strength that is proportional to the weight of the generating aircraft, the Huntsville data suggest an equation that relates vortex strength to the square root of the rotorcraft weight. The current study indicates that this dependence is incorrect and that the Huntsville results may reflect the inconsistent quality of the CH-54 data.

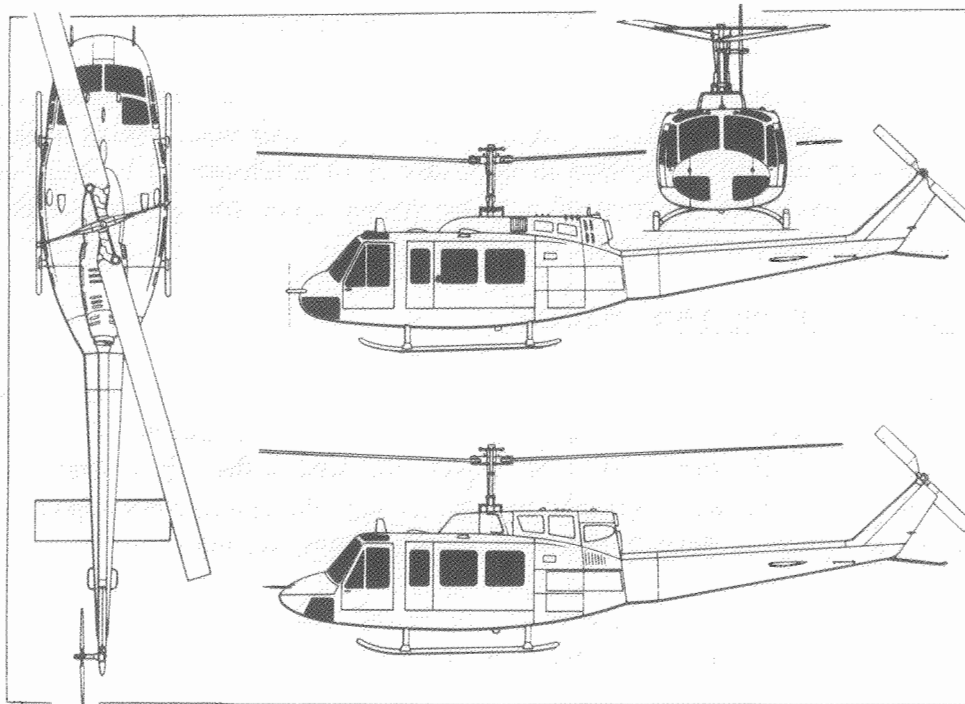


FIGURE 1-4. BELL UN-1H HELICOPTER SCHEMATIC (REFERENCE 12)



Photo courtesy of 177 FW, NJANG

FIGURE 1-5. SIKORSKY CH-54 HELICOPTER

Section 4 of reference 2 fitted analytical models to the measured undecayed wake vortex profile of rotorcraft. These models were then combined with a particular wake vortex hazard model for fixed-wing following aircraft (described in appendix A of reference 2) to yield an analytical prediction for the maximum severity of a wake vortex upset for a given rotorcraft vortex generator and fixed-wing probe aircraft.

#### 1.4 DESCRIPTION OF PRESENT STUDY.

The goal of the flight test program was to characterize the strength, persistence, movement, and decay of helicopter wake vortices out-of-ground effect under conditions of low atmospheric turbulence. These tests, described in section 2, were initiated in the fall of 1985 and concluded in the fall of 1987. The tests were designed to scientifically characterize helicopter wake vortices and to address the following deficiencies with previous rotorcraft tests:

- a. A lack of flow visualization for the heavy helicopters.
- b. Incomplete characterization of meteorological testing conditions.
- c. Uncertainties in the measurement of low helicopter airspeeds.
- d. A lack of vortex probing by test aircraft.

Five helicopter types were tested using LDV measurements and probes with small fixed-wing aircraft: The Bell UH-1H, Sikorsky S-76A, Sikorsky CH-53E, Boeing Vertol CH-47D, and Sikorsky UH-60A (figures 1-4, 1-6, 1-7, 1-8, and 1-9 respectively).

The outline of the report will be as follows:

The remainder of this chapter will present a description of the analytical background of wake vortex strength and an analytical expression for the vortex hazard. Chapter 2 will present a description of test vehicles and measurements. Chapter 3 will describe the LDV measurements, and the LDV results will be presented in chapter 4. Full-scale probe testing, which will be described in chapter 5, gave a direct indication of required safe separation for the rotorcraft tested. In addition, probe tests were intended to help "calibrate" the LDV measurements and hazard models for translation into separation requirements. Chapter 6 will discuss the consistency of the LDV and probe data and the limitations of the test methods. Finally, the conclusions and recommendations of the report are presented in chapters 7 and 8.

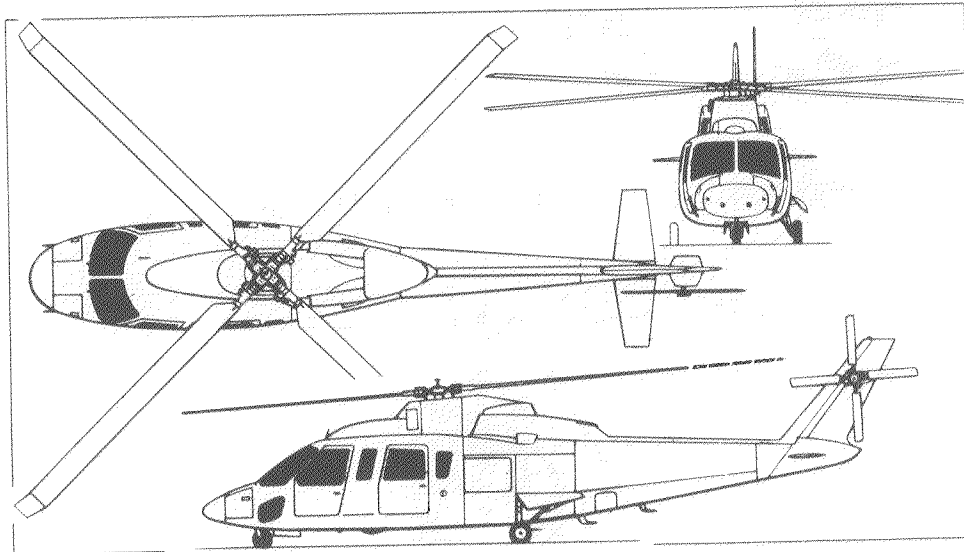


FIGURE 1-6. SIKORSKY S-76A HELICOPTER SCHEMATIC (REFERENCE 12)

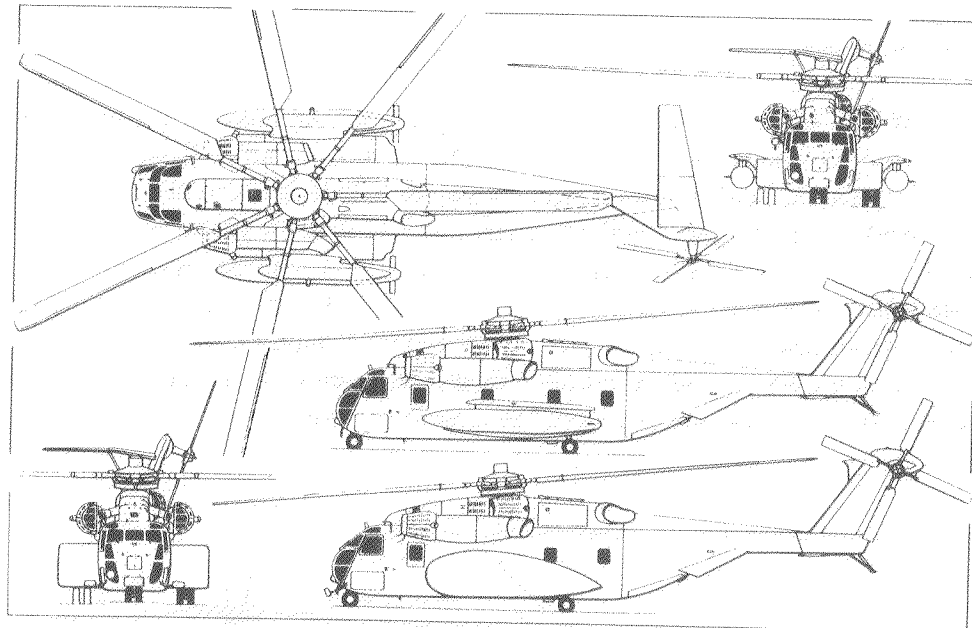


FIGURE 1-7. SIKORSKY CH-53E HELICOPTER SCHEMATIC (REFERENCE 12)

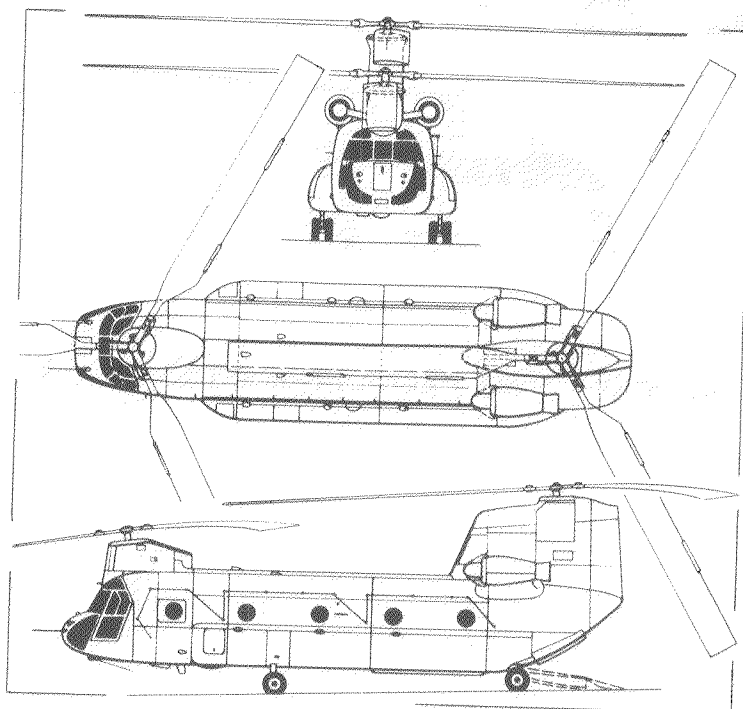


FIGURE 1-8. BOEING VERTOL CH-47D HELICOPTER SCHEMATIC (REFERENCE 12)

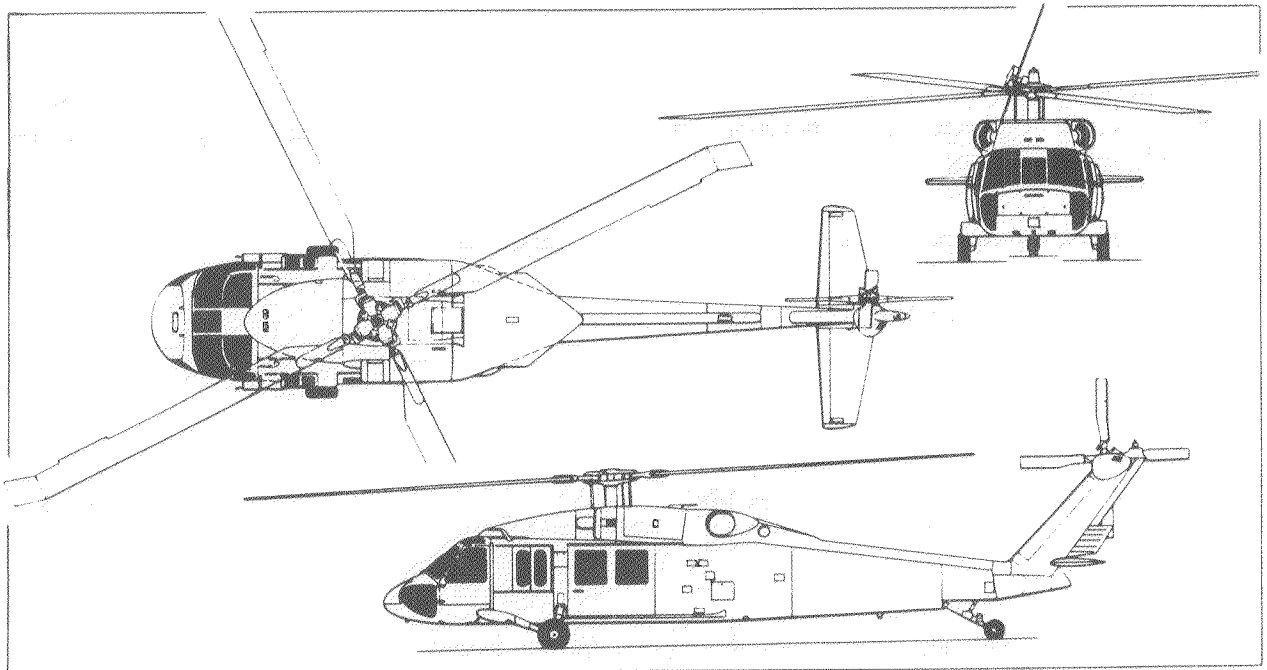


FIGURE 1-9. SIKORSKY UH-60A HELICOPTER SCHEMATIC (REFERENCE 12)

### 1.5 ANALYTICAL BACKGROUND.

The classical equation for total circulation of trailing wake vortices from generating airplanes predicts the following dependence of vortex circulation upon weight  $W$ , airspeed  $V_g$ , wingspan  $b_g$ , and air density  $\rho$  as

$$\Gamma_{\infty} = KW/\rho V_g b_g \quad (1-1)$$

For an airplane,  $\Gamma_{\infty}$  is the bound circulation around the midpoint of the wing. The constant  $K$  is determined by the shape of the lift distribution and takes values of unity for uniform lift and  $4/\pi$  for elliptical loading.

The spacing  $b'$  between the two vortices is given by

$$b' = b/K \quad (1-2)$$

The validity of equation 1-1 for helicopters has been questioned for two reasons:

- a. Rotorcraft wake vortices are formed in a much more complex fashion than those generated by fixed-wing aircraft.

- b. A helicopter can fly at zero forward airspeed (hover). Thus, the vortex strength predicted by equation 1-1 becomes infinite in hover and cannot be accurate.

Despite these limitations, equations 1-1 and 1-2 are useful first approximations for the wake vortex properties of helicopters operating above the speed of translational lift, generally from about 35 knots to  $V_{max}$ .

The classical equation for circulation at any radius is given by

$$\Gamma(r) = 2 \pi r v(r) \quad (1-3)$$

The average circulation is given by

$$\Gamma'(r) = \frac{1}{r} \int_{-r}^r \pi r' v(r') dr' \quad (1-4)$$

In reference 5 a simplified model was developed for the circulation and velocity profiles of a wake vortex.

The circulation at any radius is given by

$$\Gamma(r) = \Gamma_{\infty} / [1 + (r_c/r)^2] \quad (1-5)$$

where  $r$  is the vortex radius. Using this equation, the circulation is half  $\Gamma_{\infty}$  at the core radius  $r_c$ , which is the radius of highest tangential velocity.

The vortex tangential velocity is given by

$$v(r) = \frac{\Gamma_{\infty}}{2\pi r} \left\{ \frac{1}{1 + \left(\frac{r_c}{r}\right)^2} \right\} \quad (1-6)$$

Although equations 1-5 and 1-6 have no particular theoretical justification, they have been found by some to give reasonable representations of vortex measurements. Further, these equations have the virtue of straightforward mathematical manipulation.

As an example, the average circulation  $\Gamma'$  out to radius  $r$  can be expressed as

$$\Gamma'(r) = \Gamma_{\infty} [1 - (r_c/r) \arctan(r/r_c)] = \Gamma_{\infty} [Fn(r/r_c)] \quad (1-7)$$

## 1.6 HAZARD MODEL.

In accordance with the hazard model of reference 2, the average circulation at radius  $r = b_e/2$  is closely related to the maximum vortex-induced rolling moment on an encountering aircraft with a wingspan of  $b_e$ . In this model, the ratio  $f$  of the maximum vortex-induced rolling moment to the roll control capability of the encountering aircraft is given by

$$f = 3\Gamma'(b_e/2)/(\pi b_e V_e \dot{\phi}) \quad (1-8)$$

where  $\dot{\phi}$  is the maximum nondimensional roll rate of the encountering aircraft. This roll rate is typically 0.06 for commercial aircraft and 0.08 for general aviation airplanes. If  $f$  is greater than 1.00, the encountering aircraft is assumed to be out of control. Several studies (reference 4) have indicated that  $f > 0.50$  is hazardous, particularly for encounters near the ground.

Combining equations 1-1, 1-7, and 1-8 yields the following "calculated expression" for the hazard generated by an undecayed fixed-wing wake vortex:

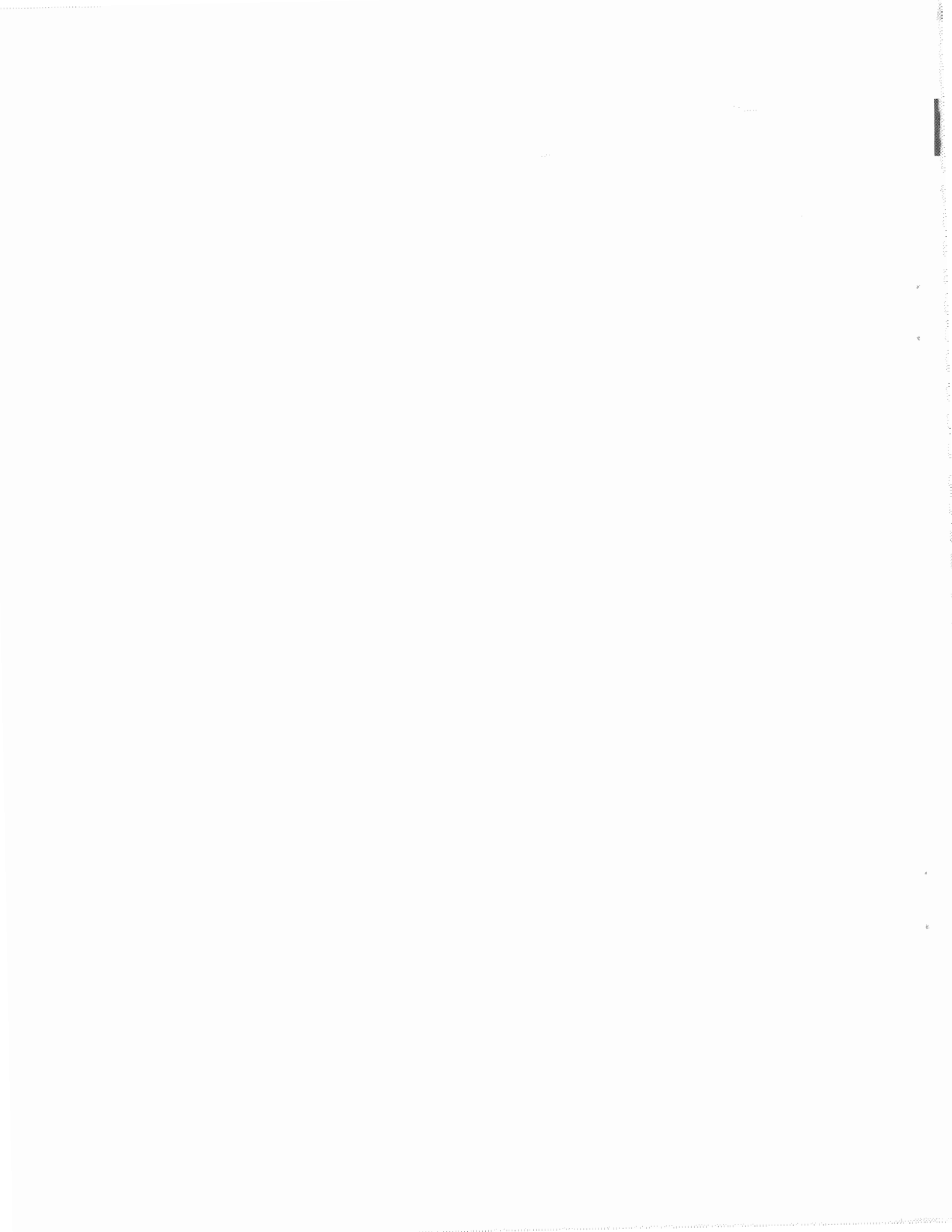
$$f = 3KW F_n(b_e/2r_c)/(\pi \rho \dot{\phi} b_e b_g V_e V_g) \quad (1-9)$$

As can be seen, according to this model, the hazard varies inversely with the product of the airspeeds of the generating and encountering aircraft.

By rearranging equation 1-8 and inserting typical values for a landing jet transport aircraft of  $V = 130$  knots and  $\dot{\phi} = 0.07$ , a first estimate of the assumed average strength hazard threshold for a typical landing situation can be expressed as

$$\Gamma'_T(b_e/2) \approx 5fb_e \quad (\text{m}^2/\text{s}) \quad (1-10)$$

This equation was used to estimate the hazard, times, and distances from the LDV measurements during the tests.



## 2. TEST DESCRIPTION.

### 2.1 AIRCRAFT TYPES.

The tests were performed at the FAA Technical Center, the home base of the FAA S-76A helicopter which was the primary test rotorcraft. Four other helicopters were tested, a UH-1H provided by the Pennsylvania Army National Guard; a CH-53E provided by the U.S. Marines, Quantico, VA; a CH-47D provided by the US Army, Ft. Eustis, VA; and a UH-60A provided by the U S. Army, Ft. Dix, NJ.

Table 2-1 presents the basic characteristics of these aircraft.

TABLE 2-1. CHARACTERISTICS OF WAKE VORTEX GENERATING HELICOPTERS

<u>PARAMETER</u>	<u>UH-1H</u>	<u>S-76A</u>	<u>UH-60A</u>	<u>CH-47D</u>	<u>CH-53E</u>
Max. Takeoff Weight (lbs)	7,650	10,300	16,260	50,000	69,750
Rotors	1	1	1	2	1
Blades	2	4	4	3/3	7
Advancing Blade	Stbd	Stbd	Stbd	Stbd/Port	Stbd
Rotor Diameter (ft)	48	44	53'8"	60	79
Max. Level Flight Speed (kts)	100	145	176	155	170

### 2.2 FLOW VISUALIZATION.

For a probe aircraft to find a wake vortex, the vortex must be marked using smoke or some other visualization method. Furthermore, Huntsville tests showed that satisfactory LDV measurements require that extra aerosols be injected into the wake of the generating aircraft. A major technical issue of the test program, therefore, was to install smoke generating equipment on all test rotorcraft. The following sections describe the flow visualization systems used in the test program.

One of the basic procedures for generating smoke behind an aircraft is to inject an atomized smoke oil into an area of intense heat. The oil responds to this heat by vaporizing and then condensing into a very dense, opaque cloud which is neutrally buoyant and thus moves with any ambient winds into which it is injected. Careful installation and skilled operation of a properly designed flow visualization system are essential requirements for the safe generation and operational effectiveness of smoke.

A typical installation used by the UH-1H is illustrated in figure 2-1. Note the ring shaped oil injection manifold aft of the engine exhaust. The system produces an intense smoke, as illustrated in figure 2-2.



FIGURE 2-1. BELL UH-1H SMOKE GENERATOR



FIGURE 2-2. BELL UH-1H SMOKE TRAIL

### 2.2.1 CH-53E.

The CH-53E, a three-engine helicopter (figure 1-7), has two prominent engine exhaust ducts, one each located on either side of the fuselage just behind the main rotor area. Smoke generation for the CH-53E is fairly straightforward and similar to the UH-1H system; atomized smoke oil is pumped into the engine exhaust directly aft of the exhaust tube where it vaporizes (figure 2-3). Corvus smoke oil was carried aloft in two 55-gallon drums contained in the cargo area of the helicopter, along with the necessary plumbing and pumping apparatus. By virtue of the tremendous lifting capacity of the CH-53E, missions could be launched with a full supply of smoke oil, which would last for roughly one hour of continuous operation. This smoke generating arrangement was convenient, reliable, and safe, as it provided long durations of smoke without the need for an auxiliary heat source.

It was observed that the inclined tail rotor of the CH-53E drew a substantial portion of the smoke upwards, away from the main body of the wake. This smoke suggests the presence of a third vortex that was above the primary pair generated by the rotorcraft.



FIGURE 2-3. CH-53E WAKE VORTEX FLOW VISUALIZATION SYSTEM

### 2.2.2 CH-47D.

The CH-47D used the same flow visualization system as the CH-53E. Corvus oil was injected into the exhaust of the two engines mounted at the rear of the aircraft, as illustrated in figure 2-4. It was observed that most of the smoke was drawn into the starboard vortex, especially at high speeds, as seen in figure 2-5. This phenomenon could be due to the more complex flow field of the tandem rotor.

### 2.2.3 UH-60A.

The UH-60A used the same flow visualization system as the CH-53E. Corvus oil was injected into the exhaust of the two engines mounted on the top of the aircraft, just under the rotor, as illustrated in figure 2-6. A typical smoke trail for the aircraft is illustrated in figure 2-7. Note the evidence of individual blade vortices in the near field.

### 2.2.4 S-76A.

The engine exhaust design of the S-76A (centerline, atop the fuselage) makes smoke generation on this helicopter more complicated as direct oil injection cannot be utilized. Smoke generators, manufactured by the Frank Sanders Aircraft Corporation, were mounted on each end of a specially constructed boom attached to the airframe, which placed each generator roughly four feet outboard of the fuselage. The Sanders smoke generators consist of a gasoline-powered heat source, an oil atomizer, and injection system which are housed in an aluminum cylinder roughly one foot in diameter and five feet long. The system, illustrated in figure 2-8, produces a very dense white smoke, as seen in figure 2-9.

These generators were initially designed for installation and use on fixed-wing aircraft and rely on ram air for proper operation. For operation at the low forward speeds of rotorcraft, the generators were modified to include an auxiliary air supply system. This auxiliary air system consisted of two high-capacity compressed air tanks mounted in the cabin of the helicopter, and pressure regulation and plumbing to the air inlet tube of each smoke generator. As modified, the smoke generators were somewhat temperamental, particularly at airspeeds below 60 knots, and were very sensitive to ignition, oil injection timing, and auxiliary air pressure. Below 40 knots airspeed, the smoke generators were placarded inoperative and flow visualization was accomplished by arrays of red smoke grenades mounted outboard of the generator units. Both systems (generators and grenades) are pictured in operation in figures 2-8 and 2-9.

The addition of the smoke generation system to the S-76A placed the aircraft in the experimental category until they were removed.



FIGURE 2-4. CH-47D WAKE VORTEX FLOW VISUALIZATION SYSTEM



FIGURE 2-5. CH-47D SMOKE TRAIL



FIGURE 2-6. UH-60A WAKE VORTEX FLOW VISUALIZATION SYSTEM



FIGURE 2-7. UH-60A SMOKE TRAIL



FIGURE 2-8. S-76A WAKE VORTEX FLOW VISUALIZATION SYSTEM



FIGURE 2-9. S-76A WAKE VORTEX FLOW

### 2.3 TEST SCHEDULE.

The tests were carried out in December of 1985; June, August, and October of 1986; and September, October, and November of 1987. On many days, two or three test sequences were carried out, with a break in between to replenish the flow visualization system. Table 2-2 summarizes the LDV testing for each helicopter type.

TABLE 2-2. LDV RUNS

<u>HELICOPTER</u>	<u>DATE(S)</u>	<u>LDV RUNS</u>
S-76A	June, Oct. 1986	111
CH-53E	Aug., Oct. 1986	106
CH-47D	Sept., Oct. 1987	89
UH-60A	November 1987	37

### 2.4 TEST PROCEDURES.

The LDV test procedure was designed to measure rotorcraft wake vortex tangential velocities in low-turbulence air. LDV tests, therefore, were conducted immediately after dawn, before solar heating of the ground produced thermal turbulence at the typical test altitude of 600-feet AGL. Probe tests were conducted at a typical altitude of 5500-feet MSL where surface thermal effects did not occur until later in the day, and safety of flight was enhanced. These test requirements dictated that testing on a given day with suitable weather would begin with an LDV test sortie. Following the completion of this test sequence, the smoke generator and aircraft fuel would be replenished and a probe test would be launched.

### 3. LDV MEASUREMENTS.

The LDV was first sent to the FAA Technical Center in December 1984, but the S-76A flow visualization system was not ready for testing. When the LDV was being returned to the FAA Technical Center via highway transportation, its housing was destroyed in a mishap. The LDV was rebuilt into a new housing based on a standard 40-foot shipping container (see figure 3-1) and moved to the FAA Technical Center in May of 1986. Accordingly, only vortex flow visualization and probe flight tests were conducted at the FAA Technical Center in the fall of 1985.

Figure 3-2 illustrates the location of the LDV and other equipment at the FAA Technical Center. Figure 3-3 pictures the LDV and the adjacent trailer that housed the recording equipment for the meteorological sensors mounted on the 65-foot telephone pole in the background.

#### 3.1 METEOROLOGICAL MEASUREMENTS.

Three ground based meteorological measurement systems were utilized to characterize the atmosphere during the wake vortex measurements<sup>1</sup>. The first meteorological system was mounted in a kytoon, a kite type balloon, which can be unreeled to altitudes of up to 1000-foot AGL. This system reports wind speed and direction, temperature, and dewpoint as a function of altitude about every 30 seconds. Unfortunately, this system was damaged by high winds during the first flight test period and generated no useful data.



FIGURE 3-1. CH-53E DATA FLIGHT OVER LDV HOUSING

---

<sup>1</sup>None, however, gave usable data at the 300- to 600-foot (AGL) altitude of vortex generation.

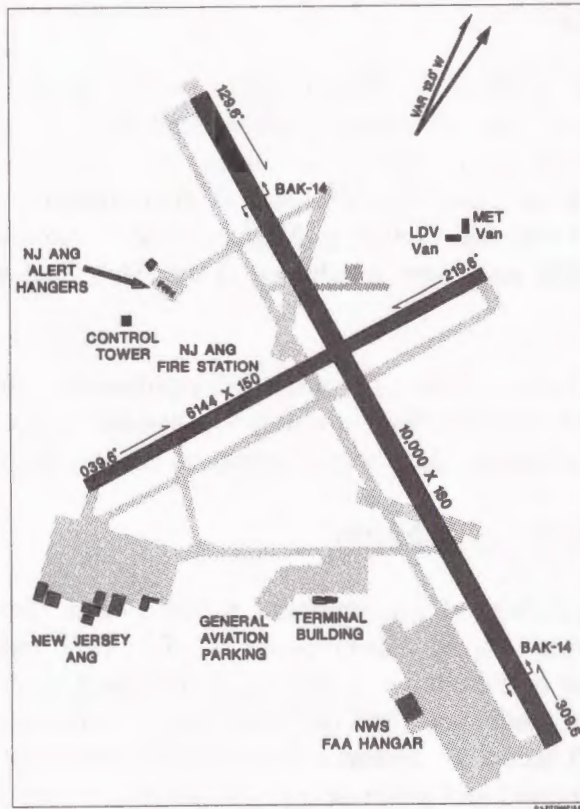


FIGURE 3-2. LDV INSTALLATION AT FAA TECHNICAL CENTER



FIGURE 3-3. S-76A DATA FLIGHT OVER EQUIPMENT VAN

The second system measured the wind speed and direction and temperature at four levels, 8-, 24-, 45- and 63-feet AGL with sensors mounted on the telephone pole shown in figure 3-4. The temperature measurement system consisted of one temperature sensor and three differential temperature sensors. The system was designed to obtain accurate differential temperature measurements necessary to calculate the Richardson number, a measure of turbulence that was recommended in reference 6 for vortex persistence correlation. The Richardson number characterizes whether or not atmospheric wind shear and temperature gradient will produce turbulence. The pole-mounted meteorological system was not operational during the October 1986 tests.

Only meteorological data from the lowest sensor level (8 feet) and the highest sensor level (63 feet) were directly used in the analysis. Using the most widely separated sensors gives the greatest accuracy for measuring temperature inversions and wind shears. Hence, the intermediate-level met data values were used only as a guide to the overall health of the met data collection system during that day's test. The wind data collected at the highest sensor level showed generally poor agreement with wind data reported at the helicopter altitude (600 feet), indicating the presence of a considerable wind shear near the ground during many of the flight tests.



FIGURE 3-4. METEOROLOGICAL MEASUREMENT SYSTEM AT TEST SITE

The third meteorological system that was utilized was the weather balloon (radiosonde) released daily by the National Weather Service Station at the Atlantic City International Airport. This balloon was released every morning at 0800 local and gave wind and temperature measurements. Unfortunately, the vertical resolution of the radiosonde data was too coarse to characterize the atmosphere at the level of the flight tests. As a result of the aforementioned shortcoming, additional UH-1H flights were conducted at the start of the LDV testing to gather data on ambient atmospheric conditions from the surface to the flight test altitude.

### 3.2 AIRCRAFT TRACKING.

During the flight tests, the Technical Center operated one of two aircraft tracking systems; one system utilized a laser tracker aimed at a retroreflector on the aircraft and the other used a conventional (NIKE) tracking radar. Both tracking systems were located at least a half mile from the LDV and provided tracking data in the form of the cartesian location of the helicopter as a function of time. The coordinate system normally originated at a runway threshold with one of the axes aligned with the runway centerline. The cartesian helicopter coordinates were typically printed each 0.1 second. This method proved to be a very reliable way to obtain test helicopter ground speeds.

### 3.3 PHOTOGRAPHY.

For most runs, a 35-mm camera was mounted on a tripod next to the LDV van with the camera lens pointed straight up. The camera had an automated sequencer programmed to take a picture at fixed intervals. For each run, the goal was to have two or three pictures that included the helicopter and perhaps seven or eight pictures of the wake behind it. Using the displacement of the helicopter, from frame to frame, the helicopter ground speed could be accurately estimated. From the displacement of a particular puff of smoke from frame to frame, the headwind and crosswind at the vortex altitude could be accurately estimated.

The camera was started just before the helicopter reached the van. For slow airspeeds of 60 knots or less, the frame rate was typically one frame per second. For faster runs (above 60 knots), the frame rate was increased to 2 frames per second to ensure that at least two frames included the helicopter. A log of the frame rate for each run was maintained by the camera operator.

The camera put the day number, hour, and minute on each photograph, so it was possible to assign a sequence of pictures to a given run. For most days the camera clock was synchronized to the LDV computer clock, but for a few days the two times were off by a few minutes and these discrepancies were noted on the day's log sheet.

### 3.4 AIRSPEED/GROUND SPEED.

For airspeeds above 40 knots, the airspeed indicator aboard a helicopter is accurate and reliable. Below this speed, however, the difference between the static and dynamic pressure on the aircraft's pitot static system is small and is greatly influenced by the rotor flowfield. Thus, this difference was difficult to measure reliably. If the winds aloft and the ground speed are recorded, however, one can compute the helicopter airspeed.

For most runs the aircraft position and ground speed were obtained from laser or radar tracking. For the higher speed runs, the helicopter reported airspeed was considered accurate (no correction for indicated airspeed versus actual airspeed). By comparing this airspeed and the resulting ground track of the aircraft, estimates of the wind aloft on the test day were made. The results of this method were compared to the photographic method described in section 3.3 for confirmation.

Reliable estimates of the wind aloft were needed for two purposes. With this data, reasonable estimates of airspeed for runs flown at less than 40 knots were made and modifications made to yield corrected values of the wake vortex duration. As most runs were flown over the LDV under the influence of a headwind, the wind aloft blew fresher parts of the wake over the LDV. In other words, the headwind kept active parts of the wake over the LDV for a longer time, thus giving an artificially long result for the wake vortex duration. Once the wind aloft was known, its influence upon wake duration was calculated and subtracted from the duration measured, thus yielding an accurate measurement of vortex lifetime.

### 3.5 LDV SYSTEM.

The LDV (reference 5) scans a plane perpendicular to the aircraft path, as illustrated in figure 3-5. A typical scan pattern consists of three to five sweeps in elevation angle at stepped, fixed ranges and is called a scan "frame." Though the elevation angle scanner can cover the full range of 0 to 180 degrees from horizon to horizon, it can only scan 60 degrees at a given time. A system operator ensures that the desired aircraft wake remains in the LDV field of view by tracking that wake with adjustments in scan parameters. Useful LDV ranges are about 50 to 300 meters. Since range resolution decreases with range as the square of the range, at large ranges all range resolution is lost. At small ranges the resolution is so fine that the vortex core cannot be measured unless the range passes very close to the core. The ranges selected for the scan pattern, therefore, are designed to fit the range resolution. For vortices generated at 600 feet (about 200 meters), initial ranges of 230, 200, 170, and 140 meters might be selected. As the vortices descend, the ranges 120, 100, 90, and 80 meters might be added and the highest ranges dropped. For vortices generated at 300 feet (about 100 meters), starting ranges might be 110, 100, 90, and 80 meters, with 70, 60, and 50 meters added as the wake descends. As the wake descends, the angular separation between the individual vortices becomes greater and can exceed the 60 degree maximum LDV scan angle.

The LDV measures the absolute value of the line-of-sight component of the wake velocity field (and any ambient wind associated with it). LDV data consisted of the velocity "spectrum," averaged over the range response function and over the time of a data point (4 milliseconds). The resulting spectrum is complex and is processed to obtain the highest measured velocity above the noise level, which gives a reasonable estimate of the vortex tangential velocity. The vortex velocities for each frame are displayed in real time so that the tracking parameters can be adjusted to keep the vortices centered in the scan area, as discussed in the previous paragraph.

The LDV has an assumed error of three velocity "bins" (velocity bins are internal software processing devices in the LDV system). This translates into a velocity overread of approximately 1.65 meters per second, as discussed in reference 2.

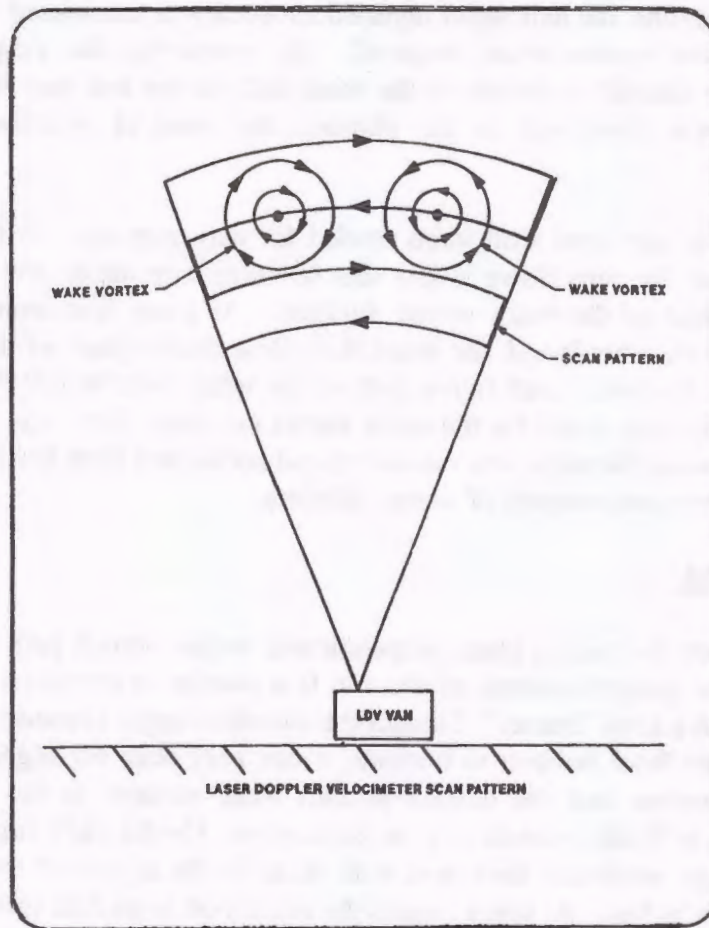


FIGURE 3-5. LDV SCAN METHODOLOGY

### 3.6 DATA COLLECTION.

The best LDV data are obtained when the wake vortices are located directly above the LDV scanner, the cylindrical object mounted on the top of the right hand container illustrated in figure 3-6. For angles far away from vertical, the measurements are affected by the ambient wind and the mutual interference of the two vortices. Therefore, the LDV scan plane is normally oriented perpendicular to the ambient wind direction to minimize wind effects. The standard helicopter flight path passed directly over the LDV, most often at fixed airspeed and altitude. An altitude of 600-feet AGL was preferred for ease in vortex tracking, as the vortices were observed to descend as much as 300 feet. The flight path was usually oriented directly into the wind so that the wake would not drift away from the LDV. Since the ambient winds, which were in the 5- to 10-knot range for most of the tests, did vary in direction, the rotorcraft heading had to be adjusted occasionally in azimuth to prevent excessive lateral drift of the wake. For those runs when the helicopter airspeed was below 40 knots, the helicopter flew with the wind to prevent excessively long approach times to the LDV. For all flyovers, the smoke generators were operated long enough to assure that the wake above the LDV contained smoke until the wake decayed.



FIGURE 3-6. CH-53E DATA FLIGHT OVER LDV VAN

A series of level runs at constant altitude were flown to obtain baseline information on wake behavior. In addition to these level runs, some runs were made with the rotorcraft descending or climbing. Accurate glideslope descents were made with the assistance of a Precision Approach Path Indicator (PAPI). Sites were laid out along three headings for PAPI locations which gave glideslope angles of 3, 5, 7, and 14.7 degrees at altitudes of 300 or 600 feet over the LDV. Climbing runs were accomplished by maintaining a given airspeed and initiating a specified rate of climb at a position slightly upwind of the LDV.

Some runs were made in ground effect in an attempt to assess the effect of the ground on vortex decay. The helicopter flew at a 300-foot lateral offset with respect to the LDV (marked by a parked vehicle location) so that the vortices would be at a large enough range for tracking. Both 100- and 300-foot altitudes were flown.

The philosophy used to plan the flight tests considered a number of factors. The basic goal was to fill out a matrix of the desired aircraft performance parameters, primarily airspeed and glideslope angle. At least two runs were planned for each test configuration and condition to check on data consistency. To eliminate the effects of changing meteorological conditions during the test period, runs with different configurations were run sequentially so that the effect of a particular parameter could be isolated from any meteorological effects. Glideslope effects, for example, were studied by flying a level run and following that run immediately with a 7 degree glideslope run at the same altitude and airspeed.

Data collection was initiated as soon after dawn as possible to take advantage of the calm atmospheric conditions most conducive to long vortex lifetimes. On some days, equipment problems delayed the beginning of the tests until later in the morning. By this time, normal thermal activity had already begun and vortex lifetimes were seriously reduced. On other days, ambient winds were strong enough even at dawn to both reduce vortex lifetimes and make vortex tracking more difficult. In all, only one or two days of the test sequence for each helicopter were conducive to maximum vortex lifetimes. In an effort to take advantage of turbulent conditions, some runs were deliberately repeated later on particular test mornings to study the effects of atmospheric turbulence on vortex persistence as a function of vortex altitude.

### 3.7 DATA REDUCTION.

The data reduction process involved two manual steps before the automatic data analysis programs could be utilized. In the first step, the velocity profiles from each arc scan were examined by a specially trained operator. The start of a given run was signaled by a large velocity spike in the scan which occurred when the LDV beam bounced off the airframe ("skin hit"). The velocity profiles were random for a number of scans until the two vortices have rolled up. Following vortex rollup, the scan showed each vortex as two velocity peaks with a sharp dip in between, which was caused by the reversal of the sign of the velocity at the center of the vortex (the LDV cannot sense the velocity sign). The centers of the vortices were marked (in angle) by the operator in each scan. These centers were marked by the operator until it was certain that the vortex structure had broken down and only random turbulence remained. The vortex structure appeared gone to the operator when the dip in the velocity profile disappeared and only random lumps were remaining in the velocity profile.

The second step of the data reduction took place after the run had been marked in the procedure outlined in the preceding paragraph. In this step, the range and angle locations of the vortices were computer-plotted versus a function of vortex age (figure 3-7). Since the range values generally have considerable scatter, a fitted line was drawn manually with the computer cursor through the data points to give a smooth function of range versus time. These selected range values were then used to select the measured velocity profile from the range scan closest to the selected vortex range and to change the profile from elevation angle to vortex radius as the independent variable. The software had the option of fitting the lateral position of the vortices (X,Y coordinates) instead of the range (R,Theta coordinates). This option was useful when the vortices were moving laterally at constant speed, but gave a singular point for a vortex located directly above the LDV.

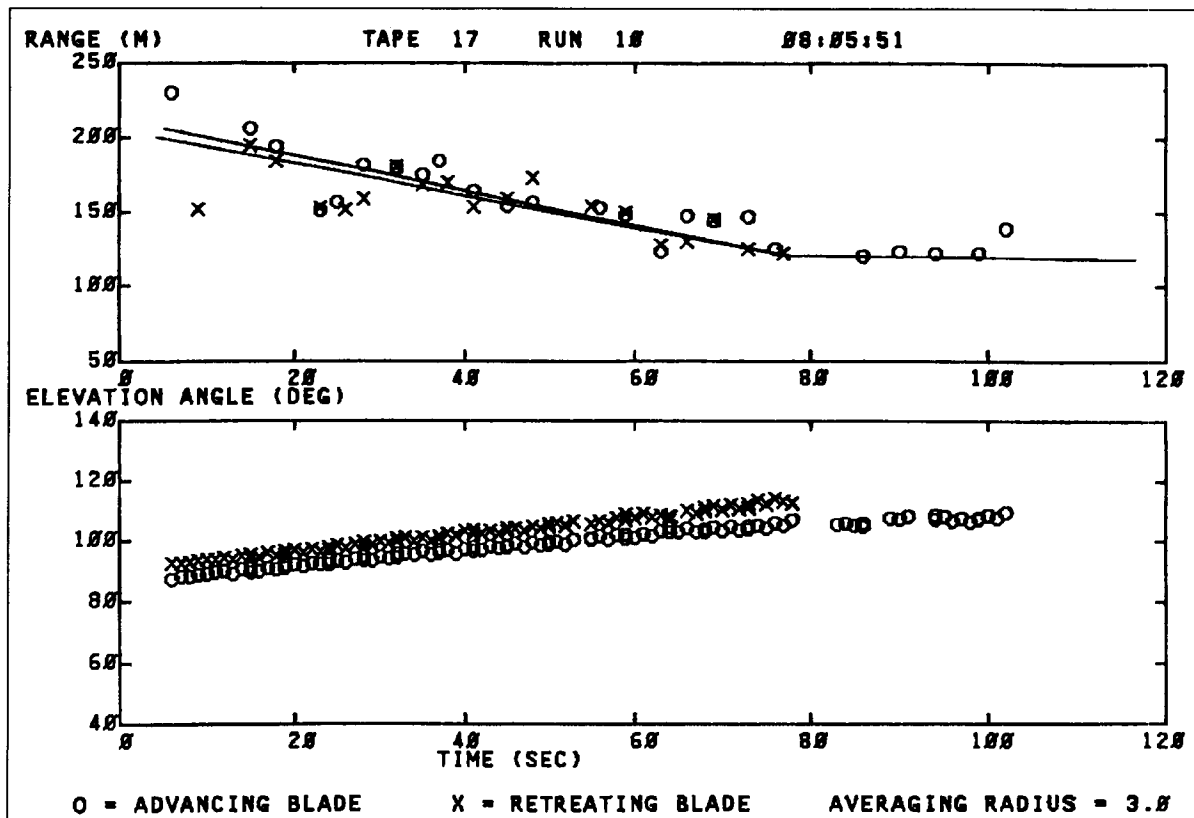


FIGURE 3-7. RANGE AND ELEVATION ANGLE VS. TIME

### 3.8 DATA ANALYSIS.

The LDV data reduction process produced vortex trajectory and vortex velocity profiles every three to five seconds. From this information a variety of data plots can be generated:

- a. The basic plot (figure 3-8) shows the velocity profiles for both vortices for all scan frames. As can be seen, the correct velocity signs are assigned by processing routines to give a downdraft between the vortex centers and an updraft outside of the centers.
- b. A full-size plot (figure 3-9) of the velocity profiles can be generated for any selected vortex age.
- c. Once the vortex velocity profile is corrected for vortex motion along the LDV line of sight, the velocity profile becomes symmetrical. A velocity profile can then be converted to two circulation profiles [ $\Gamma(r)=2\pi r v(r)$ ] (equation 1-3), one from each side of the vortex. Plots can be generated showing circulation profiles for all times or for a selected time (figure 3-10).
- d. The hazard model (reference 2) used with LDV data relates hazard to the circulation  $\Gamma$  averaged over the semispan of the following aircraft. Profiles of

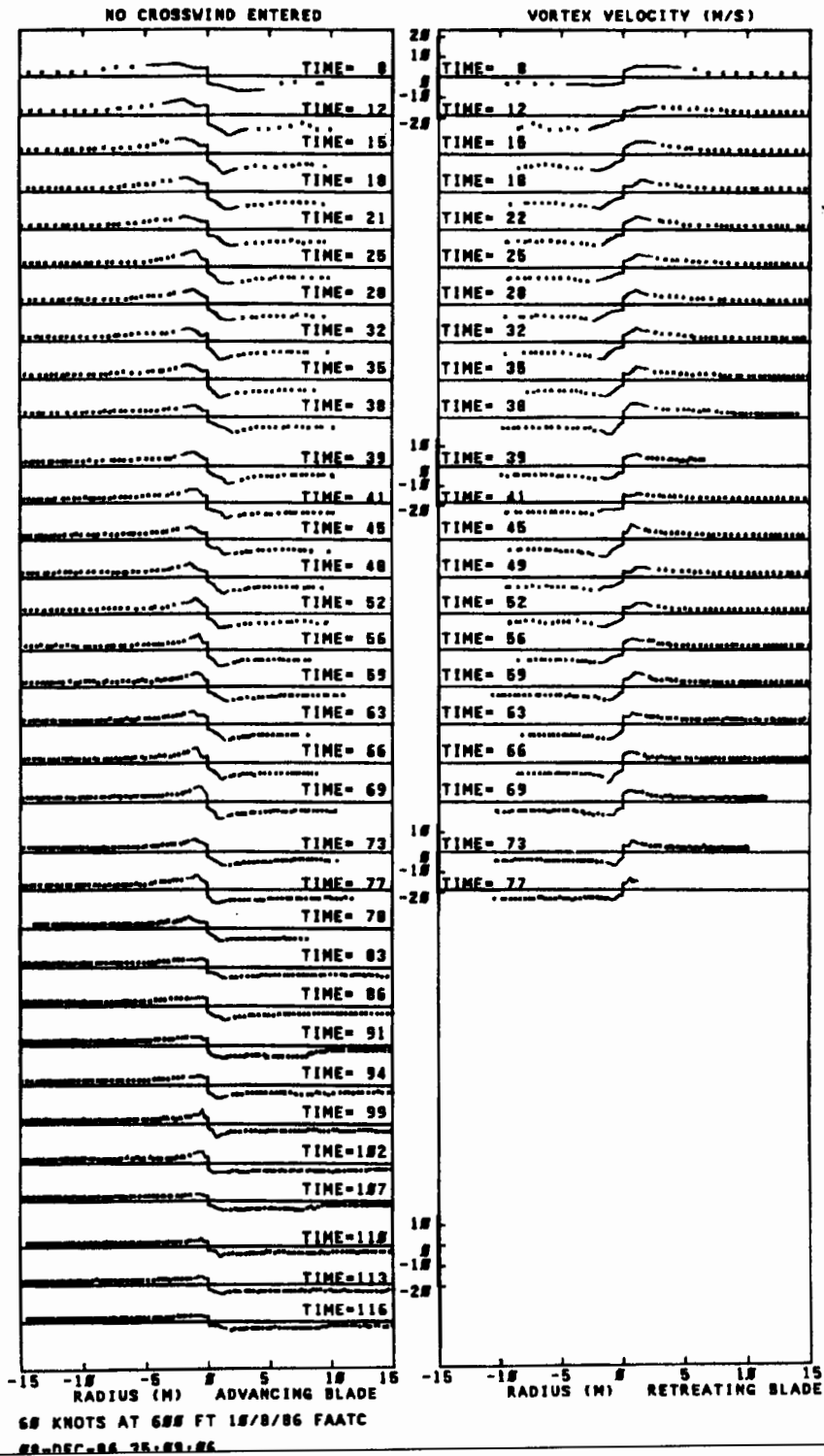


FIGURE 3-8. S-76A VELOCITY PROFILE TIME HISTORY

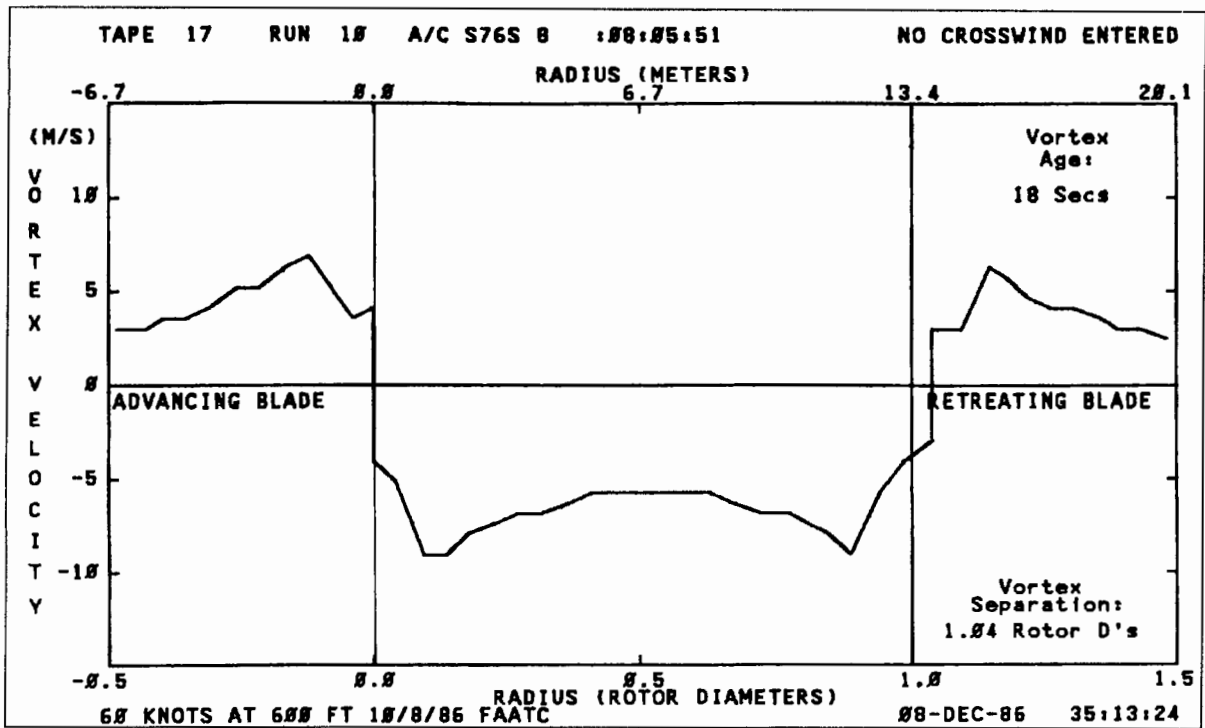


FIGURE 3-9. FULL-SIZE S-76A WAKE VELOCITY PROFILE

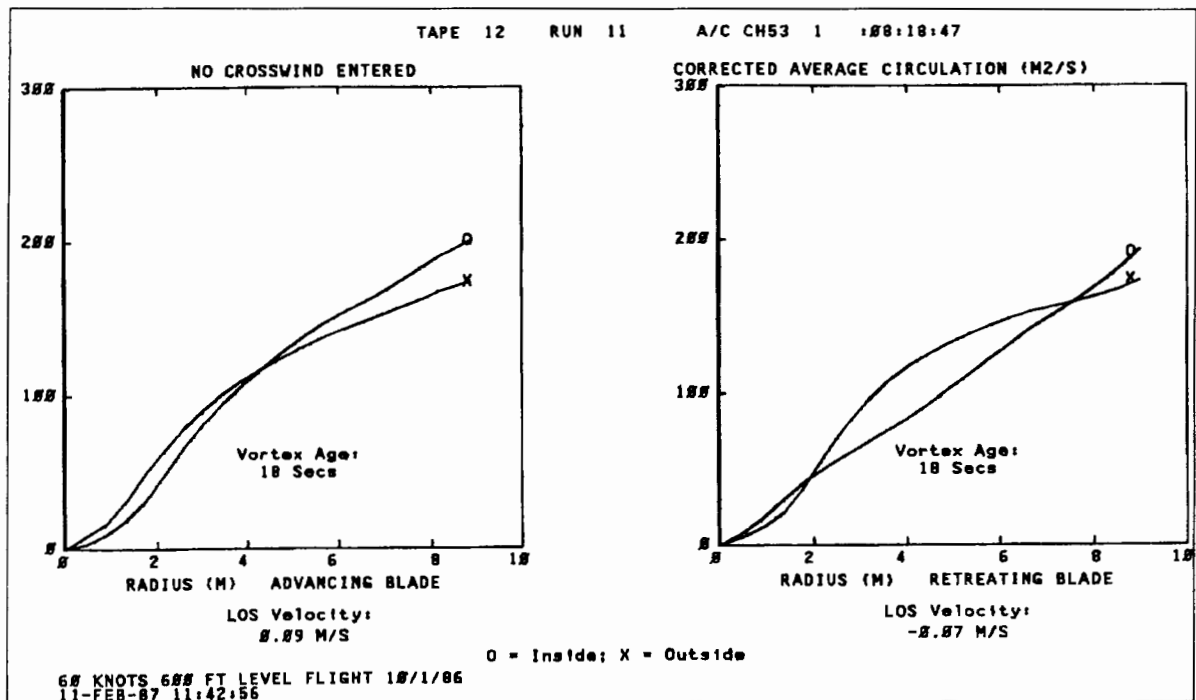


FIGURE 3-10. CH-53E CIRCULATION PROFILES

average circulation ( $\Gamma$ ) versus averaging radius can be generated for selected times. Time histories of average circulation for several averaging radii (5, 10 meters, etc.) can also be plotted (figure 3-11). Plots can also be generated for the induced rolling moment vs. separation distance for two specific following aircraft, the T-37 and DC-9, though no example of these plots is reproduced here.

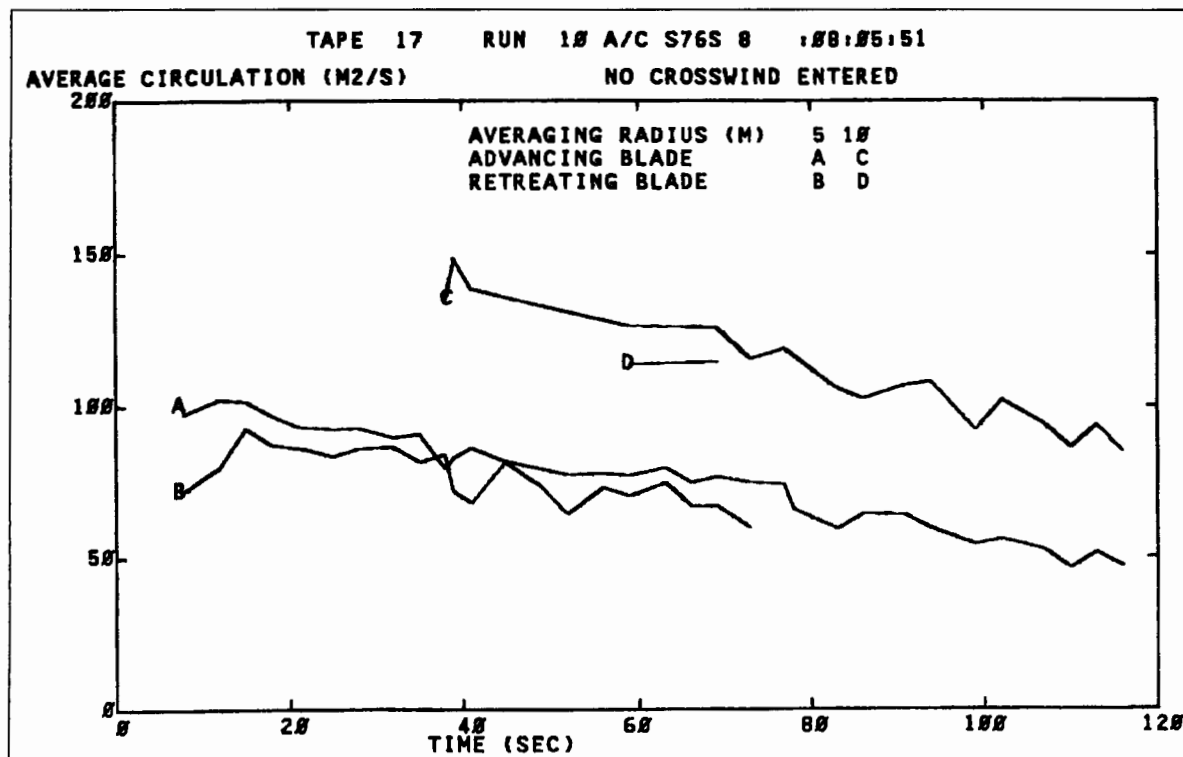


FIGURE 3-11. S-76A AVERAGE CIRCULATION VS. TIME

In all the aforementioned plots, only the two described in paragraph 3.8d (the average circulation and the induced rolling moment) are corrected for the assumed 1.65-meter-per-second velocity error of the LDV. Since this assumed correction factor may not be valid for rotorcraft results (having been derived for fixed-wing flight tests, reference 2) and hence may lead to significant errors in velocity measurements and circulation calculations, the results presented in section 4.1 must consider the sensitivity of the measurements to this assumption.

In contrast to previous reports (references 2 and 5), no new analysis plots will be presented in this report. Instead, information from the many plots generated was extracted from data plots and incorporated into large spreadsheets that served as data bases.

Because of the large amount of labor involved in the data processing, not all the data collected were processed into the data bases. The data tapes with the longest lasting vortices were analyzed along with representative tapes with shorter lasting vortices.

## 4. LDV RESULTS.

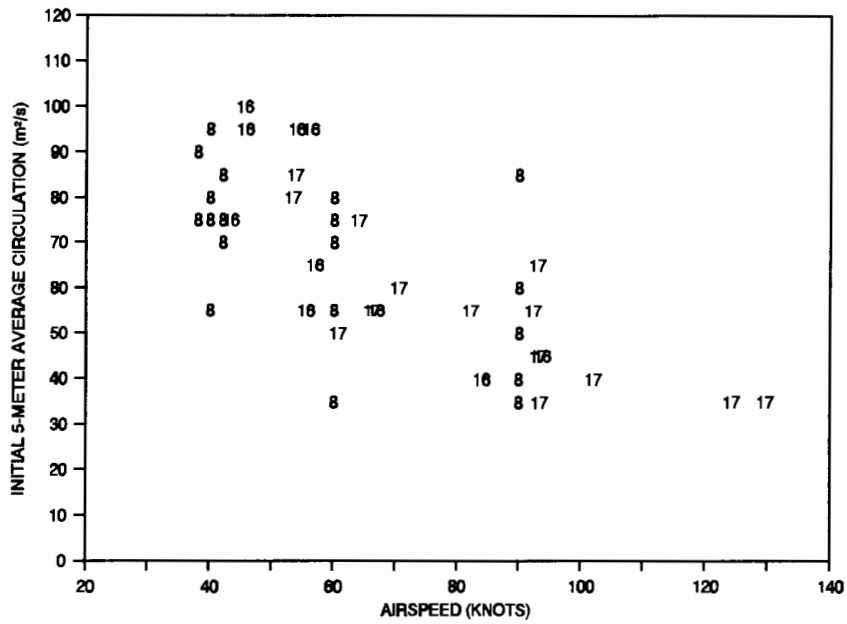
This section presents the results of the LDV measurements. The nature of the helicopter generated wake vortices and their strength is examined first, followed by considerations of initial transport properties and measurements of vortex decay.

### 4.1 INITIAL VORTEX STRENGTH.

As discussed in section 1.5, the average circulation of a vortex out to radius  $r$ ,  $\Gamma'(r)$ , gives an indication of the maximum vortex-induced roll on a following aircraft of wingspan  $2r$ . An averaging radius of five meters was chosen to compute average vortex strengths for two primary reasons:

- a. Larger values of averaging radii are not practical. At larger values of averaging radius, the flow field of one vortex begins to significantly affect the outer flow field of the other vortex.
- b. The wingspans of the probe aircraft used in the study were about ten meters.

Figures 4-1 through 4-4 are plots of the initial five-meter vortex average circulation  $\Gamma'(5)$  versus helicopter airspeed for each of the four helicopters studied. The points are labeled by their respective tape number, which represents the day on which the runs were made. For all runs, the starboard (on the pilot's right) vortex was used in the plots. At higher airspeeds, the starboard vortex, which corresponds to the advancing side of the helicopter rotor, is somewhat stronger than the port vortex for single-rotor helicopters (references 1,4). The vortex average circulations for these plots were computed at a vortex age of 10 to 15 seconds, when the vortices have rolled up completely but little decay has occurred. In general, the plots show the inverse airspeed dependence predicted by equation 1-1. The few runs below 40-knots airspeed show much diminished vortex average circulation. In the transition region to hover (zero airspeed) the wake does not appear to completely roll up into cohesive vortices despite the vorticity shed by the individual blades. The data indicate that equation 1-1 fails at airspeeds below about 40 knots.



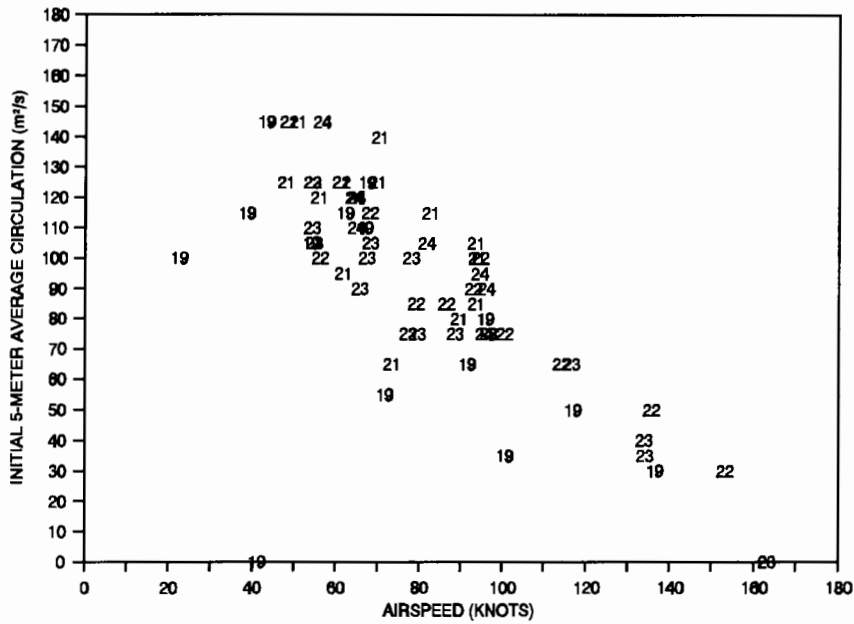


FIGURE 4-3. CH-47D 5-M INITIAL AVERAGE CIRCULATION VS. AIRSPEED (KNOTS)

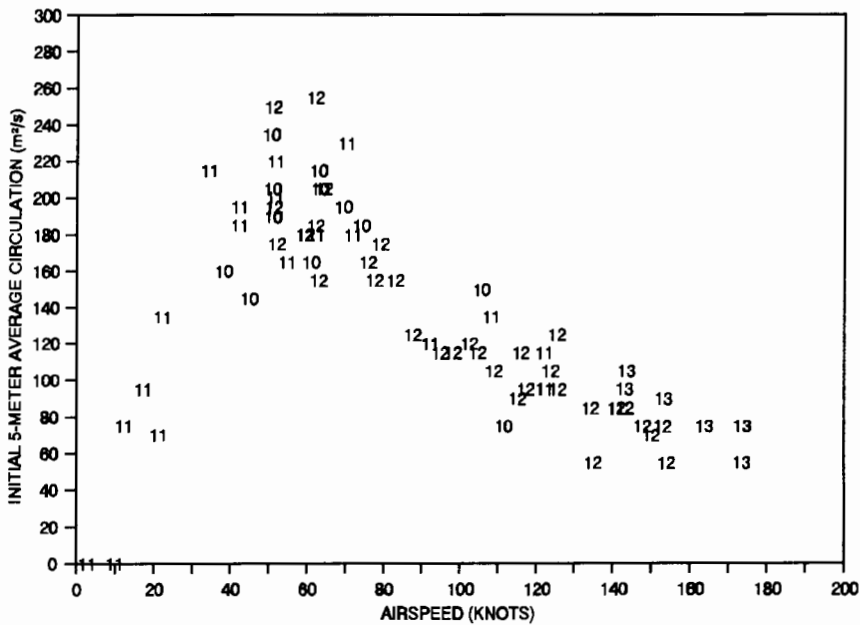
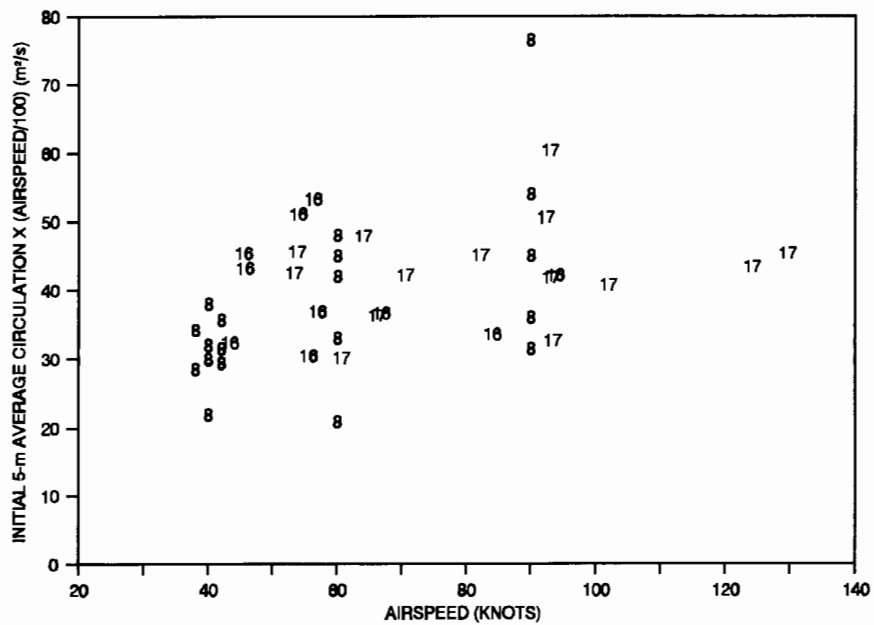


FIGURE 4-4. CH-53E 5-M INITIAL AVERAGE CIRCULATION VS. AIRSPEED (KNOTS)

Equation 1-1 suggests that the product of circulation and airspeed be constant for any specific aircraft. With this in mind the average circulation data of figures 4-1 through 4-4 were multiplied by their respective airspeeds in knots and divided by 100 knots to maintain proper dimensions and to provide a scaling for speed. The results of these calculations are shown in

figures 4-5 through 4-8 to illustrate how well equation 1-1 fits the data. Above airspeeds of 50 knots, the product of vortex average circulation and airspeed is more or less constant for all four helicopters. A visual fit to the data between 60 and 120 knots in figures 4-5 through 4-8 gives the values shown in the third line of table 4-1 for the average circulation at 100 knots ( $V/100 = 1.0$  in the figures). The two larger helicopters (figures 4-7 and 4-8) show a trend toward lower values of  $K$  at the highest airspeeds.



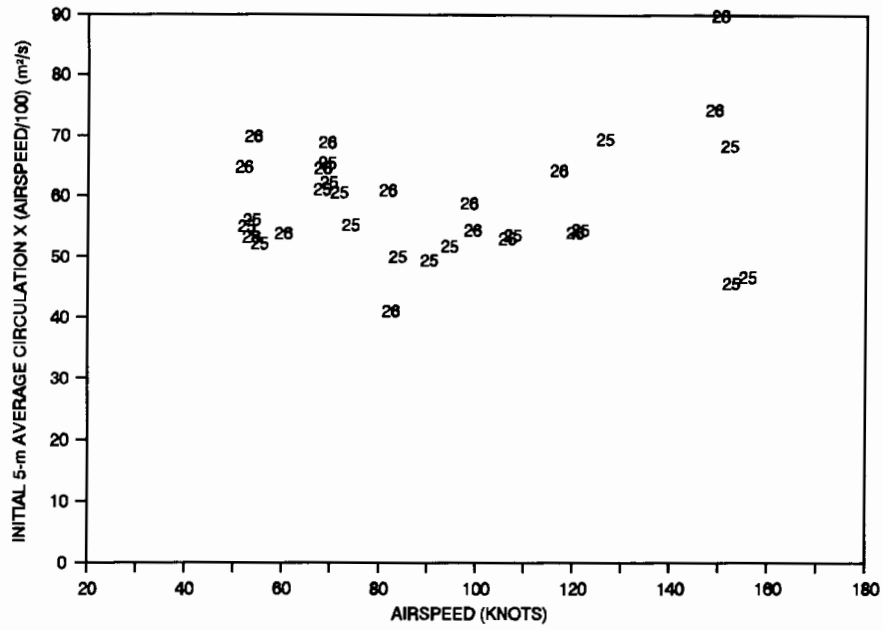


FIGURE 4-6. UH-60A 5-M INITIAL AVERAGE CIRCULATION X (V/100) VS. AIRSPEED (KNOTS)

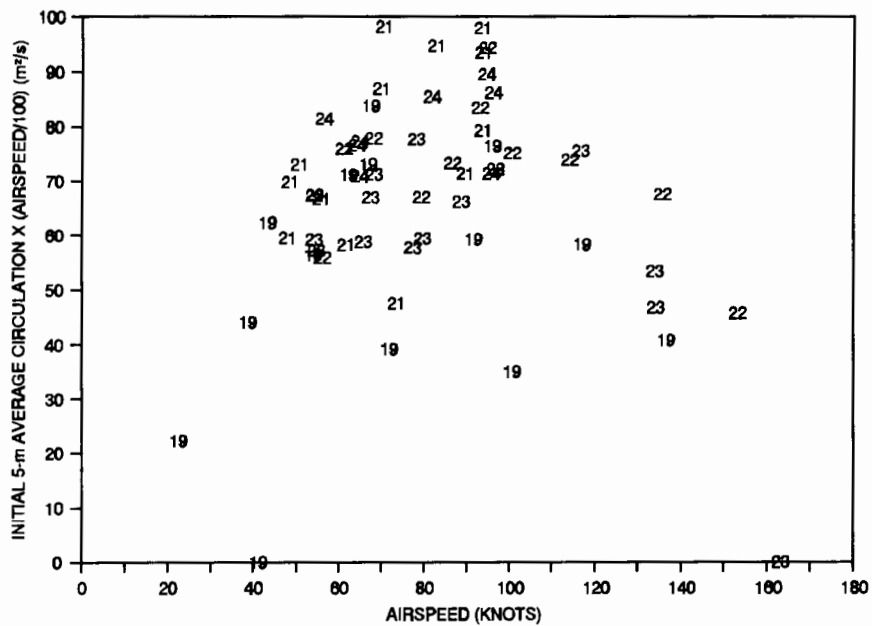


FIGURE 4-7. CH-47A 5-M INITIAL AVERAGE CIRCULATION X (V/100) VS. AIRSPEED (KNOTS)

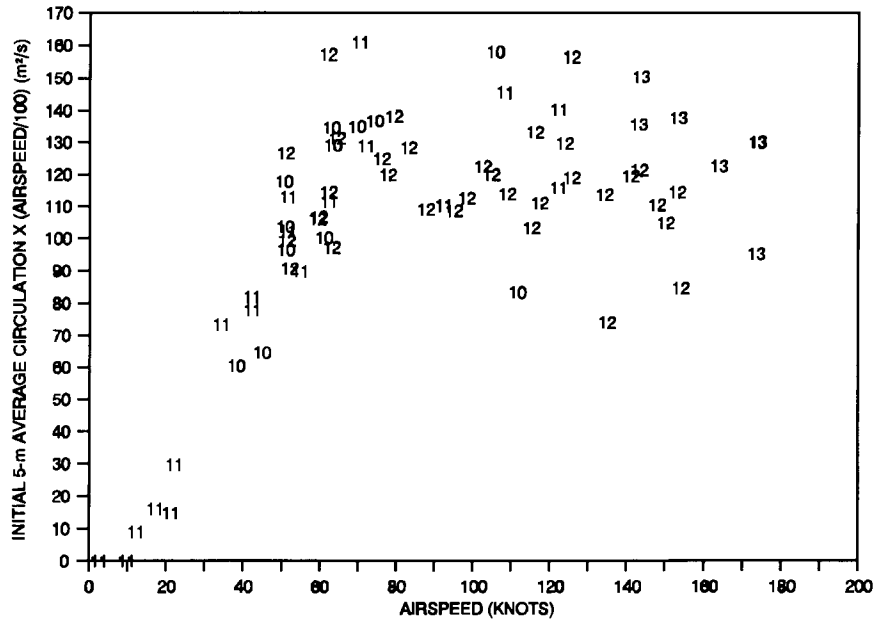


FIGURE 4-8. CH-53E 5-M INITIAL AVERAGE CIRCULATION X (V/100) VS. AIRSPEED (KNOTS)

Table 4-1 represents an analysis of the measured 5-meter average circulation data and compares it to the total circulation predicted by equation 1-1. The weight for each helicopter is an estimate of the test weight during the flight period and was obtained from the flight test log sheets and its maximum takeoff weight.

Reference 4 reports that the core radius of a helicopter wake vortex is approximately ten percent of the rotor diameter. The fourth line in table 4-1 computes the ratio of average circulation to the total circulation for this core radius using equation 1-7. The fifth line in the table shows the resulting calculated value for  $\Gamma_{\infty}$  based on measurements. The next line shows the theoretical values for the vortex circulation from equation 1-1 using an air density,  $\rho$ , of  $1.23 \text{ g/m}^3$  ( $10^{\circ}\text{C}$  at sea level),  $V = 52 \text{ m/s}$ ,  $b = d$  (rotor diameter) and  $K = 1$ . The last line in the table shows the ratio of the calculated to theoretical values. Single-rotor helicopters show a consistent value of about 1.6, while the tandem-rotor CH-47D shows a ratio of 1.0.

The lower ratio for the CH-47D suggests that not all the vorticity from both rotors is rolled up into the final wake vortices, or that some sort of destructive interference is taking place in the flowfield. The measurements indicate that the final vortices may represent primarily the wake of only one of the two rotors and that the wake of the other rotor is mostly lost. The CH-47D vortices were anomalous in another respect in that they tilted soon after generation (reference 4). In any case, the wake vortices from the CH-47D appear to be less hazardous than those from a single-rotor helicopter of the same size.

TABLE 4-1. WAKE VORTEX CIRCULATION ANALYSIS

<u>PARAMETER</u>	<u>S-76A</u>	<u>UH-60A</u>	<u>CH-47D</u>	<u>CH-53E</u>
Weight (Lbs)	8,000	15,000	37,000	56,000
Rotor Diameter d (m)	13.41	16.36	18.29	24.08
Fitted $\Gamma'(5 \text{ m})$ ( $\text{m}^2/\text{s}$ ) at 100 knots	43	58	75	125
$\Gamma'(5 \text{ m})/\Gamma_\infty$ @ $r_c = 0.1 \text{ d}$ from equation 1-7	0.65	0.59	0.55	0.46
Calculated $\Gamma_\infty$ ( $\text{m}^2/\text{s}$ ) at 100 knots (52 m/s)	66	98	136	272
Theoretical $\Gamma_\infty$ ( $\text{m}^2/\text{s}$ ) from equation 1-1	42	64	141	162
Ratio Calculated/Theoretical	1.57	1.53	0.96	1.68

The observed numerical factor of 1.6 between the calculated and theoretical total circulation values may be related to a number of factors:

- a. The factor K in equation 1-1 may be larger than 1.00 (see section 4.2).
- b. The effective core radius may be smaller than 0.10 d or may be influenced by other factors such as disk loading, blade loading, or blade number.
- c. The LDV velocity error may be larger than the 1.65 m/s measured for the B-747 and assumed in this analysis (reference 4 contains further discussion on this issue). Note, however, that a larger correction would cause figures 4-5 through 4-8 to decrease more at high airspeeds and hence would be less consistent with a constant K in equation 1-1.
- d. Finally, one cannot dismiss the possibility that a helicopter simply cannot be related to those from fixed-wing aircraft via equation 1-1.

#### 4.2 INITIAL VORTEX SEPARATION.

Figures 4-9 through 4-12 show the initial separation between the port and starboard vortices (normalized to the rotor diameter) for each of the four helicopters as a function of airspeed and glideslope angle. The separation is measured from the center of one vortex to the center of the other vortex at a time of 10 to 15 seconds after the helicopter flew over the LDV van and shortly after the vortices have rolled up. According to equation 1-2, the ratio of the rotor diameter to the vortex separation should be equal to the constant, K, in equations 1-1 and 1-2. In general,

the vortex separations for airspeeds above 50 knots are close to the rotor diameter and are therefore consistent with the value of  $K = 1.00$  assumed in section 4.1. The two larger helicopters (figures 4-11 and 4-12) show a slight trend toward smaller spacings for higher airspeeds (i.e.,  $K$  becoming larger than 1.00). This trend is opposite to the slight decrease in  $K$  for high airspeeds, which was noted in figures 4-7 and 4-8. Below 50-knots airspeed the spacing increases dramatically, just as the strengths (figures 4-3 and 4-4) are decreasing, as predicted by equations 1-1 and 1-2 for small values of  $K$ . The wide vortex separation at very low airspeed was also very evident in the photographic data.

The points in figures 4-9 through 4-12 are labeled by glideslope, with the convention that a negative value denotes a climb. The S-76A runs in figure 4-9 suggest a relationship between vortex separation and glideslope, with vortices being closest together during descents and furthest apart during climbs. This relationship is present in CH-53E data which shows most of the 7-degree descent runs to have vortex separations under one rotor diameter. The effect appears to a lesser degree for the CH-47D runs which shows most of the descent runs to have vortex separations under one rotor diameter.

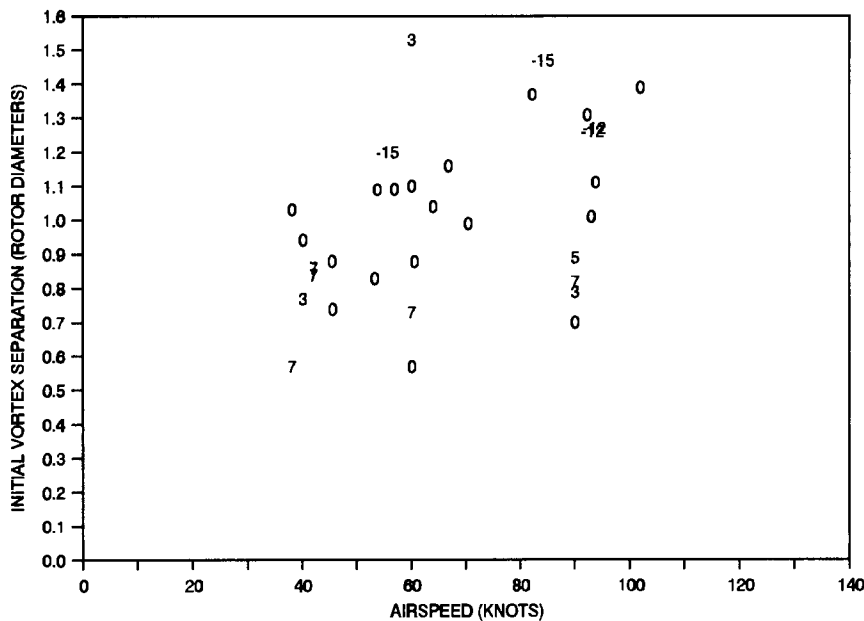


FIGURE 4-9. S-76A VORTEX SEPARATION (ROTOR DIAMETERS) VS. AIRSPEED (KNOTS)

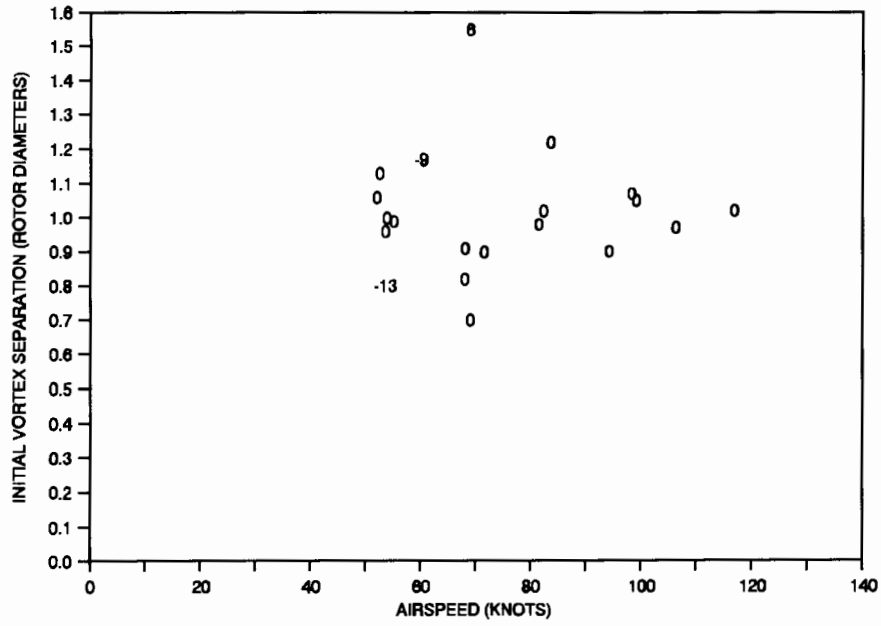


FIGURE 4-10. UH-60A VORTEX SEPARATION (ROTOR DIAMETERS) VS. AIRSPEED (KNOTS)

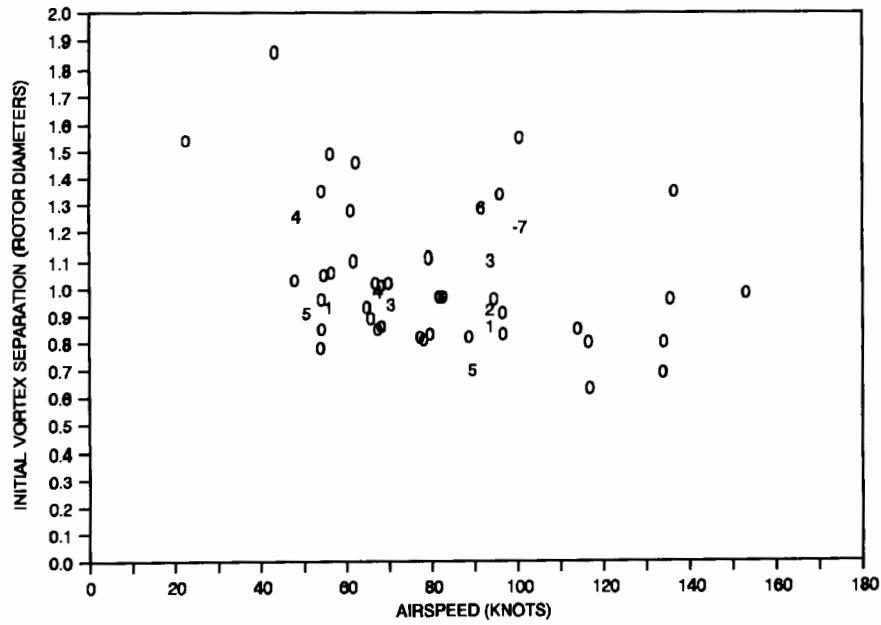


FIGURE 4-11. CH-47D VORTEX SEPARATION (ROTOR DIAMETERS) VS. AIRSPEED (KNOTS)

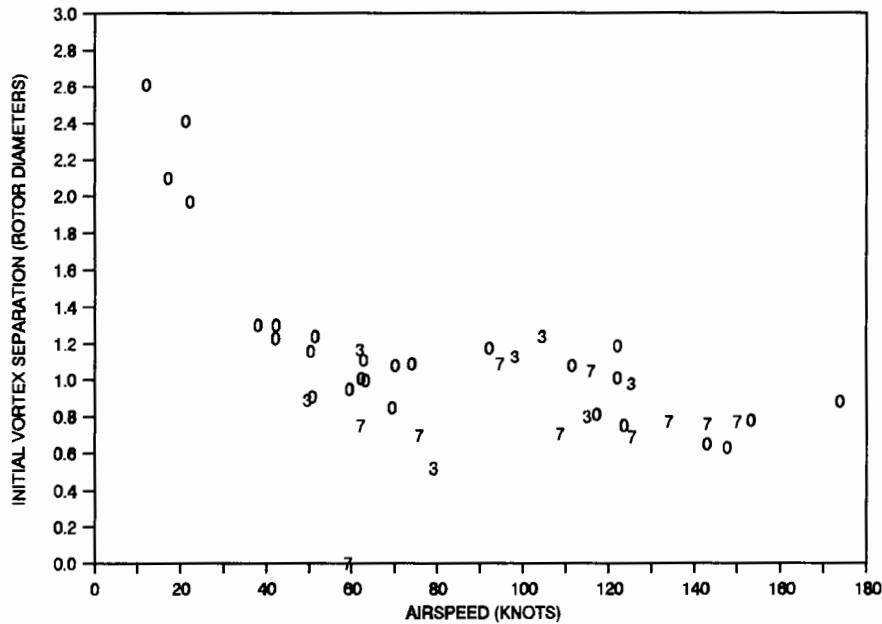


FIGURE 4-12. CH-53E VORTEX SEPARATION (ROTOR DIAMETERS) VS. AIRSPEED (KNOTS)

### 4.3 VORTEX DECAY.

Wake vortices decay by turbulent diffusion and by two types of vortex instability, core bursting and vortex linking (reference 7). Vortex linking was clearly evident in about 10 percent of the runs analyzed.

The physics of vortex decay are most naturally expressed in the time domain: the vortex hazard duration,  $T$ , is the vortex age when it is no longer hazardous. However, for final approach aircraft separation purposes, it can be more useful to examine vortex decay as a function of distance behind the generating aircraft.

If both the generating and following aircraft are flying at the same airspeed,  $V$ , the hazard distance  $D$  is given by

$$D = VT \tag{4-1}$$

The simplified expression of equation 1-10 was used to define when a vortex was considered hazardous. This expression, with  $f=0.5$ , predicts a vortex to be hazardous for as long as its 5-meter average circulation,  $\Gamma(5\text{ m})$ , is greater than  $25\text{ m}^2/\text{s}$ . A vortex of this strength should induce a maximum rolling moment equal to half the roll control capability of an aircraft with a 10-meter wingspan (5-m semispan). This hazard definition, as discussed in section 1-6, assumes that the encountering aircraft has an airspeed of 130 knots. For significantly different airspeeds, equation 1-8 should be used. It should be noted that other investigators, including NASA Dryden

(DFRF), have used  $f=1.0$  for defining the vortex hazard in full-scale vortex probe flight tests. Section 6.1 describes an analysis of the sensitivity of the hazard duration to the assumed values for  $f$ .

#### 4.3.1 Predicted Hazard Duration.

The LDV is stationary in space rather than moving with the ambient wind. Therefore, it does not measure  $T$  (the modeled hazard time of a particular vortex) directly, except under zero wind conditions. As a result, the LDV measures different segments of the aircraft wake trail at different times; under headwind conditions the LDV sees progressively fresher portions of the vortex and the real hazard duration will thus be shorter than the measured duration. Any predicted hazard duration, therefore, must be corrected by the amount of headwind relative to the aircraft speed.

The correction is given by equation 4-2:

$$T = (G/V)T_{LDV} \quad (4-2)$$

where  $G$  = helicopter groundspeed.  
 $V$  = helicopter airspeed.  
 $T_{LDV}$  = Elapsed time between the helicopter overflying the LDV (the "skin hit") and the time the portion of vortex over the LDV showed no hazard.

On the vast majority of the runs the helicopter flew into a headwind, so the groundspeed  $G$  was less than the airspeed  $V$ , and  $T$  was therefore less than  $T_{LDV}$ .

Figures 4-13 through 4-16 show the predicted vortex hazard duration  $T$  versus airspeed for the four helicopters. The predicted hazard durations are for the starboard vortex on each run, which usually remains hazardous longer than the port vortex (reference 4). The data points in these figures are labeled by the tape number discussed earlier. Statistics on predicted hazard duration are presented in table 4-2.

From figures 4-13 to 4-16 and table 4-2, it is clear that the primary factor in how long a vortex is predicted to remain hazardous is the ambient weather on a particular day (represented by tape number in the figures). Ambient weather appears to be even more important than the size of the helicopter generating the vortices. Using the hazard model discussed in section 1.6 with  $f=0.5$ , the longest lasting hazardous vortices were generated by the S-76A, the smallest helicopter flown during the flight tests. See section 6.1 for further discussion.

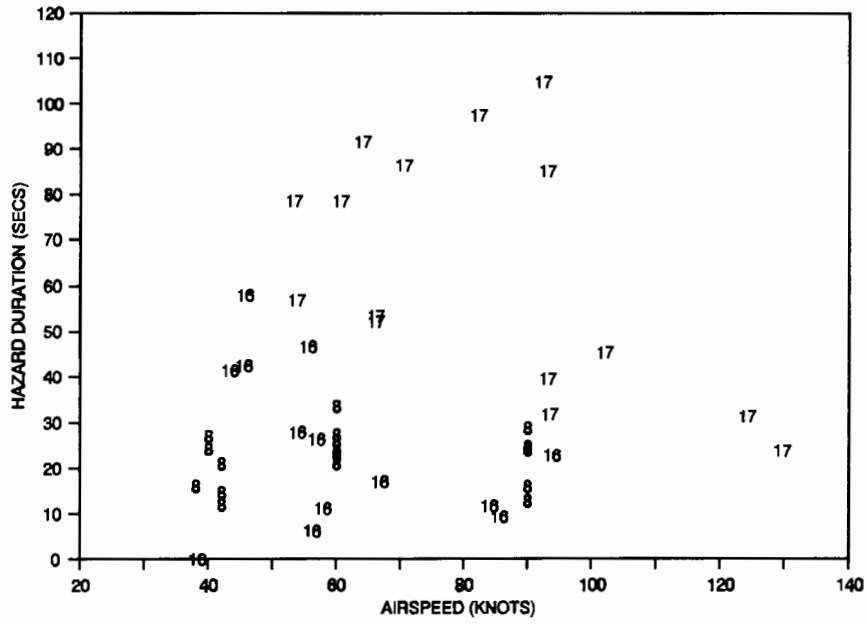


FIGURE 4-13. S-76A MODELED VORTEX HAZARD DURATION VS. AIRSPEED (KNOTS)

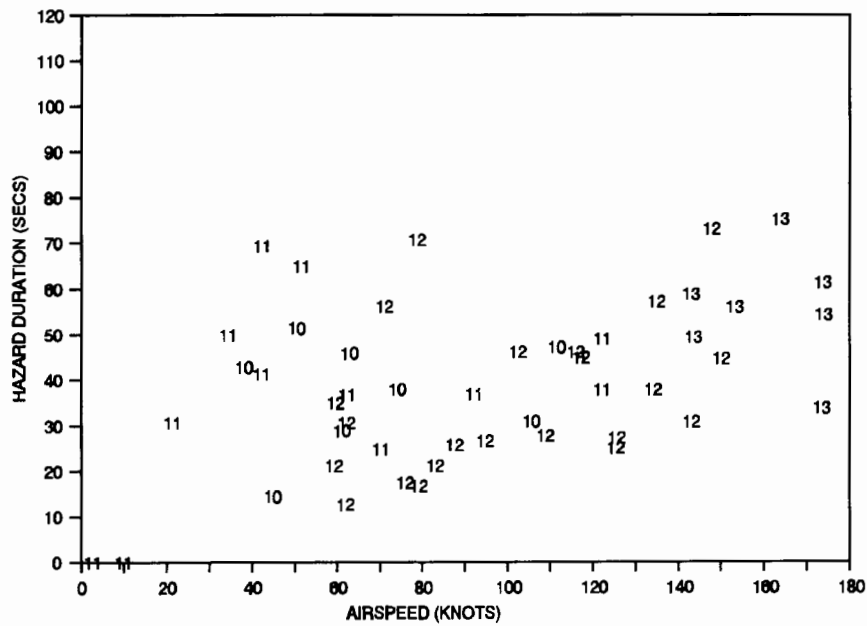


FIGURE 4-14. UH-60A MODELED VORTEX HAZARD DURATION VS. AIRSPEED (KNOTS)

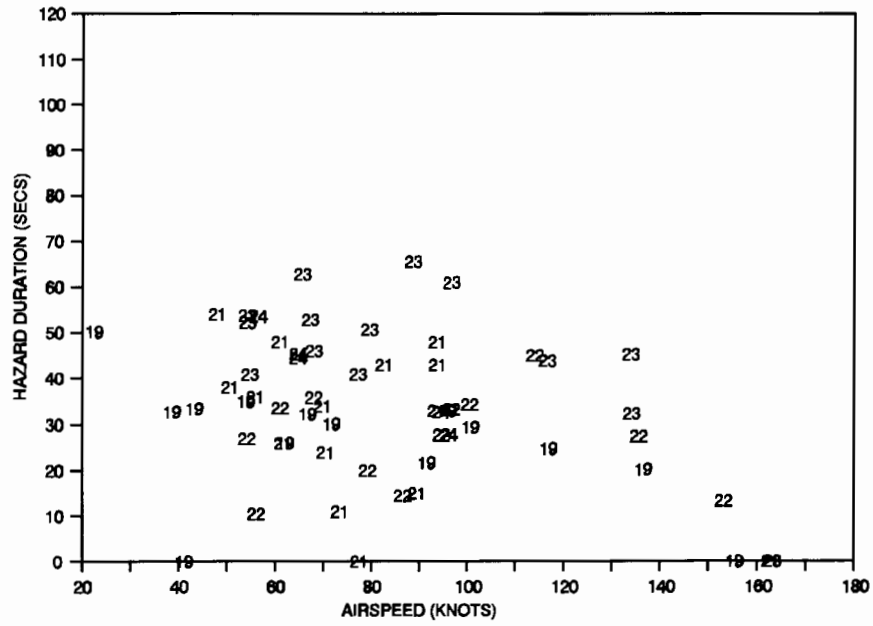


FIGURE 4-15. CH-47D MODELED VORTEX HAZARD DURATION VS. AIRSPEED (KNOTS)

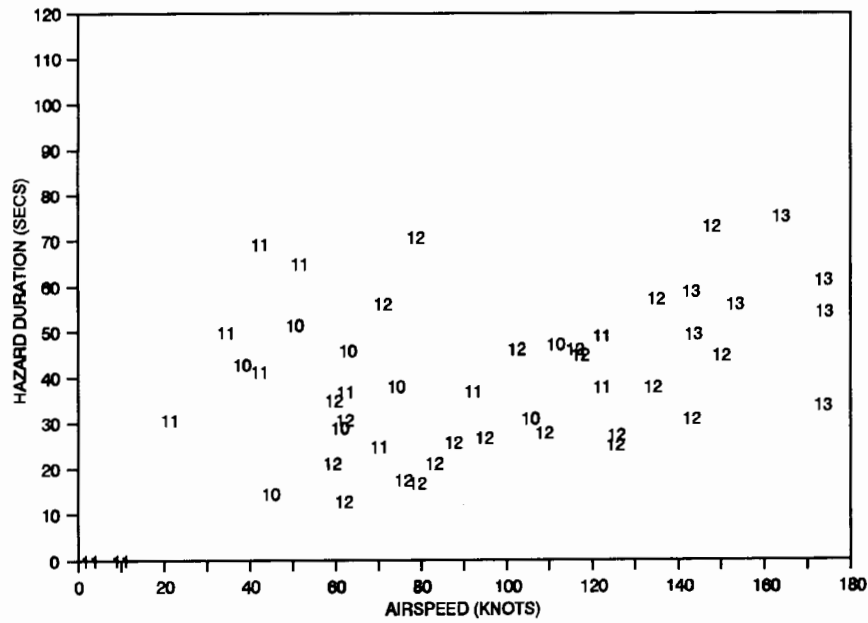


FIGURE 4-16. CH-53E MODELED VORTEX HAZARD DURATION VS. AIRSPEED (KNOTS)

TABLE 4-2. PREDICTED HAZARD DURATION, T

<u>PARAMETER</u>	<u>S-76A</u>	<u>UH-60A</u>	<u>CH-47D</u>	<u>CH-53E</u>
Maximum T (s)	105	64	65	75
Percentage of Runs, T > 60	15	3	5	12
Median T (s), All Airspeeds V	28	35	35	38
Median T (s), V > 80 knots	28	35	32	45
Median T (s), V < 80 knots	28	35	37	35
<u>Desegregate by tape number:</u>				
Median T (s) (Tape Number)	20(8)	33(25)	30(19)	40(10)
Median T (s) (Tape Number)	25(16)	38(26)	38(21)	38(11)
Median T (s) (Tape Number)	58(17)		28(22)	30(12)
Median T (s) (Tape Number)			46(23)	55(13)

The longest lasting vortices observed for all helicopters were recorded on tape 17, which was spectacular in terms of vortex duration. The typical S-76A vortex on that tape lasted more than two to three times longer than the S-76A vortices measured on other days. Other tapes that contained long-lasting vortices (though not as dramatic as tape 17) were tape 23 for the CH-47D and tape 13 for the CH-53E. On each of these two tapes, measured vortices were predicted to be hazardous about 50 percent longer than on other tapes for the same helicopter. The long median modeled hazard duration of 45 seconds on tape 24 for the CH-47D has relatively little significance since predicted hazard durations were available for only five runs.

There does appear to be a small relationship between helicopter weight (and size) and the predicted vortex hazard duration. The median CH-53E hazard durations were the longest and the median S-76A hazard durations were the shortest.

There is little apparent relationship between vortex hazard duration and airspeed for a given helicopter. The CH-53E data gave an impression (probably false) that the vortices last longer at higher airspeeds. The data are biased, however, because all of the tape 13 runs, which had long-lasting vortices, were flown at high airspeeds. If half of the modeled hazard durations based on tape 13 observations had occurred at low airspeeds, then there would be little difference between the median CH-53E predicted hazard durations for low and high airspeed runs.

The only apparent relationship between predicted hazard duration and airspeed occurs at the extremes of airspeed. Very low airspeed LDV runs were flown only with the CH-53E. At airspeeds below about 20 knots there was no modeled hazard duration, because the vortices failed to roll up and thus average circulation is zero. A potential hazard generated by the rotor downwash, however, may exist at these low speeds. For the S-76A, UH-60A, and CH-47D helicopters, the predicted hazard durations fall off rapidly above 120 knots for the S-76A and 130 knots for the UH-60A and the CH-47D. At such high airspeeds, the vortices from these helicopters are initially very weak and quickly decay below the modeled hazard threshold. The CH-53E vortices are still strong enough at the maximum CH-53E airspeed (about 175 knots) to

remain hazardous to light aircraft, according to the model, for as long as the vortices generated at lower airspeeds.

In summary, the initial strength of the vortices seems to play a secondary role, compared to the ambient weather, in how long vortices will remain hazardous. Vortices that are initially strong, either because of a heavy generating helicopter or a low airspeed, apparently decay substantially faster than the vortices that are initially less strong, so that the resulting predicted hazard duration is about the same for initially strong or initially weak vortices.

#### 4.3.2 Predicted Hazard Distance.

Figures 4-17 through 4-20 plot the predicted vortex hazard distance  $D$  (equation 4-2) versus airspeed  $V$  for the four helicopters.  $D$  is the actual distance behind the helicopter that its starboard vortex is still hazardous. References 1 and 4 show that the starboard vortex (corresponding to the advancing blade) is predicted to remain hazardous for as long as or longer than the port vortex in the great majority of runs. Statistics on vortex hazard distances are presented in table 4-3.

From figures 4-17 through 4-20 and table 4-3 it is clear that the greatest predicted hazard distances occur behind helicopters flying at high airspeeds. In section 4.3.1 it was shown that predicted hazard duration is essentially independent of airspeed. Hence, for relatively equal hazard duration times, the greatest hazard distances will occur at higher airspeeds.

For the S-76A, UH-60A, and CH-47D helicopters, the predicted hazard distances increase with airspeed up to about 130 knots. Above 130 knots predicted hazard distances begin to fall off rapidly since at such high airspeeds the vortices are initially very weak and have a strength just above the calculated hazard threshold and decay beneath that threshold after a very short time. Predicted hazard distances for the CH-53E helicopter increase as the airspeeds reach the maximum CH-53E airspeed because the vortices are still strong enough at that high airspeed to remain hazardous for a considerable time.

Each point in figures 4-17 through 4-20 is labeled by the tape number (one tape for each test day). As expected, the days with the longest predicted hazard durations are the days with the greatest calculated hazard distances. Data on these days were recorded on tape 17 for the S-76A runs, tape 23 for the CH-47D runs, and tape 13 for the CH-53E runs.

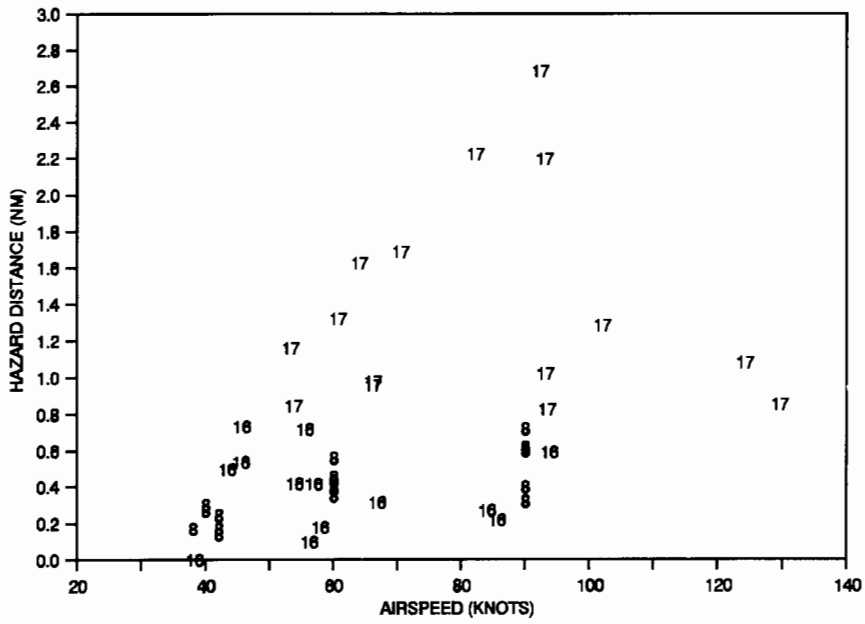


FIGURE 4-17. S-76A PREDICTED VORTEX HAZARD DISTANCE (NM) VS. AIRSPEED (KNOTS)

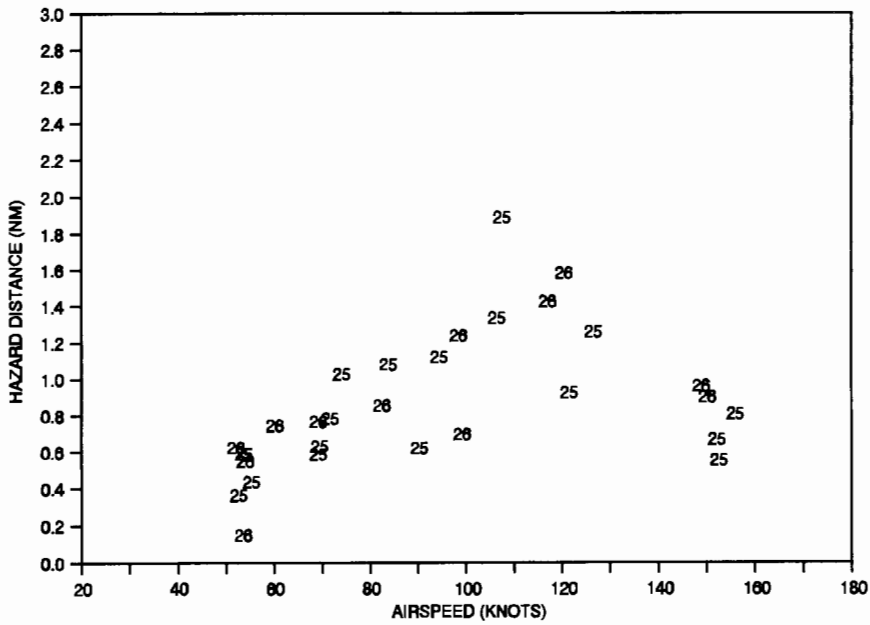


FIGURE 4-18. UH-60A PREDICTED VORTEX HAZARD DISTANCE (NM) VS. AIRSPEED (KNOTS)

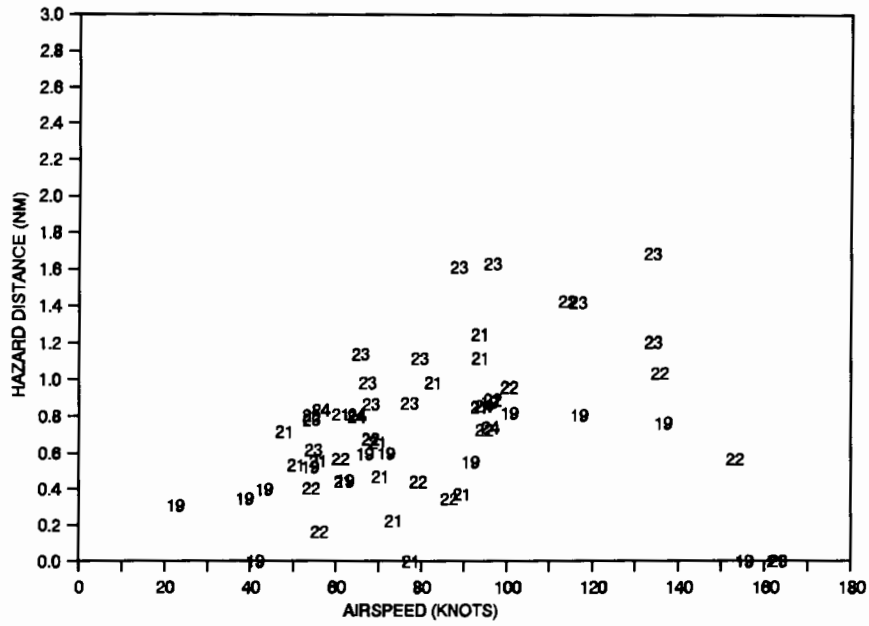


FIGURE 4-19. CH-47D PREDICTED VORTEX HAZARD DISTANCE (NM) VS. AIRSPEED (KNOTS)

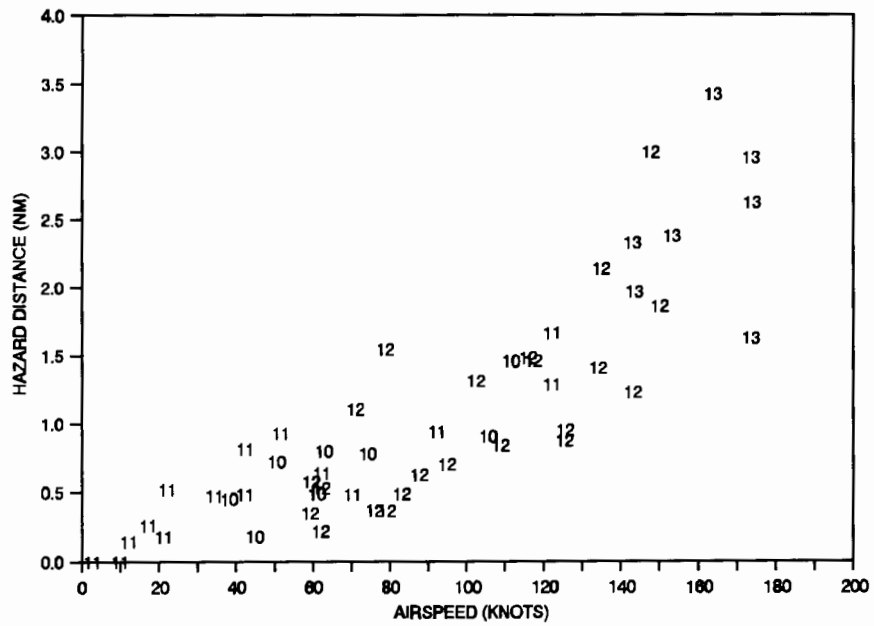


TABLE 4-3. PREDICTED HAZARD DISTANCE, D

<u>PARAMETER</u>	<u>S-76A</u>	<u>UH-60A</u>	<u>CH-47D</u>	<u>CH-53E</u>
Max. Hazard Distance D (nm)	2.6	1.9	1.6	3.4
Percentage Runs D > 2 nm	7	0	0	13
Median D (nm)	0.6	0.8	0.7	0.8
Median D, V < 80 knots	0.5	0.6	0.6	0.5
Median D, V > 80 knots	0.8	1.0	0.8	1.5

## 5. PROBE TESTING.<sup>1</sup>

The smoke marked helicopter vortices were probed by small airplanes to obtain a direct assessment of vortex hazard as a function of distance behind the generating helicopter. These tests were designed to provide data (1) for establishing Air Traffic Control separation criteria, (2) for comparison with theoretical calculations, and (3) for correlation with LDV data.

Appendix A lists the probe test sorties including the helicopters, probe airplanes, dates and times.

### 5.1 PROBE AIRPLANES.

The Beechcraft T-34C was the primary probe airplane. The Bellanca "Decathlon" airplane was used as a secondary probe airplane. Both have the required structural and performance characteristics for helicopter wake vortex probing. They are also similar in size to the small general aviation aircraft most likely to be affected by rotorcraft wake vortices. Two other aircraft, the Beechcraft T-34A and the Aero Commander 680E (a twin engine aircraft), were used in preliminary testing during the fall of 1985. Appendix A lists relevant parameters of the probe airplanes.

In previous probe tests studying the wakes from jet transport aircraft, the probe aircraft were instrumented to record aircraft dynamic response parameters. Unfortunately, funding and time limitations of the helicopter tests precluded instrumenting the probe airplanes with the flight test instrumentation required to obtain and record precise airplane motion and control responses. Although the lack of quantitative response data was an obvious disadvantage, it was largely overcome by using a test pilot with considerable experience in probing fixed-wing aircraft wake vortices in past FAA/NASA programs.

The first heavy aircraft separation criteria were based on the flight tests described in reference 9 which utilized the Air Force Lockheed C-5A and the Boeing 747 as wake generators. The first results from these tests were based on FAA and NASA pilot qualitative observations. Subsequent analysis of recorded airplane upset data gave almost identical results. Other flight tests (summarized in figure 25 of reference 10) showed consistency between the pilot's hazard assessment and distances where the measured maximum vortex-induced rolling moment was equal to the roll control capability of the probe aircraft.

### 5.2 PROBE TEST PILOT'S HAZARD CRITERIA.

Test pilot assessments are a valid measure of the wake vortex hazard due to the manner in which these assessments evolved. It is helpful to recall the procedures and criteria used in prior wake vortex research: The FAA and NASA test pilots involved in the first flights behind the C-5A, 747, and 707 airplanes had previously performed research in approach and landing characteristics and aircraft handling qualities in simulators, instrumented test airplanes, and variable stability airplanes. Prior to flight, the pilots were briefed by the FAA project test pilot on a generalized criteria to be used to determine the limits of upsets (roll, pitch, yaw, and any accelerations)

---

<sup>1</sup>The material of section 5 was summarized and presented at an earlier date in reference 8.

which, if encountered during an instrument approach at the published minimums of 200-foot ceiling and 1/2-mile visibility, would permit continuation of the approach rather than a go-around.

An additional criteria was to consider the amount of control used and the most severe airplane excursions which the pilots would tolerate in the most turbulent crosswinds in which they would attempt to land a particular airplane. For want of a more definitive criterion, a rule of thumb was evolved that suggested that the maximum acceptable bank angle at published minimums would be that obtained by dividing 1200 by the wingspan in feet. Thus, the limits for the Boeing 747 and Beechcraft T-34 (spans 196 feet and 34 feet respectively) would be, in approximate terms:

$$1200/200 = 6 \text{ degrees of bank for the B747}$$

$$1200/34 = 35 \text{ degrees of bank for the Beechcraft T-34}$$

For the purpose of these tests, the hazardous roll angle limit for evaluating the current probe tests was rounded off to 30 degrees.

### 5.3 TEST PROCEDURES.

The probe tests involved three aircraft:

- a. The wake generating helicopter equipped with a flow visualization system.
- b. The probe aircraft.
- c. The safety/photo/chase helicopter that flew near the probe aircraft, generally on the up-sun side.

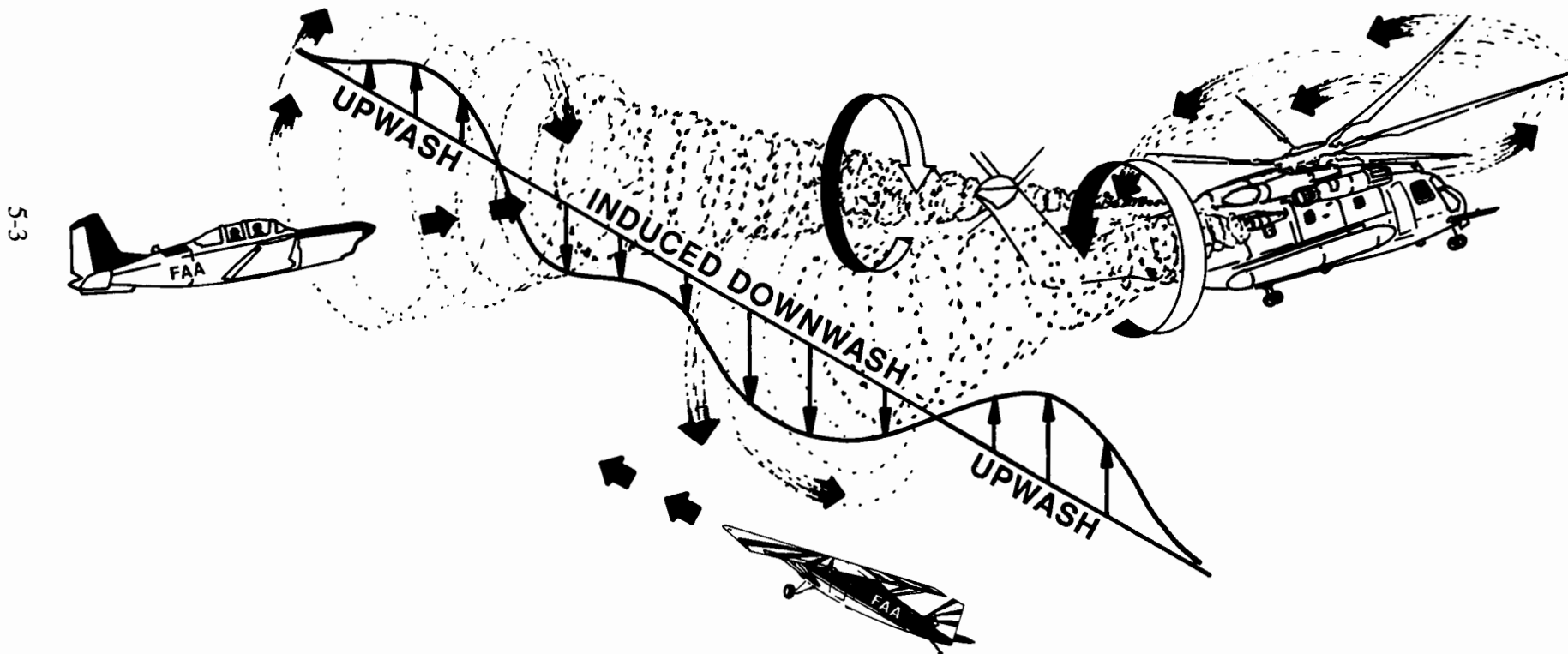
The three aircraft flew to the test altitude together and then set up the desired test pattern. A common radio frequency was used to coordinate operations and the airspace used for probing was selected so as to be free of conflicting air traffic.

The probe tests were conducted in level flight as well as in climbs and descents. All encounters were carried out at altitudes above 3000-feet AGL to allow room for recovery or bailout from severe upsets or structural failure.

#### 5.3.1 Vortex Probing Techniques.

The techniques developed during previous FAA/NASA fixed-wing vortex test programs were adapted to these tests. The two techniques used were parallel and crosstrack penetrations (figure 5-1).

**VORTEX PROBING TECHNIQUES**  
**T-34C ILLUSTRATES PARALLEL PROBE TECHNIQUE**  
**DECATHELON ILLUSTRATES CROSS TRACK PROBE TECHNIQUE**  
**(OBVIOUSLY CONDUCTED AT DIFFERENT TIMES BY EITHER AIRPLANE)**



5-3

FIGURE 5-1. VORTEX PROBE TECHNIQUES: PARALLEL AND CROSSTRACK PENETRATIONS

The parallel probing technique is the most obvious and involves flying into the vortex trail behind and below the helicopter, as visualized by the Corvus oil vapor or "smoke trail." This probing would commence at the maximum distance that the smoke trail was visible or where some airplane reaction was felt. At helicopter airspeeds above 70 knots, the probe airplane would attempt to probe at a constant separation distance until the vortex characteristics were fully evaluated. At slower helicopter airspeeds, the probe airplane could no longer fly the same speed as the helicopter and would fly its normal approach speed (70 knots for the Decathlon and 80 knots for the T-34C). In this case, the probing was necessarily conducted at decreasing separation until control was either completely lost or the pilots became concerned that they were in danger of overrunning the helicopter.

In conducting the probes, the vortex penetration angle was made as small as possible and entries were made from all directions (above, below, left, and right). Two different probe techniques were used in these tests; the first simulates an unexpected encounter.

- a. In a few cases the controls were kept neutral to observe the airplane's response.
- b. In most cases, the controls were applied against the upset and the upset angle, and the amount of control was recorded.

The aircraft flew a long race track pattern, with the long sides of the pattern oriented to give good contrast for viewing the vortex entrained smoke by the probe aircraft pilots. Flight along each long side of the pattern lasted for about four minutes and constituted one run. Since the wake generating helicopter could produce vortex visualization smoke for about one hour (except in the case of the S-76A) approximately 15 test runs could be flown for each sortie. On some occasions, particularly those involving slow helicopter airspeeds, the runs would last for over ten minutes, thus providing time for thorough vortex hazard evaluations.

The safety/photo/chase helicopter flew parallel to the probe airplane to document a vortex-induced upset when it occurred and to assist in determining test separation distance, to advise on the location of the vortex core, and to order the breaking off of the test run when the separation between helicopter and probe airplane became too small. A high test efficiency was attained in these parallel probes, and the probe pilots felt confident that they had explored the "hazard volume" very thoroughly for all test helicopters and that entry into both vortices had been adequately accomplished from almost all conceivable angles.

Crosstrack probing (figure 5-1) involved maneuvers which would allow the probe airplane to probe the vortex trail at angles up to 90 degrees. This was done especially in the near field when a parallel probing effort was broken off and a right or left 270-degree turn would be made to penetrate the vortex trail at acute and perpendicular angles to evaluate the severity of the vortices in angular penetrations. A series of "S turns" would be flown through the vortices to provide the pilots with an assessment of the energy in the vortex trail as a function of the distance behind the generating helicopter. The crosstrack penetrations resulted in a very short sharp vertical jolts (pitching excursions) rather than excursions in roll or yaw. These vertical impacts were of concern for structural damage rather than for loss of control. The information gained could be applicable for analysis of airplanes operating on runways perpendicular to helicopter flight paths.

### 5.3.2 Aircraft Separation.

The distance between the helicopter (vortex generator) and the probe airplane was obtained by different methods, depending on the available equipment installed in the aircraft:

<u>Probe Airplane</u>	<u>Distance Measuring Method</u>
T-34A	Air-to-Air Distance Measuring Equipment (DME) installed in both airplane and helicopter
All Others	Distances calculated by measuring the distance between the helicopter and the probe airplane to a DME station aligned with the flight path of both aircraft. Distance between the aircraft is the difference in these two distances.

The safety/photo/chase helicopter would also verify the distance between the aircraft and ensure that the probe aircraft did not overtake the generating helicopter. This was especially important at very close separation distances where the smoke density would obscure the probe pilot's vision of the helicopter wake vortex generator and would create the danger of the probe overrunning the helicopter at lower airspeeds.

### 5.3.3 Data Recording and Photo-Video Coverage.

Data was manually recorded and consisted primarily of separation distances, bank angle, estimates of yaw angles, control inputs, vertical accelerations, and general comments. There was a concerted effort to photograph the upsets from the safety/chase helicopter, from the ground (where possible), and from a fixed video camera in the probe airplane. Two pilots were generally used in the probe airplane in order to locate the vortex cores or maximum smoke density to record data.

Figures 5-2 and 5-3 represent typical ground based photographs of probe aircraft encounters. Although the dynamics of an encounter are obviously lost in a fixed image, both photographs illustrate the excursions in yaw that typically resulted during a probe test run. Unfortunately, obtaining ground photographs of upsets was problematic due to the extremely long ranges involved. No images of roll excursions could be located, though these excursions were well documented by video tape recorders aboard the safety/photo/chase helicopter.

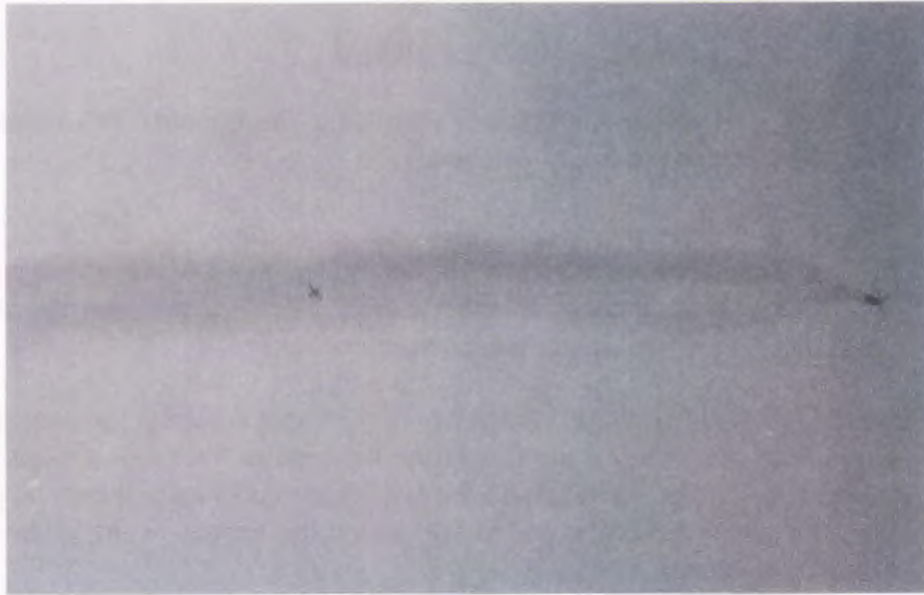


FIGURE 5-2. PROBE TEST (NOTE ASYMMETRY OF WAKE TRAIL)



FIGURE 5-3. PROBE TEST  
(NOTE PROBE AIRCRAFT EXCURSION IN THE VORTEX CORE)

## 5.4 TEST RESULTS.

### 5.4.1 Vortex Upsets.

The primary measurement of the probe tests is the observed bank angle generated by a vortex encounter. The two main variables effecting the encounter are the helicopter airspeed and the separation distance. Figures 5-4 through 5-7 present composite plots of bank angle versus separation distance for four helicopters, UH-1H, UH-60A, CH-47D, and CH-53E. Although three sorties were carried out, insufficient upsets were experienced behind the S-76A to generate a plot. Roll control data (section 5.4.2) indicated that the S-76A had less vortex hazard than the UH-1H; however, it should be noted that the most severe upsets behind the UH-1H occurred at airspeeds that were below the minimum speed permitted for the flow visualization system installed on the S-76A.

For small separation distances at low airspeeds, the upsets are more severe for slower airspeeds than for the higher airspeeds (see figure 5-4 for the UH-1H). At larger separations, the upsets tend to be more severe for higher airspeeds because the vortices formed at the lower airspeeds, though initially stronger, have already substantially decayed by the time that the probe airplane reaches them.

Figures 5-8 through 5-10 show plots of bank angle versus separation for selected bands of helicopter airspeed. A more consistent plot would be expected for a narrow band of airspeeds. Figures 5-9 and 5-10 represent the expected operational airspeeds for these helicopters. The effects of testing at different times of the day can be studied with these plots. The CH-47D data in figures 5-8 and 5-9 were collected on three days. On one day (points plotted as "Morning") the test period was 1055 to 1252 hours. The other days' testing started at 1300 hours. Figure 5-8 shows no difference between morning and afternoon. Figure 5-9 shows slightly greater upsets in the morning. The CH-53E data in figure 5-10 were also collected over three days. The morning data were collected very early in the day (0657 to 0907) and should have represented conditions of minimal atmospheric turbulence. The morning results were more consistent, but the afternoon results covered the same range of upsets. These observations suggest that the probe test results for these two helicopters were minimally affected by atmospheric turbulence.

### 5.4.2 Roll Control Power.

Criteria to establish separation distances have been greatly refined for instrumented airplanes (references 9 and 10). Basically, these involve comparing the maximum vortex-induced rolling moment to the total roll capability of the encountering airplane (the same ratio,  $f$ , used in equation 1-6). A direct determination of this relationship was made early one morning (10/8/86) under extremely stable weather conditions. The probe pilot was able to "balance" the small Decathlon probe airplane in a sideslip condition for several seconds in the wake of the S-76A helicopter and thus achieve a good assessment of the roll and yaw control power required to overcome the vortex-induced roll and yaw. These tests were conducted at 5,500-foot AGL, with airspeed for both aircraft decreasing from 110 to 70 knots. Approximately 1/2 aileron and rudder were required at 100 knots and increased to 3/4 at 80 knots, all at a distance of 1/2 mile behind the S-76A. At 70 knots and a separation of 0.4 miles, 3/4 to full control input was required.

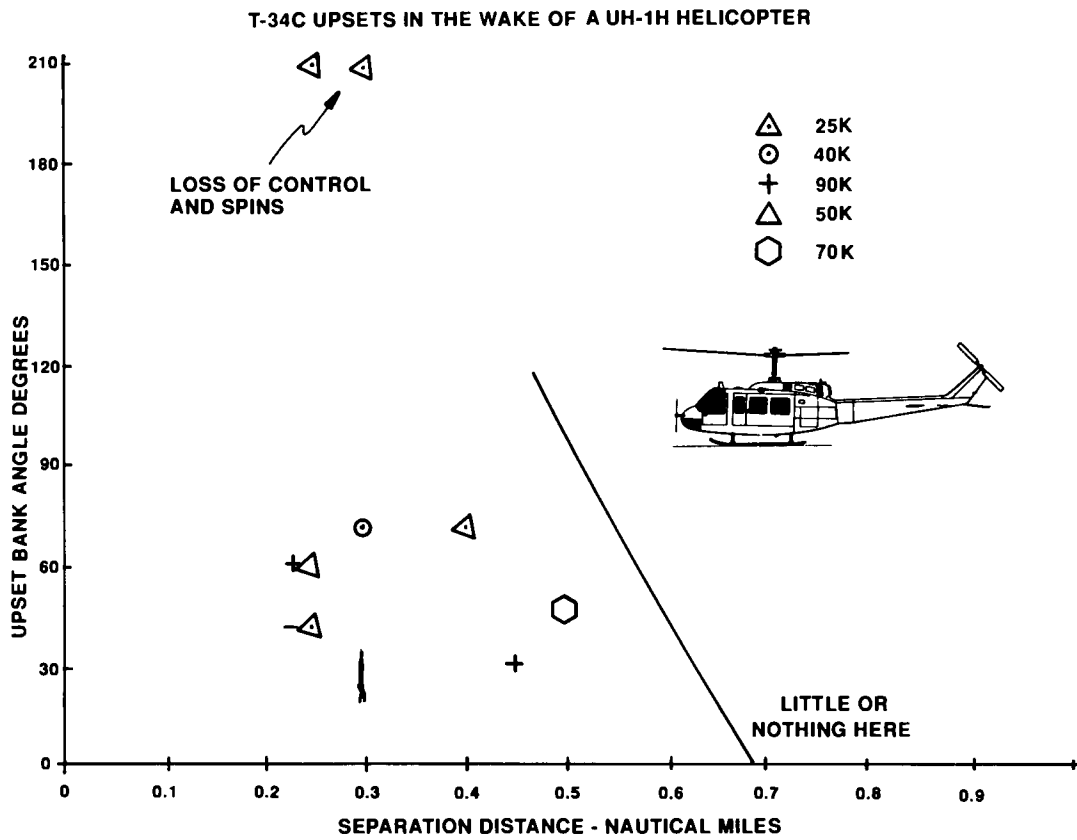


FIGURE 5-4. T-34C UPSETS IN THE WAKE OF A UH-1H HELICOPTER

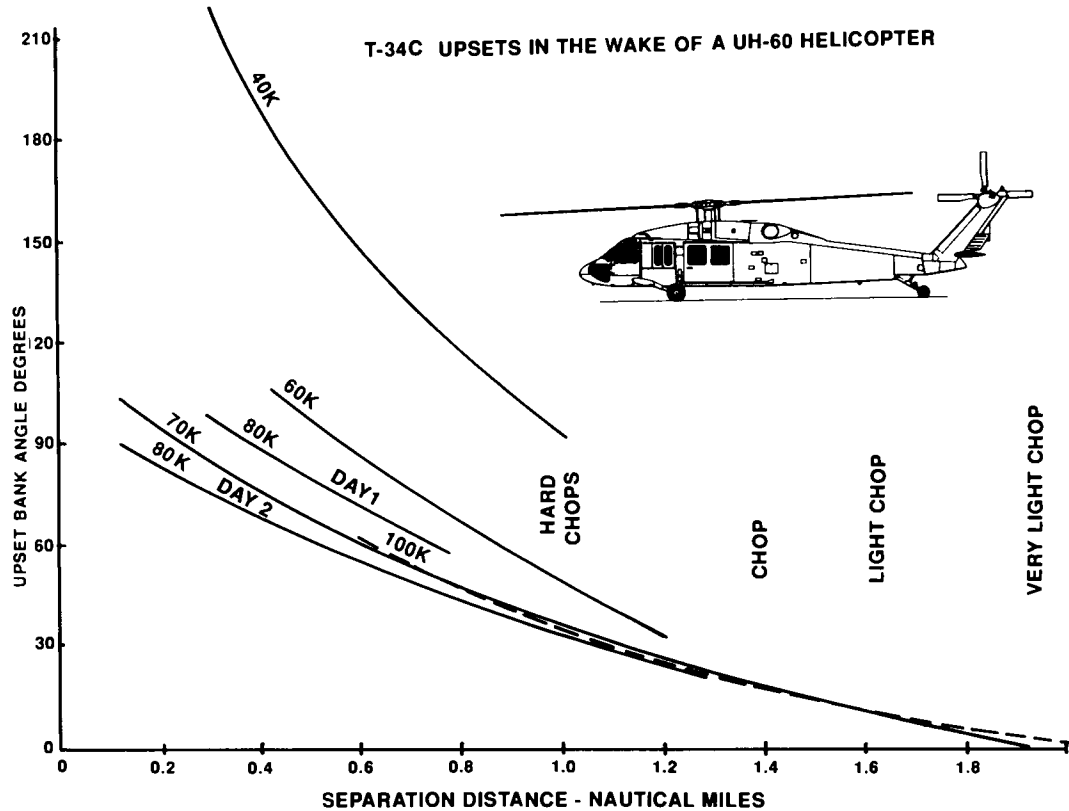


FIGURE 5-5. T-34C UPSETS IN THE WAKE OF A UH-60A HELICOPTER

6-5

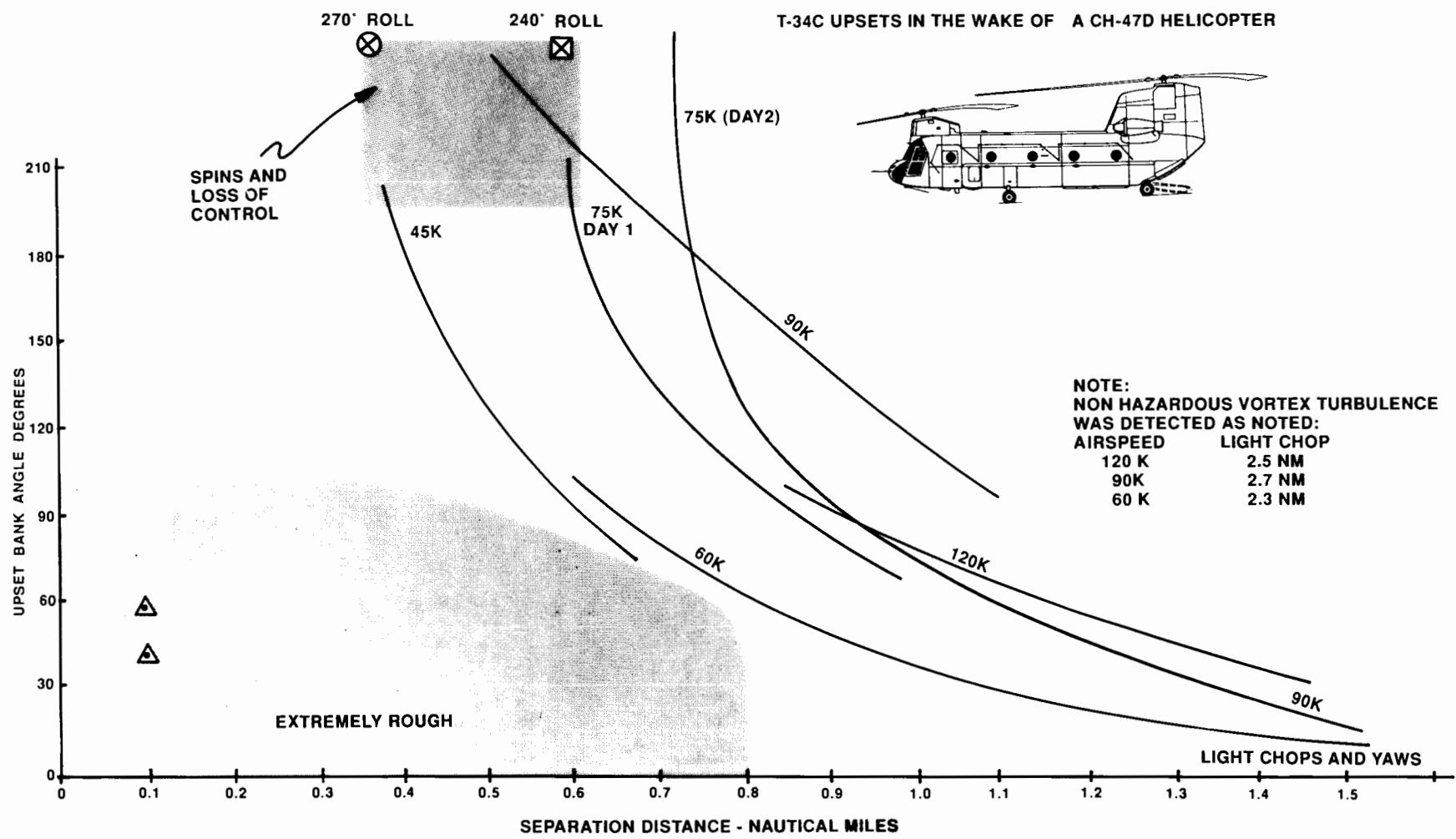


FIGURE 5-6. T-34C UPSETS IN THE WAKE OF A CH-47D HELICOPTER

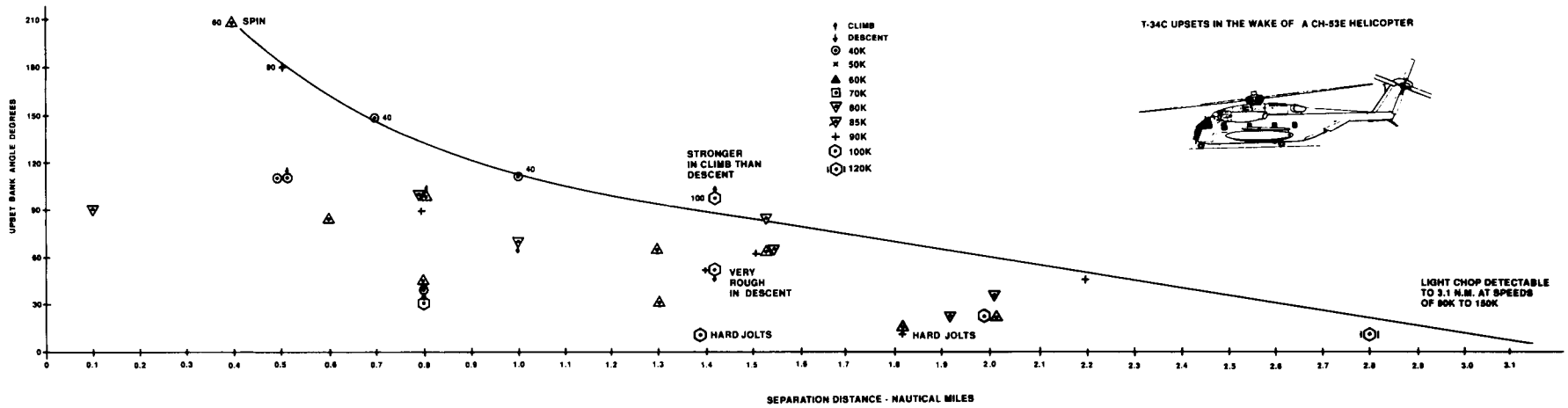


FIGURE 5-7. T-34C UPSETS IN THE WAKE OF A CH-53E HELICOPTER

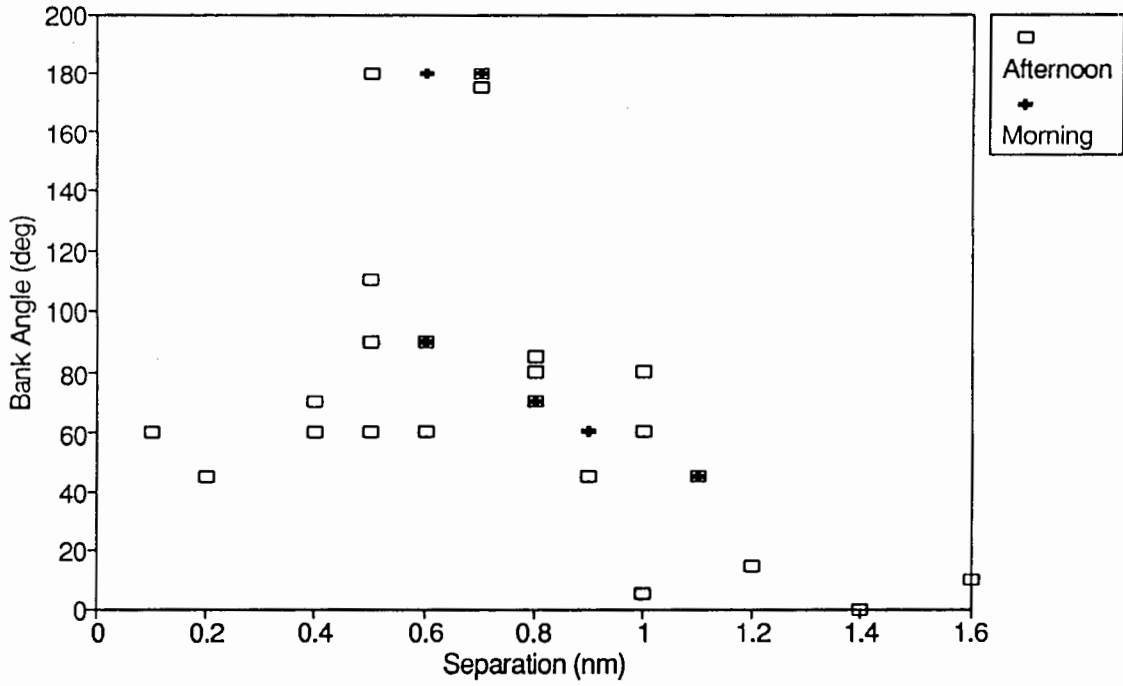


FIGURE 5-8. BANK ANGLE VS. SEPARATION FOR CH-47D (45-75 KNOTS AIRSPEED)

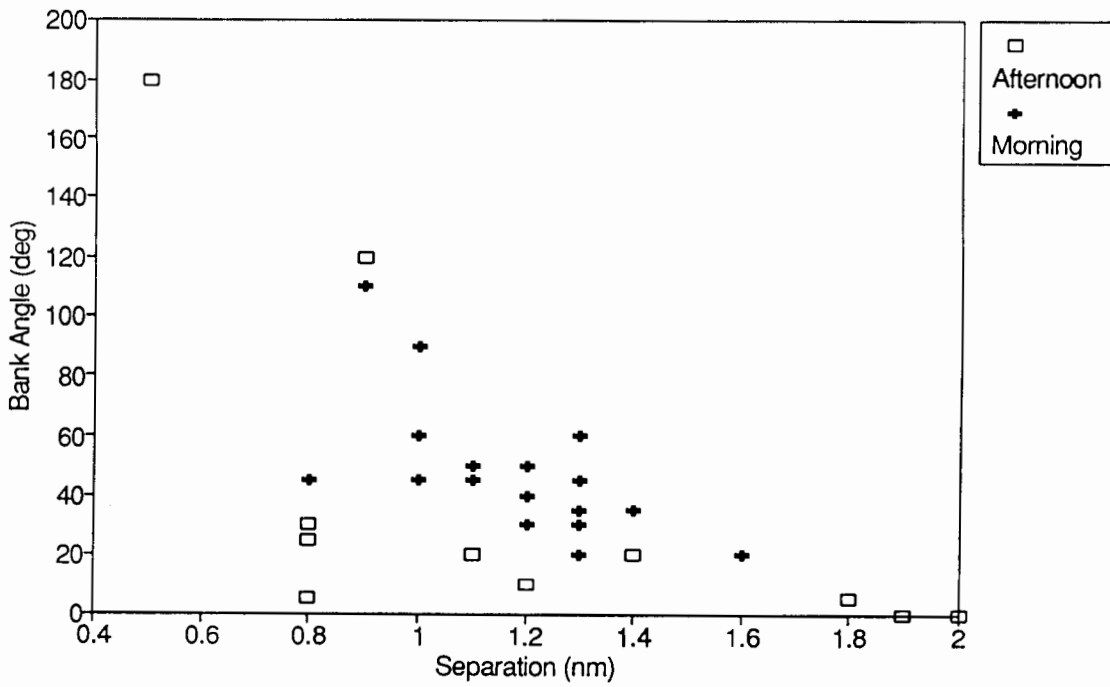


FIGURE 5-9. BANK ANGLE VS. SEPARATION FOR CH-47D (90-120 KNOTS AIRSPEED)

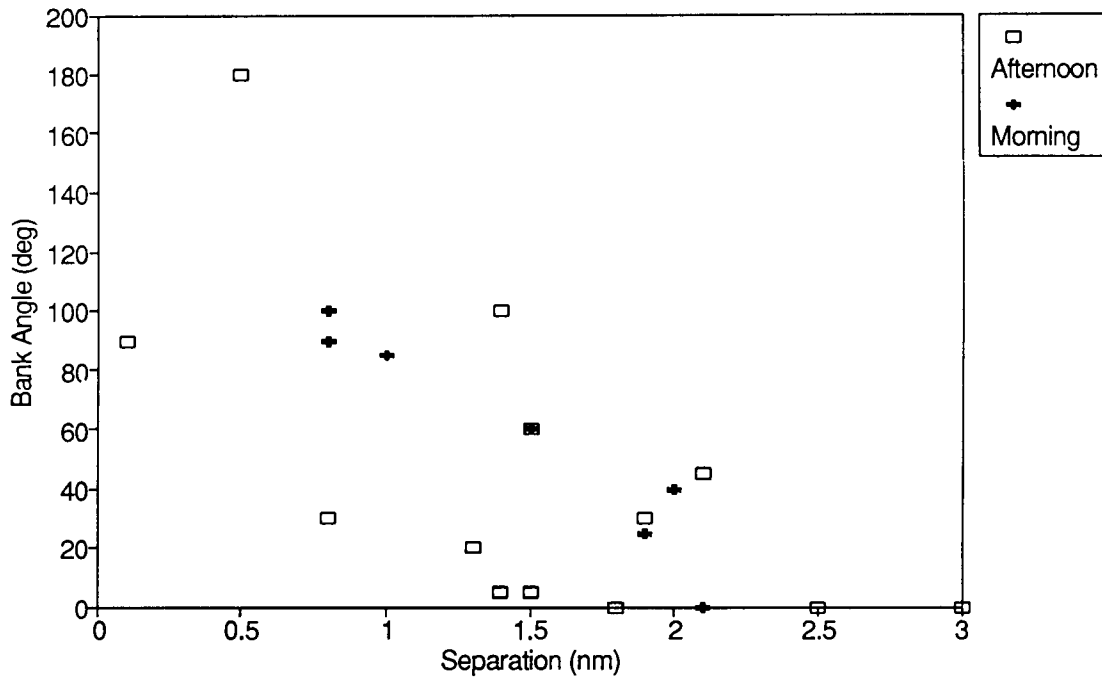


FIGURE 5-10. BANK ANGLE VS. SEPARATION FOR CH-53E (80-120 KNOTS AIRSPEED)

#### 5.4.3 Vortex Upset Hazard.

The capability of the vortex to cause an unexpected departure of the encountering aircraft from controlled flight depends on the size, weight, and speed of the “vortex generator” and on the vortex age. Operationally, the vortex age is reflected in terms of the distance of the encounter behind the vortex generating aircraft. The upset depends upon the type of encounter:

- a. In following flight, the upset is an abrupt roll, yaw, or pitch excursion. This type of upset is the primary concern of this report since it determines the longitudinal separation standards.
- b. In crossing flight, the upset is a rapidly varying vertical acceleration.

The following parameters are useful for establishing separation distances for small airplanes behind helicopters:

- a. Detectability — The maximum distance at which the influence of the helicopter’s wake vortex can be detected by the probe airplane.
- b. Hazard Distance — This is a distance, obtained under test conditions, which results in a nominal 30-degree bank upset.

Table 5-1 shows the results of this analysis for these two parameters. Note that the helicopter airspeed was not explicitly considered for this analysis but will be addressed in section 6.1.3.

In addition, table 5-1 lists a suggested minimum separation based on the probe tests alone. This final suggested distance includes allowances for pilot reaction time, more stable atmospheric conditions, and other operational factors.

TABLE 5-1. PROBE TEST SEPARATION DISTANCES (NM)

<u>HELICOPTER</u>	<u>MAXIMUM DETECTABILITY DISTANCE</u>	<u>MAXIMUM DISTANCE 30-DEG UPSET</u>
UH-1H	1.0	0.7
S-76A	1.0	0.7
UH-60	2.4	1.4
CH-47D	2.7	1.5
CH-53E	3.1	2.5

### 5.5 STRUCTURAL DAMAGE CONSIDERATIONS.

It should be noted that the probe tests were continued to less than 0.1 nm behind all helicopters with no evidence of structural damage although violent upsets, including loss of control and/or spins, resulted in most cases. Similar exposure behind large or heavy airplanes would be far more hazardous.

On two occasions the probe pilots abandoned a run while flying the light Bellanca Decathlon airplane in the wake of the CH-53E at a high speed because of an unexpected “shudder” or apparent flapping of the wings. This phenomenon was the first ever reported in probe testing and justified immediate abandonment of the runs because of concerns over exciting a catastrophic wing flutter mode. This reaction of the airplane to pulsing vortex inputs felt as though the vortices of individual helicopter rotor blades were still present or that some other rhythmic pattern was at work. Note that the wake flow visualization generally showed the effects of individual blade vortices.

### 5.6 QUALITATIVE OBSERVATIONS.

The following qualitative observations are offered; many concern comparisons with the wakes from fixed-wing aircraft. It should be noted that the probe tests of fixed-wing wakes made use of jet transport aircraft that have significantly larger weights and wingspans.

### 5.6.1 Visual Characteristics.

In forward flight, the port and starboard vortices appear distinctly different as seen by the density of the entrained smoke and the apparent cross-sectional areas of the vortex trails. On American single-rotor helicopters, the starboard vortex is produced by advancing rotor blades and the port vortex by retreating rotor blades. The retreating blades are at a higher angle of attack in order to produce as much lift as the advancing blades but at a much lower effective airspeed. The vortex behind the advancing rotor is smaller, tighter, and more coherent, especially as the forward speed increases above 80 knots. In almost every case, a distinct advancing blade vortex could be seen by the probe pilots or the photo/chase pilot. The vortex behind the retreating blade is characterized by a larger diameter, less dense smoke marking, and a greater cross-sectional area. This visual assessment was also reflected in the vortex effects on the probe airplane; the advancing blade vortex is generally more “solid” and results in more abrupt roll and yaw excursions than the retreating blade vortex.

The area “contaminated” by the helicopter wake turbulence is clearly larger than that of an airplane of comparable size and weight, especially at speeds below 70-80 knots.

### 5.6.2 Wake Vortex Trajectories.

The lateral distances between vortex centers appeared to expand initially and then to contract approximately eight rotor diameters behind the helicopter. Similarly, the densest smoke first descended behind the helicopter and then rose. These effects are likely due to the location of the smoke generators near the centerline of the helicopter. The smoke is first driven down by the rotor downwash. It is then swept outward and upward by the vortex flow field.

The helicopter wakes did not descend in the same predictable manner as do those for fixed-wing airplanes; the same effect was observed in the LDV data. The wakes appeared to be more buoyant. Helicopters are known to use much more engine power than an airplane to generate an equivalent amount of lift. Perhaps the injection of this resulting excess of hot engine exhaust is responsible for the apparent buoyancy of helicopter wakes.

The vortex core separation appears to increase in descending flight and to decrease in climbing flight.

### 5.6.3 Wake Vortex Hazard Volume.

The size of the cross-sectional area filled with smoke leads the probe pilots to believe that vortex size decreases with increased airspeed in the same manner as fixed-wing airplanes. The apparent vortex size is increased with helicopter size and weight as might be expected. In addition, an increased number of rotor blades appeared to increase the vortex size. The blade number effect was identified by comparing the wakes from two helicopters of the same weight, but different number of blades; the UH-1H with two blades and the S-76A with four blades. The observation suggests that increasing the number of blades acts to alleviate the vortex in the same way that flap extension does on fixed-wing airplanes. This effect is more evident when the tandem rotor system of the CH-47D is considered. The two rotors appear to interact to inhibit the vortex rollup process.

The visual observations of vortex size were correlated with the nature of the probe airplane upsets. At lower airspeeds there was a greater “hazard volume” and the direction of the upsets in roll and yaw was less predictable than for fixed-wing airplanes, i.e., exhibiting strong roll and yaw tendencies. As the high-speed vortices decayed, these coherent effects were replaced by sharp vertical “bumps,” which decreased in severity until either the smoke trail dissipated or until turbulence was no longer evident.

#### 5.7 PROBE TEST COMMENTS.

The probe tests were successful in spite of significant missing information. The lack of probe aircraft instrumentation and meteorological measurements at the test altitudes made interpretation of the test results less precise. Future probe tests should include such measuring capability.

Although the flow visualization was adequate for the probe testing, the tests would have been more efficient if more of the smoke had been injected into the vortex core (e.g., emitting the smoke closer to the blade tips).

The probe tests were carried out with aircraft that are representative of the smallest members of the general aviation fleet. Therefore, the results should be conservative for all airplanes likely to be affected by rotorcraft operations.



## 6. DISCUSSION.

### 6.1 COMPARISON OF LDV AND PROBE RESULTS.

#### 6.1.1 Hazard Definition.

The probe tests indicated that the hazard model utilized in the analysis of chapter 4, which was developed for fixed-wing wake vortices, may overestimate the hazard due to vortices generated by rotorcraft. Helicopter vortices that generated a predicted hazard by the criteria of this model were often felt only as light chop in the probe airplane.

This disagreement could be due to a number of factors. Rotorcraft vortices of similar strength to aircraft of similar weight and airspeed were seen to have significantly smaller spacing between vortices; perhaps the close proximity of the second vortex influences the response of the probe airplane. The turbulent nature of rotorcraft wake formation (the rollup of individual blade tip vortices) could also influence the effects of these vortices on probe aircraft. Finally, the disagreement could be due to the limitations of the flight tests themselves. LDV data were collected under conditions that were more favorable to vortex duration than the ambient conditions for the probe tests, though this possibility has largely been discounted by the analysis of the probe test results. Whatever the reason for the disparity between the predicted and observed hazard, some modification to the hazard model clearly must be incorporated to make it acceptably accurate for rotorcraft applications.

The LDV hazard duration and distances reported in section 4 were based on equation 1-10, used a value of the hazard parameter  $f$  of 0.5, and assumed a following aircraft speed of 130 knots. The probe hazard data, however, indicates that an “ $f$ ” value of 1.0 and an airplane speed equal to the helicopter speed (for airspeeds above about 75 knots) would be more appropriate. For lower helicopter speeds, an appropriate airplane speed has been determined to be 75 knots. The following sections will reflect this information and will present LDV data reprocessed with the value of  $f=1.0$ , so as to provide a more direct comparison with the probe tests.

#### 6.1.2 Hazard Distance.

In general, the probe tests gave good agreement with the LDV results in terms of vortex duration, although not in terms of hazard duration. Vortices were detected by the probe aircraft, usually in the form of mild chop, at distances that were consistent with LDV measurements, though the severity of the encounters was often much less than that predicted. A vortex was detected at distances predicted to be hazardous by LDV measurements, but its effects on the probe airplane were benign enough so as not to constitute a hazard (an uncommanded 30 degree or more bank) until the separation distance was substantially reduced.

The LDV data showing the longest lived vortices for the S-76A (tape 17) and the CH-53E (tape 12) were processed for  $f=0.5$  and  $f=1.0$  as discussed in section 6.1.1. Figures 6-1 and 6-2 compare the resulting predicted hazard distances for the S-76A and CH-53E, respectively. As shown in figure 6-1, the S-76A results are very sensitive to the value of the hazard parameter  $f$ . For  $f=1.0$ , the predicted hazard distance will disappear for airspeeds of 100 knots and above. In

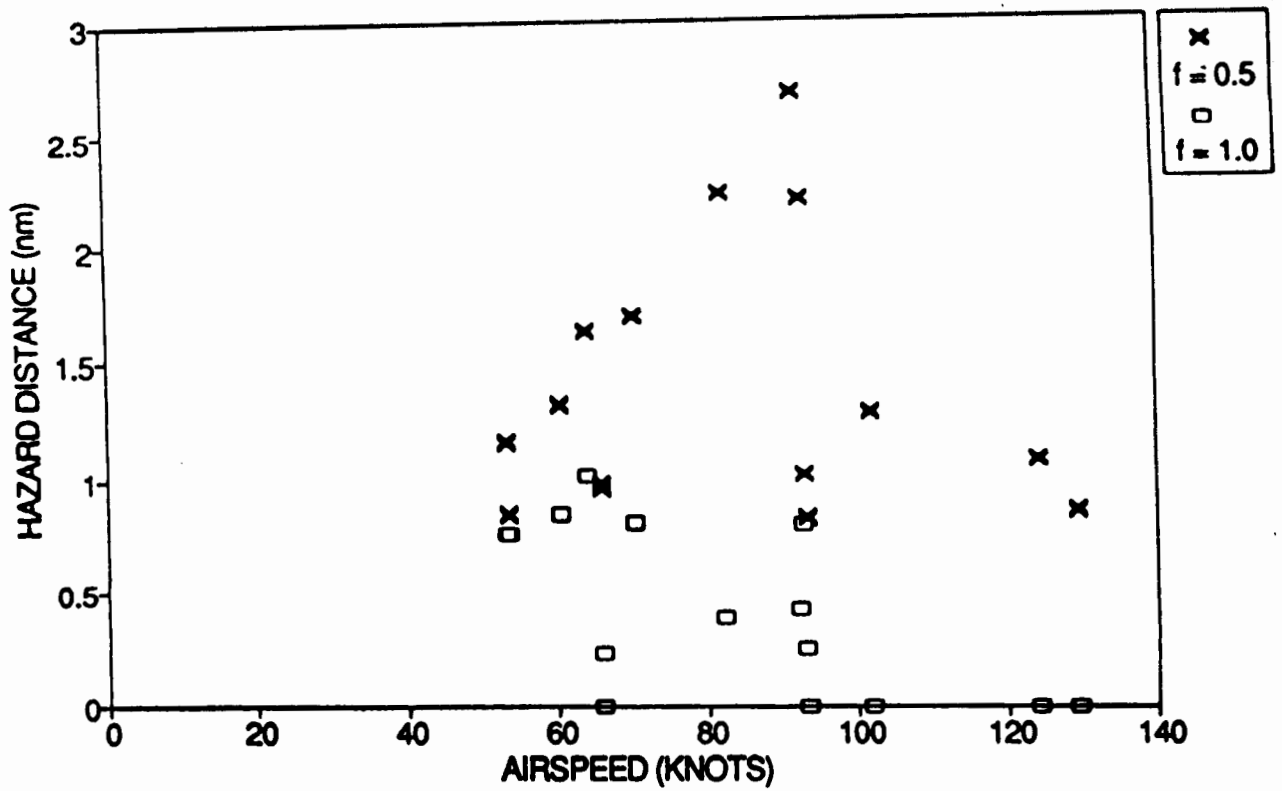


FIGURE 6-1. PREDICTED HAZARD DISTANCE VS. AIRSPEED FOR S-76A (TAPE 17)

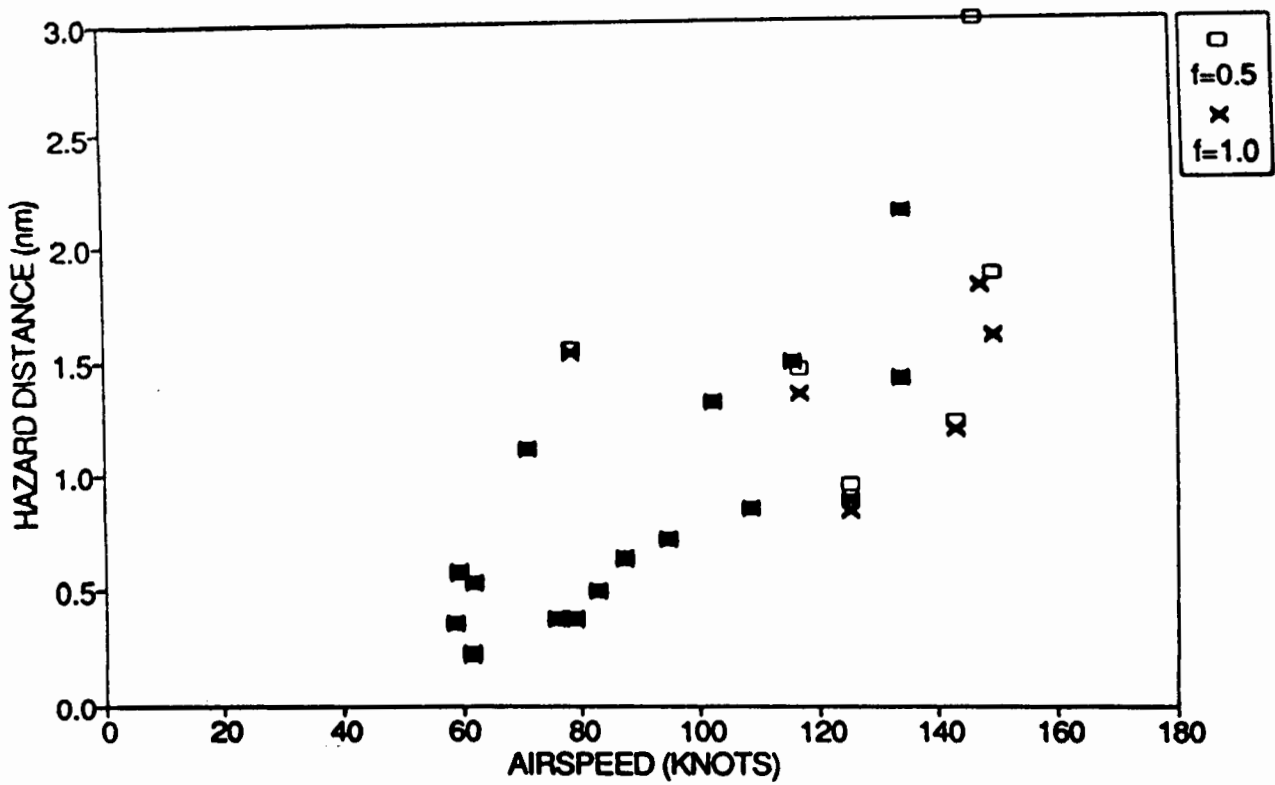


FIGURE 6-2. PREDICTED HAZARD DISTANCE VS. AIRSPEED FOR CH-53E (TAPE 12)

addition, the maximum predicted hazard distance for  $f=1.0$ , drops to 1.0 nautical mile. This value is substantially lower than the predicted value of 2.7 nautical miles reported in section 4 and is more in line with the hazard distances observed by the pilot in the probe airplane. As can be seen in figure 6-2, predicted hazard distances for the CH-53E are reduced (with  $f=1.0$ ) only for higher helicopter airspeeds. The reduction of predicted maximum hazard distance from 3.0 to 2.2 nautical miles (as hazard parameter  $f$  is increased) is significant; the initial lower vortex strengths at higher helicopter airspeeds permitted some sensitivity to the selected hazard threshold.

Table 6-1 compares maximum calculated hazard distances (based on LDV data) to the maximum observed hazard distances (based on probe tests). The LDV derived data is based on calculated distances reported in figures 4-17 through 4-20 and in figures 6-1 and 6-2. Probe test data are those reported in table 5-1. As can be seen, the LDV values calculated for the hazard parameter  $f=0.5$  are larger than the observed probe values. LDV hazard distances recalculated for a value of  $f=1.0$ , however, give good agreement with the probe results.

TABLE 6-1. HAZARD DISTANCE COMPARISON

<u>HELICOPTER</u>	LDV		<u>PROBE</u>
	<u>f=0.5</u>	<u>f=1.0</u>	
S-76A	2.7	1.0	0.7
UH-60A	1.9		1.4
CH-47D	1.7		1.5
CH-53E	3.4	2.6	2.6

### 6.1.3 Hazard Duration.

As discussed in the previous section, the probe aircraft was able to detect the presence of active vortices at distances with reasonable agreement to those predicted by the LDV measurements. The LDV analysis, however, predicted that these detections would be hazardous, which was not the case. This section will compare the actual probe results with the modified hazard model discussed in the previous sections.

The probe airplane upset bank angle generated by encounters with the vortices of CH-47D and CH-53E are presented in figures 6-3 and 6-4. Figures 6-3 and 6-4 show the "oldest" hazardous encounters (defined as a uncommanded bank of 30 degrees or greater) are for vortex ages of 60 and 95 seconds, respectively. The comparable maximum hazard duration calculated from LDV measurements (figures 4-15 and 4-16 generated by the application of equation 1-10 with  $f=0.5$ ) would be 68 and 77 seconds for these two rotorcraft. The probe tests, therefore, reveal a slightly shorter maximum vortex hazard duration for the CH-47D and a substantially longer vortex hazard duration for the CH-53E than that calculated by LDV measurements.

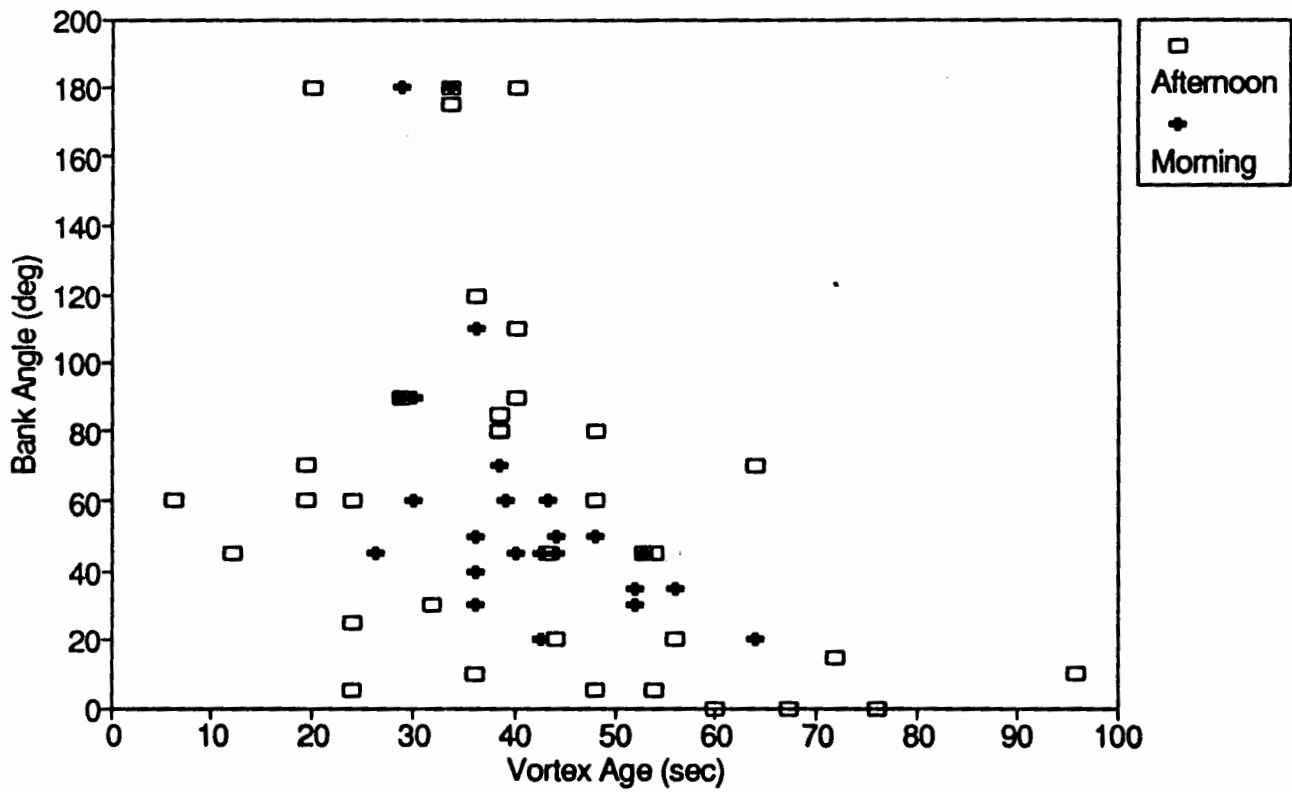


FIGURE 6-3. PROBE UPSET BANK ANGLE VS. VORTEX AGE FOR CH-47D

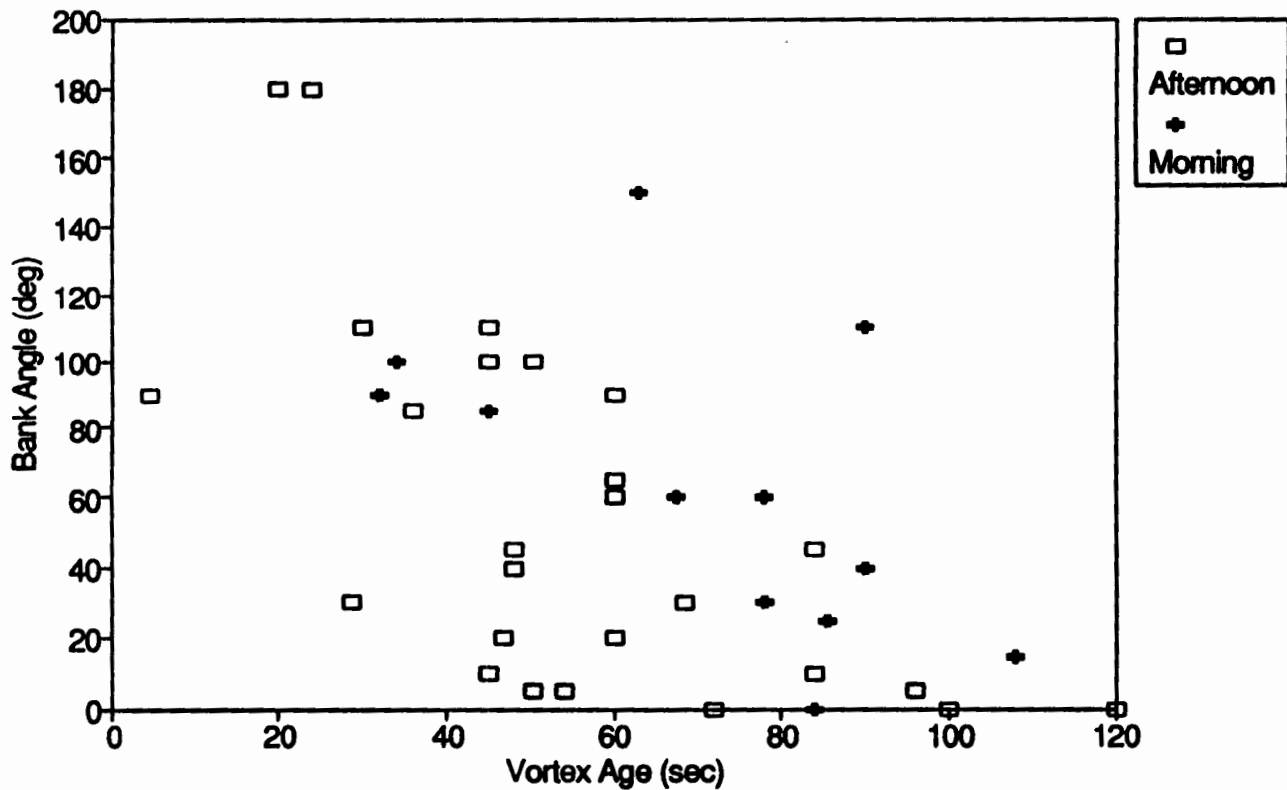


FIGURE 6-4. PROBE UPSET BANK ANGLE VS. VORTEX AGE FOR CH-53E

Figures 6-5 and 6-6 depict the calculated hazard duration for the S-76A and CH-53E using the reprocessed LDV data depicted in figures 6-1 and 6-2. As seen in the figures, the calculated hazard duration for the S-76A drops from 105 to 58 seconds when the value of the hazard parameter  $f$  is increased from 0.5 to 1.0. In contrast, the maximum calculated hazard duration for the CH-53E drops only slightly when this increased value for the hazard parameter is employed.

#### 6.1.4 Vortex Core Spacing.

LDV and probe interpretations differed in the effects of climbs and descents on vortex spacing. Probe pilots (and a ground observer) saw the vortex spacing to be reduced with helicopter climb and to expand on descent relative to straight and level flight. The LDV data (see figures 4-9 through 4-12) indicate the opposite; that vortex spacing increases with climb and decreases with descent. As a result, no definitive conclusion can be made as to the effects of climbs and descents on vortex spacing.

### 6.2 COMPARISON WITH CALCULATIONS.

The most direct comparison between LDV-based calculated hazard and the actual hazard as observed by the probe airplane occurred with the S-76A helicopter and the Decathlon airplane. As discussed in section 5.4.2, the pilot of the Decathlon was able to balance the induced roll from one of the S-76A's wake vortices with the roll control of the aircraft and was able to remain in this balanced condition for an extended period for several different helicopter airspeeds at a separation distance of 0.4 to 0.5 nautical mile (740-930 meters). These observed "roll balances" can be compared with the predictions of equation 1-9, as demonstrated in the following table. Note that conversion to metric units is required for consistency.

$$f = 3KWFn(b_g/2r_c)/(\pi\rho\hat{\rho}b_e b_g V_c V_g) \quad 1-9$$

where:

<u>Variable</u>	<u>Parameter</u>	<u>Value</u>
K	Span load factor	1.0
W	Generator weight	9000 lbs (40090 Newtons)
$\pi$	Pi	3.14159
$b_g$	Generator rotor diameter	44 ft (13.41 meters)
$r_c$	Vortex core diameter	1.31 meters (10% $b_g$ )
$b_e$	Encountering A/C span	32 ft (9.8 meters)
$\rho$	Atmospheric density	1.25 kg/m <sup>3</sup>
$\hat{\rho}$	Nondimensional roll factor	0.08
$F(b_g/2r_c)$	$F=1-(r_c/r)ARCTAN(r/r_c)$	0.64

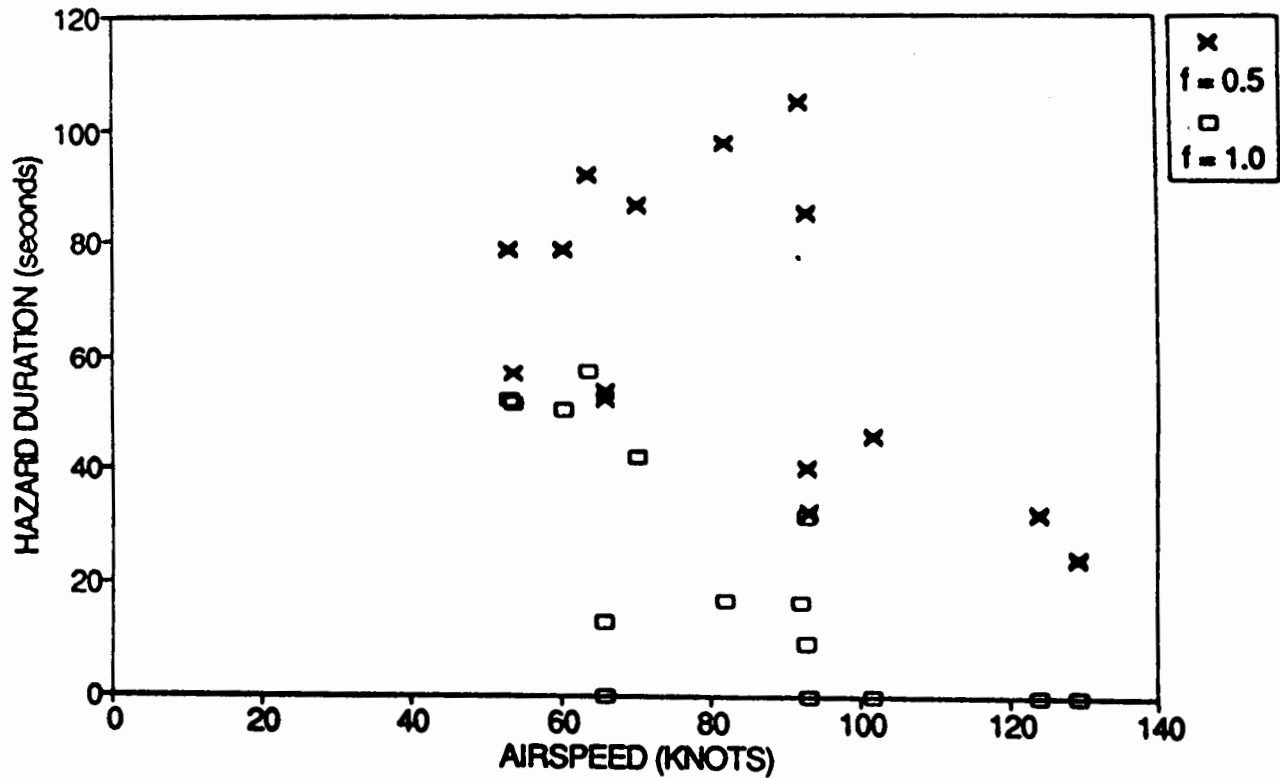


FIGURE 6-5. RECALCULATED HAZARD DURATION VS. AIRSPEED FOR S-76A

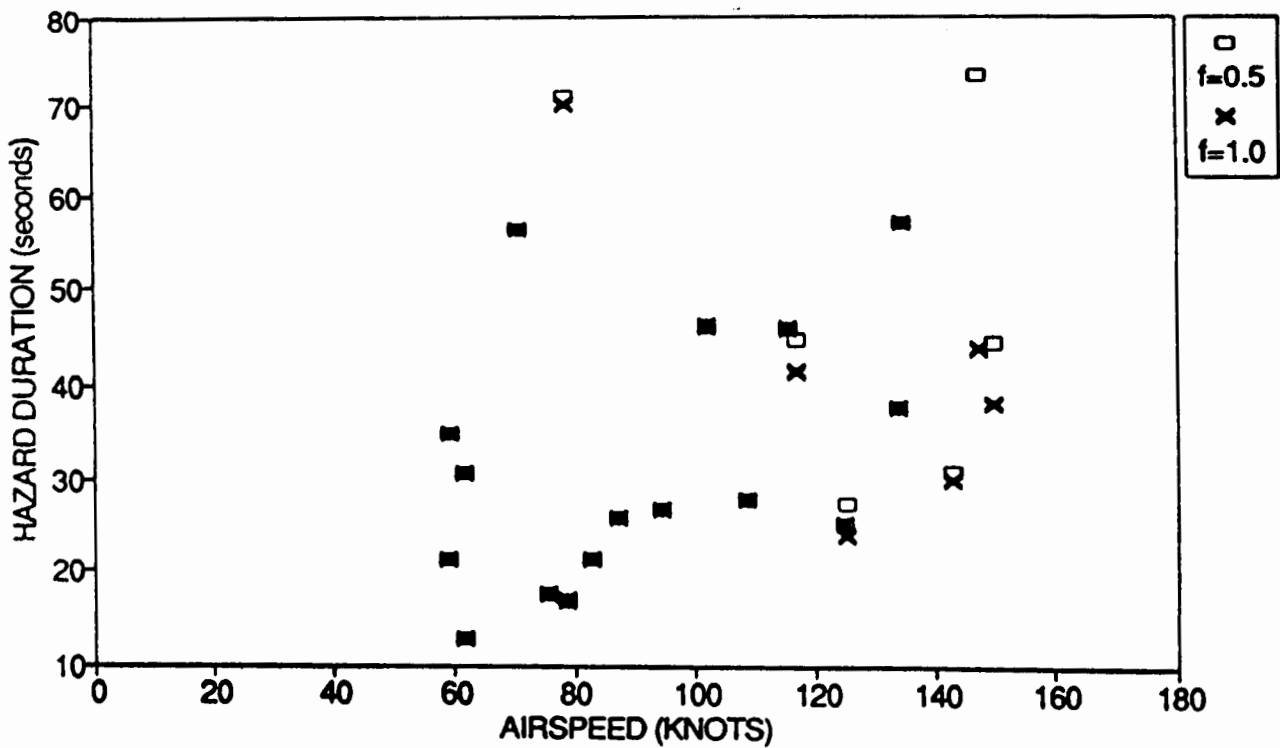


FIGURE 6-6. RECALCULATED HAZARD DURATION VS. AIRSPEED FOR CH-53E

Table 6-2 compares the observed and calculated values of the variable  $f$  and the ratio between them. The observed value of  $f$  is derived from the percentage of available control actually used to hold the aircraft in equilibrium under the influence of the encountered wake vortex. For example, if the aircraft is in equilibrium inside the wake vortex with an applied stick deflection of 75 percent,  $f$  is defined to be 0.75 under these conditions. The calculated value of  $f$  is generated by the application of equation 1-9, as discussed above, and assumes a vortex decay of 20 percent by the time of encounter. The agreement between the observed and calculated hazard outlined in the table is remarkable, considering that the induced roll measurement is subjective and that the hazard model makes numerous assumptions.

TABLE 6-2. COMPARISON OF OBSERVED AND CALCULATED ROLL MOMENTS

Sikorsky S-76A and Bellanca Decathlon			
Airspeed $V_g=V_e$	100 kts (52 m/s)	80 kts (42 m/s)	70 kts (36 m/s)
Vortex age*	18 sec	22 sec	19 sec
Probe $f^{**}$	0.5	0.75	1.00
Model $f^{***}$	0.7	0.89	1.16
Ratio: Model/Probe	1.4	1.2	1.2

\* Time separation between passage of vortex generating helicopter and arrival of probe aircraft at time of encounter.

\*\* As determined by the percentage of applied corrective control: 50% stick equates to an  $f=0.5$ .

\*\*\* As calculated via equation 1-9 and assuming a 20% vortex decay at the time of probe aircraft encounter.

Table 4-1 presents a comparison of the LDV derived vortex strength measurements to the calculated values determined from equation 1-1. In contrast to the good agreement between the probe tests and the adjusted hazard model, the strengths indicated from the LDV measurements were considerably greater than those predicted from those calculated via equation 1-1. Possible explanations for these differences have been discussed in sections 3.8 and 4.1.

### 6.3 OPERATIONAL CONSIDERATIONS.

Before this test program was initiated, many people held the misconception that rotorcraft do not generate cohesive wake vortices. The image of figure 6-7 conclusively dispels this misconception. Others suggested that rotorcraft wake vortices would decay much more quickly than vortices generated by fixed-wing aircraft due to the turbulent nature of their formation (the rotorcraft wake vortex is composed of the rolled up tip vortices of the individual rotor blades). Still others believed that the strength of rotorcraft wake vortices could be predicted with accuracy using the fixed-wing wake vortex equation (equation 1-1) and that rotorcraft wake vortices could be generated at low forward airspeed which rivaled the strength of the wake vortices generated by heavy fixed-wing aircraft.



FIGURE 6-7. S-76A WAKE VISUALIZATION

### 6.3.1 Current Separation Standards.

The critical location for wake vortex encounters for aircraft on approach is between the middle marker and touchdown. When an encountering aircraft is further from touchdown while on the glideslope or approach path, wake vortex encounters are (1) less likely because of the height available for normal vortex descent and (2) less dangerous because of the increased altitude available for recovery from a vortex-induced upset.

The separation standards currently in use for fixed-wing aircraft are defined for aircraft classes delineated by maximum certificated gross takeoff weight (MCGTOW). Table 6-3 outlines the weight limits that classify fixed-wing aircraft as heavy, large, and small.

TABLE 6-3. WAKE VORTEX CLASS WEIGHT LIMITS

<u>CLASS</u>	<u>WEIGHT LIMITS (MCGTOW)</u>
Heavy	More than 300,000 Lbs.
Large	12,500 to 300,000 Lbs.
Small	Less than 12,500 Lbs.

Table 6-4 lists the current separation standards between fixed-wing aircraft.

TABLE 6-4. IFR WAKE VORTEX APPROACH SEPARATION STANDARDS  
(Nautical Miles)

<u>FOLLOWING AIRCRAFT CLASS</u>	<u>LEADING AIRCRAFT CLASS</u>		
	Heavy	Large	Small
Heavy	4	3	3
Large	5	3	3
Small	6	4	3

It should be noted that the above standards are based on separation distance, not on separation time, though time is a more accurate measurement of the duration of the wake vortex hazard. The relationship between vortex hazard duration and hazard distance is straightforward. If vortices remain hazardous for a certain time  $T_H$ , the safe separation  $D_s$  is related to the approach airspeed  $V$  by the following relationship:

$$D_s = VT_H \quad (6-1)$$

For a fixed hazard duration,  $T_H$ , the safe separation distance is clearly proportional to airspeed. Lower airspeeds will thus allow closer separation distances from a wake vortex standpoint. Equation 6-1 is based on the assumption that both aircraft are flying at constant, equal airspeeds. Clearly, if the approach speeds of the aircraft are different, the safe separation distance (as well as the physical distance between the aircraft) will increase or decrease (depending on the relative position of the faster aircraft) with the aircraft position along the approach path.

### 6.3.2 Decelerating Approach.

Helicopters normally decelerate during their landing approach. Typically, an S-76 helicopter will initiate an ILS approach at 120 knots, decelerate to 70 knots at the runway threshold, and touch down at a maximum of 40 knots. This same helicopter flying a steep MLS approach (6 degrees) to a helipad near the runway may initiate the approach at 90 knots, decelerate to 60 knots ( $V_{mini}$ ) by the decision height, and complete the approach at near zero airspeed. This deceleration will generate two adverse effects on the wake vortex hazard. First, the strength and the size of the helicopter wake vortex both increase as the airspeed of the helicopter decreases. Second, the distance between the helicopter and a following fixed-wing (and faster, fairly constant speed) airplane is constantly reducing. Under these conditions, it is important that the safe separation between the helicopter and any following traffic (as defined by equation 6-1) be maintained up to the point that the helicopter has landed. Thus, a larger separation than that specified by equation 6-1 will have to be maintained along the glideslope or approach path so that this minimum separation distance is not reached before the helicopter has landed.

The loss in separation distance arising from a decelerating approach can be estimated. Following the example of reference 11, a typical approach velocity profile can be modeled as a constant 0.05 g deceleration. The loss in separation distance,  $S$ , for such a deceleration will depend on

the initial approach airspeed ( $V_o$ ) and the final airspeed ( $V_f$ ) which is achieved when the helicopter leaves the runway at the completion of its approach and/or landing:

$$S = (V_o - V_f)^2/2a \quad (6-2)$$

where  $a = 0.05g$  (deceleration)

If  $V_o$  is 90 knots and  $V_f$  is 40 knots,  $S$  will assume a value of 0.4 nautical mile, a relatively minor correction. If  $V_f$  drops to 10 knots before turnoff,  $S$  will rise to a more significant 0.9 nautical mile; clearly the nature and final values of the deceleration will have a strong effect on the required additional separation distances. For practical applications, it is felt that the addition of an extra 0.5 nautical mile initial separation is adequate to compensate for the continuously decreasing separation discussed.

### 6.3.3 Comparison with Fixed-Wing Vortices.

#### 6.3.3.1 Initial Strength.

LDV data indicate that the strength of wake vortices generated by large rotorcraft cannot be accurately predicted by the fixed-wing vortex strength equation (equation 1-1) for helicopter airspeeds below about 50 knots. The data show that the wake vortex will reach its maximum strength as helicopter airspeeds approach the 40-60 knot range and that this strength will fall off as airspeeds drop below about 40 knots. LDV data collected for smaller rotorcraft showed the same phenomenon, but shifted downward in airspeed; maximum vortex strength for these helicopters was observed at airspeeds around 40 knots. LDV data collected for the tandem rotor CH-47 showed a wake vortex strength that was approximately 2/3 that which would be generated by a single rotor machine of equivalent weight under identical conditions.

Probe tests indicated that rotorcraft wake vortices resemble fixed-wing vortices. This resemblance became especially evident when rotorcraft airspeeds were 80-100 knots and above.

#### 6.3.3.2 Vortex Decay.

Table 6-1 illustrates that both LDV and probe tests give similar results for wake vortex hazard durations, and hence vortex decay, when appropriate factors are used.

The LDV data showed a series of S-76A wake vortices which lasted longer than those of all of the larger helicopters. Two possible explanations for this anomaly are:

- a. Unique meteorological conditions existed on the day that were conducive to the abnormally long vortex lifetimes that were recorded. These conditions were not observed during tests for the other helicopters.
- b. Vortex decay may be accelerated for helicopters with higher disk loadings or a greater number of blades. Since larger helicopters typically have larger disk loadings and greater blade numbers, their vortices may intrinsically decay more rapidly, leading to a limit on vortex lifetime.

The longer lasting CH-53E vortices observed during the probe tests (see figure 6-4) give some added credence to the first possibility; perhaps there was an abnormally stable atmosphere at the probe test altitude for this series of runs. Probe tests showed that the probe aircraft response was reasonably independent of atmospheric conditions; hazard distance (and hence vortex duration) was shown to be primarily dependent on rotorcraft type and airspeed. A conclusive determination of the nature of these extended lifetimes is not possible at this time.

#### 6.3.4 Uncontrolled Airports.

Operations at uncontrolled airports present potential wake vortex hazards when rotorcraft are mixed with small fixed-wing traffic. Wake vortex problems have been noted when medium sized rotorcraft operate at airports where relatively low performance, light, single, and multi-engine general aviation aircraft are operating. Typical separation distances between light aircraft at uncontrolled fields can be as little as 3000 feet, roughly 30 seconds elapsed time at standard pattern airspeeds.

Medium weight helicopters, such as the S-76A and UH-1, can easily fit into the traffic pattern at smaller uncontrolled airports and can leave active, potentially hazardous vortices for up to 90 seconds. Separations for small aircraft behind these rotorcraft should therefore be in the 90-second range. Larger helicopters such as the CH-47D and CH-53E can also fit into these uncontrolled fields and were observed to have longer hazard times. A 120-second separation should be adequate for operations behind these rotorcraft. Likewise, takeoffs for small aircraft behind helicopters should use the same time as currently specified for operations at uncontrolled airports.

Information on the wake vortex hazard behind these rotorcraft, including delineation by class, should be included in the Airman's Information Manual and the Wake Vortex Advisory Circular.



## 7. CONCLUSIONS.

The following conclusions were drawn from this investigation.<sup>1</sup>

1. From the data generated, helicopters may be separated into two categories based on maximum gross takeoff weight, with the division in classes occurring at 25,000 lbs.
2. Helicopter vortex circulation is seen to follow the circulation equations for fixed-wing aircraft (equations 1-1 and 1-2) for helicopter airspeeds above 40 knots. In this speed regime, which is well above the area of rotorcraft translational lift, the wake vortex circulation as measured by the LDV is seen to be inversely proportional to airspeed and directly proportional to helicopter weight.
3. Vortex circulation, as measured by the LDV, diminishes with decreasing airspeed for helicopter airspeeds below 40 knots. At these lower speeds, the wake vortex structure begins to break down and changes to a distinct downwash flowfield that contains the individual tip vortices of each rotor blade.
4. The advancing-blade vortex is stronger, has a smaller core radius, and is more hazardous than the retreating-blade vortex. For American standard helicopters, the advancing blades are on the starboard side of the helicopter.
5. The observed vortex duration depends strongly on ambient meteorological conditions. A variance of up to 300 percent was observed for vortex duration on those days most conducive to vortex persistence and duration compared with those observed on typical days.
6. Stronger vortices appear to decay more rapidly than weaker vortices under similar meteorological conditions.
7. The maximum duration of vortex life as measured by the LDV shows the following:

<u>Aircraft</u>	<u>Max. Duration</u>
CH-53E	75 Seconds
CH-47D	70 Seconds
UH-60A	75 Seconds
S-76A	105 Seconds

---

<sup>1</sup>Hazards associated with the rotor wash generated by helicopters in hover or in air taxi were not a part of this investigation.

8. The maximum distance of vortex life as determined by probe tests shows the following:

<u>Aircraft</u>	<u>Maximum Detectability</u>
CH-53E	3.1 nm
CH-47D	2.7 nm
UH-60A	2.4 nm
S-76A	1.0 nm

9. The core size was seen to increase as the helicopter weight increased. Typically, helicopters with higher gross weight, larger rotor diameters, and larger numbers of rotor blades generated vortices of larger core diameters. This increase in vortex core size could be due to the increased size of the generating rotor disk or could be analogous to the effects of extending the flaps on fixed-wing aircraft. The interference generated by a larger number of individual blade vortices could mimic the interference caused by the introduction of a separate flap vortex on fixed-wing aircraft.
10. Probe tests and ground observations of flow visualization revealed an increased vortex core separation between vortices in descending flight and a decreased core separation in climbing flight.
11. Probe tests revealed that helicopter vortices did not descend in the same predictable manner as for fixed-wing aircraft. Some vortices descended; some remained level; and some initially descended, leveled off, and ascended above the altitude of the generating helicopter.
12. Probe tests showed that encounters with helicopter vortices generated much more yaw response than those generated by fixed-wing aircraft.
13. Flight tests revealed an unexpected type of aircraft response to a wake vortex, which was felt as a rhythmic slapping of the aircraft and sometimes unaccompanied by any organized roll or yaw. This response often resembled "chop" and could be due to probe aircraft interactions with individual blade vortices, though the causal mechanism should be more carefully studied. In at least one encounter, this response resulted in excessive flapping of the wing structure of the probe aircraft. Should this response generate vibrations at frequencies close to any natural mode of the wing or tail assembly of an encountering aircraft, structural failure could result.
14. The probe tests indicate that the value of the wake vortex model parameter  $f$  should be set at 1.0 rather than the value of 0.5 used in much of the analyses of the LDV measurement data. Good agreement was observed between the steady-state encounters and the wake vortex encounter model.

15. *The measured vortex strength for a tandem-rotor helicopter appears to be only 2/3 of that for a single-rotor helicopter with the same weight and rotor diameter.*
16. The residual nonhazardous “roughness” generated by a tandem-rotor helicopter is evident to the probe aircraft at a distance that is well beyond the hazard area for this configuration.
17. The use of full-scale probe airplanes has been shown to be a safe, efficient, and conclusive way to determine separation distances for fixed- and rotary-wing airplanes. It is considered mandatory to include fully instrumented test aircraft and sophisticated meteorological measurements for all future testing.
18. The quality of the signal received by the LDV and the calculated results were found to be dependent on the density of the aerosols in the vortex wakes being scanned.



## 8. RECOMMENDATIONS.

1. For air traffic control (ATC) separations standards, helicopters should be placed into two weight classes, with a dividing line of 25,000 pounds maximum takeoff gross weight (MGTOW). Adjective classification should be assigned by the FAA, e.g., "Helo Light" or "Helo Small" for helicopters under 25,000 lbs and "Helo Medium" or "Helo Large" for helicopters over 25,000 lbs (MGTOW).
2. ATC procedures should be established for rotorcraft making decelerating final approaches when mixed with fixed-wing traffic.
3. Characteristics of rotorcraft vortex descent should be more thoroughly investigated.
4. Future vortex probe tests should utilize fully instrumented probe aircraft.
5. Future wake vortex flight tests should include measurements of atmospheric stratification, wind shear, and turbulence at the test flight altitude.
6. The dynamic response of a rotorcraft to fixed- and rotary-wing generated wake vortices should be investigated.
7. Hazards associated with rotor wash generated by helicopters in hover or in air taxi operation should be investigated. In the absence of encounter measurements for the case of hover flight, it is recommended that small airplanes, at the same altitude and downwind of a hovering helicopter, maintain at least 500 feet of separation.



## 9. REFERENCES.

1. Ahers, R.H. and Hiering, W.A., "Evaluation of the Wake of an S-58 Helicopter," Final Report, Project No. 348-011-01V, July 1963, FAA, SRDS, Atlantic City, NJ.
2. Sullivan, T., Hallock, J., Winston, B., McWilliams, I., and Burnham, D., "Aircraft Wake Vortex Takeoff Tests at Toronto International Airport," Report No. FAA-RD-78-143, February 1979, DOT/Transportation Systems Center, Cambridge, MA.
3. Conner, A. B. and O'Brien, T. E., "A Brief Evaluation of A Helicopter Wake as a Potential Hazard to Aircraft" NASA TN-D-1227, March 1962.
4. Rossow, V.J. and Tinling, B.E., "Research on Aircraft/Vortex - Wake Interactions to Determine Acceptable Level of Wake Intensity," Journal of Aircraft, Vol. 25, No. 25, June 1988, pp 481-492.
5. Burnham, D.C., "B-747 Vortex Alleviation Flight Tests: Ground-Based Sensor Measurements," Report No. DOT-FAA-RD-81-99, DOT Transportation Systems Center, Cambridge, MA.
6. Garodz, Leo J., "FAA Full-Scale Vortex Wake Turbulence Flight Test Investigations; Past Present Future," AIAA Paper 71-97, Presented at 9th AIAA Aerospace Sciences Meeting.
7. Garodz, Leo J., et al., "Measurement of the Trailing Vortex System of Large Jet Transport Aircraft Using Tower Fly-by and Flow Visualization (Summary Comparison Application)," Report No. FAA-RD-75-127, January 1976.
8. Tymczyszyn, J.J., Biehl, K.J., and Teager, S.A., "Flight Test Investigation of the Wake Vortices Generated by Rotorcraft," Proceedings of the Aircraft Wake Vortices Conference, October 29-31, 1991, DOT/FAA/SD-92/1.1, DOT-VNTSC-FAA-92-7.1.
9. Andrews, W.H., Robinson, G.H., and Larson, R.R., "Exploratory Flight Investigation of Aircraft Response to the Wing Vortex Wake Generated by Jet Transport Aircraft," NASA TN D-6655, Washington, D.C., March 1992.
10. Garodz, L.J., Barber, M.R., and Kurkowskiski, R.L., "Flight Test Investigation of the Vortex Wake Characteristics Behind a Boeing 727 During Two-Segment and Normal ILS Approaches," FAA Report FAA-NA-75-151, Atlantic City, NJ, October 1975.
11. Demko, P.S. and Boschma, J.H., "Advances in Decelerating Steep Approach and Landing for Helicopter Instrument Approaches," Preprint No. 79-16, 35th Annual National Forum, American Helicopter Society, May 1979.
12. Taylor, John W.R., Editor, "Jane's All the World's Aircraft, 1988-89," Jane's Information Group, Limited, Surrey, United Kingdom, 1988.



APPENDIX A  
PROBE AIRCRAFT

Probe aircraft utilized during vortex work were:

T-34A, Model : N7CN, Serial Number G-76, Registration Number N-7CN

Basic aircraft (w/o fuel): 2327.0 lbs cg 86.48 in.

Initial test weight: 2950.0 lbs cg 88.92 in.

Allowable cg travel: 87.6 to 80.0 in.

Wing span: 32 ft. 9 7/8 in.

Illustrated in figure A-1

T-34C Navy aircraft Bureau Number 162637, Side Number 525

Basic aircraft (w/o fuel): 3019.5 lbs cg 85.49 inches

Initial test weight: 4220.0 lbs cg 88.72 in.

Allowable cg travel: 86.0 to 89.5 in.

Wing span: 33 ft. 3 7/8 in.

Illustrated in figure A-2

8KCAB Champion Decathlon Serial Number 339-77, Registration Number N253CA

Basic aircraft (w/o fuel): 1387.53 lbs cg 13.16 in.

Initial test weight: 1800 lbs cg 16.41

Allowable cg travel: 13.47 to 18.5 in.

Wing span: 32 ft.

Illustrated in figure A-3

AC-680E Aero Commander Serial Number 818062, Registration Number N50

Basic aircraft (w/o fuel); 5725.6 lbs cg 174.7 in.

Initial test weight: 7141.6 lbs cg 171.25 in.

Allowable cg travel: 166.01 to 175.12 in.

Wing Span: 49 ft. 1/2 in.

Illustrated in figure A-4



FIGURE A-1. T-34A PROBE AIRCRAFT



FIGURE A-2. T-34C PROBE AIRCRAFT



FIGURE A-3. 8KCAB DECATHLON PROBE AIRCRAFT



FIGURE A-4. AC-680E AERO COMMANDER PROBE AIRCRAFT





